

AN ABSTRACT OF THE THESIS OF

Nathan A. Germann for the degree of Master of Science in Mechanical Engineering presented on October 2, 2013.

Title: Analysis of Spillway Hydrodynamics for Total Dissolved Gas Prediction Downstream of Hydropower Projects with Free, Plunging Spillway Jets.

Abstract Approved:

Kendra V. Sharp

During spring and early summer hydropower projects are often forced to spill water through their spillways due to increased river flows of the runoff season. Flows which are directed through spillways—instead of through turbines—contain a substantial amount of energy. Stemming from the high energy content, spillway flows entrain air at the point of impingement with the lower reservoir; furthermore, entrained air can be carried deep into the plunge pool. This process results in the transfer of mass from air to the liquid phase, which can ultimately cause supersaturation of Total Dissolved Gas (TDG) downstream of hydropower projects. Under certain conditions, high enough levels of TDG supersaturation can harm fish and other aquatic biota. For this reason, many hydropower facilities are currently studying methods to reduce dissolved gas generation caused by spillway flows.

The present research effort utilizes Computational Fluid Dynamics to examine spillway jet characteristics for the prediction of TDG downstream of an arch dam. In seeking to make TDG predictions, flow at the spillway exit is analyzed and correlated to historical TDG data for known conditions at a specific hydropower project. Once this calibration step is complete, TDG predictions can be made by running numerical models of the spillway with potential structural modifications and analyzing hydrodynamic quantities at the spillway exit plane. Based on the results presented herein, the developed methodology appears to be a viable technique for analyzing structural alternatives for TDG abatement at hydropower projects with free, plunging jets. Results from the current work were compared to estimates made by another TDG prediction method, and similar trends were observed. Potential improvements to the developed methodology have been identified and suggested as future topics of research.

©Copyright by Nathan A. Germann
October 2, 2013
All Rights Reserved

Analysis of Spillway Hydrodynamics for Total Dissolved Gas Prediction
Downstream of Hydropower Projects with Free, Plunging Spillway Jets

by
Nathan A. Germann

A THESIS

Submitted to
Oregon State University

in partial fulfillment of
the requirements for the
degree of

Master of Science

Presented October 2, 2013
Commencement June 2014

Master of Science thesis of Nathan A. Germann presented on October 2, 2013.

APPROVED:

Major Professor, representing Mechanical Engineering

Head of the School of Mechanical, Industrial, and Manufacturing Engineering

Dean of the Graduate School

I understand that my thesis will become part of the permanent collection of Oregon State University libraries. My signature below authorizes release of my thesis to any reader upon request.

Nathan A. Germann, Author

ACKNOWLEDGEMENTS

While many people have helped shape my education, I gratefully acknowledge the following individuals for the role each has played throughout my graduate studies:

- Dr. Sharp—OSU—for her full support and mentorship throughout my master's program;
- Keith Moen—Hatch—for his generosity in facilitating the opportunity to investigate an interesting and challenging topic;
- Kim Pate—Seattle City Light—for her generosity in overseeing my work and setting up an excellent tour of Boundary Dam;
- Keith Fuller—Falls Creek Hydro—for taking me on as a maintenance assistant at the hydroelectric plant; my time there has proven invaluable in terms of career, practical mechanical understanding, and life lessons;
- Nikou Snell—Hatch—for providing me with the needed information about Boundary Dam and her CFD modeling efforts;
- And finally my family, including my father, mother, sister, brother-in-law, and girlfriend Bailey—all whom have accompanied and supported me along this journey.

TABLE OF CONTENTS

	<u>Page</u>
1. Introduction	1
1.1. Background.....	1
1.2. Problem statement and research goals.....	5
1.2.1. Problem statement.....	5
1.2.2. Hypothesis.....	7
1.2.3. Research goals	8
2. Review of relevant topics	9
2.1. Open Channel Flow.....	9
2.2. Hydraulic structures: Dams, spillways, energy dissipation.....	12
2.2.1. Dams.....	12
2.2.2. Spillways.....	13
2.2.3. Energy dissipation.....	15
2.3. Total Dissolved Gas	21
2.3.1. What exactly is Total Dissolved Gas (TDG)?.....	21
2.3.2. Mechanisms of generation.....	22
2.3.3. Plunging jets and air entrainment.....	24
2.3.4. Effects on river systems.....	31
2.3.5. Mitigation measures to date.....	33
2.4. Computational work related to TDG.....	34
3. Methods: A numerical approach.....	40

TABLE OF CONTENTS (Continued)

	<u>Page</u>
3.1. Phase I: Calibration.....	42
3.2. Phase II: Making TDG predictions	47
3.3. Parameters of interest.....	47
3.4. Software and models used	48
3.4.1. Two phase model.....	49
3.4.2. Turbulence model	50
3.5. Setup of Spillway 2 computational model	52
3.5.1. Domain.....	52
3.5.2. Meshing.....	55
3.5.3. Boundary conditions.....	58
3.5.4. Numerical methods.....	60
3.5.5. Convergence & monitoring solution data.....	60
3.6. Assumptions.....	61
4. Results & discussion	63
4.1. Assessing convergence and accuracy of numerical simulations	63
4.1.1. Calibration models	63
4.1.2. Baffle block models	69
4.2. Calibration model results.....	71
4.2.1. Sensitivity analysis.....	82

TABLE OF CONTENTS (Continued)

	<u>Page</u>
4.2.2. Observed potential for TDG reduction from operational changes.....	83
4.3. Baffle block results	84
4.4. TDG predictions	90
5. Conclusions.....	95
5.1. Goal of study.....	95
5.2. Kinetic energy and momentum correction coefficients.....	96
5.3. TDG regimes.....	96
5.4. Model limitations	97
5.5. Sensitivity.....	98
5.6. Mesh.....	98
5.7. Wall layer flow behavior	100
5.8. Concluding remarks	100
Bibliography	101
APPENDICES	105
Appendix A: Additional details of relevant research	106
Appendix B: Field data reduction.....	112
Appendix C: Modeling details	114

LIST OF FIGURES

<u>Figure</u>	<u>Page</u>
Figure 1: Columbia River Basin and a few hydropower projects of interest [6].....	3
Figure 2: Boundary Dam, located in the Northeastern corner of Washington State (“10 shot stitched photo” credited to Morse-Dayton, 2007 [12]).....	5
Figure 3: Comparing the impinging action of a coherent water jet vs. a dispersed water jet; in terms of plunging depth, $y_1 > y_2$	7
Figure 4: Depth of flow in a channel compared to a specific energy diagram (Fox et al., 2009 [17]).....	11
Figure 5: Left: Ogee spillway with a radial gate [19]. Right: Un-gated, overflow diversion structure (Falls Creek Hydropower, Oregon).....	13
Figure 6: Classification of spillways based upon inlet, regulation, channel, and outlet (Khatsuria, 2005 [20]).....	14
Figure 7: Expression of a hydraulic jump for different ranges of Froude number (USBR, 1987 [22]).....	16
Figure 8: Hydraulic jump energy losses vs. the Froude number of incoming flow— shown for channels with rectangular, parabolic, and triangular shaped cross sections (Sturm, 2010 [21]).....	17
Figure 9: Type III Stilling basin for Froude numbers greater than 4.5 and incoming velocity ≤ 60 ft/s (USBR, 1987 [22]).....	18
Figure 10: Impact energy dissipation. Left: Induced tumbling flow (Khatsuria, 2005 [20]). Right: baffled apron (USBR, 1987 [22]).....	19
Figure 11: Schematic of a free, plunging jet (adapted from Ervine et al., 1997 [23]).....	19
Figure 12: Left: air entrainment at an ogee-crested spillway. Right: location of air entrainment at a free jet (Gulliver et al., 1998 [33]).....	23

LIST OF FIGURES (Continued)

<u>Figure</u>	<u>Page</u>
Figure 13: Comparison of jets with similar turbulence intensities but issuing at substantially different velocities. Top: jet flowing at 5 m/s with a Tu of 5%. Bottom: jet flowing at 25 m/s with a Tu of 7% (Ervine & Falvey, 1987 [36]).	26
Figure 14: Schematic of liquid plunging jets: (a) evolution of the meniscus with increasing impact velocity, U_i (the minimum radius of curvature of the meniscus, r , is indicated by the dashed circle), (b) incipient conditions for shear-dominated viscous entrainment, (c) incipient conditions for low-viscosity, low-disturbance level, and (d) entrainment by large-amplitude disturbances. (Figure borrowed from Kiger & Duncan, 2012 [35]).	28
Figure 15: View of spillway jets from the top of Boundary Dam. Immediately downstream of the spillway jets the flow is white because of the large volume of air entrained by spilled flow. Further downstream (at the top of the image) it can be seen that a substantial amount of entrained air has escaped from the flow, as the river is a darker color (Photograph taken 5/13/2013).	29
Figure 16: TDG variation with depth and surface saturation (Weitkamp, 2008 [42]).	32
Figure 17: Spillway deflector schematic showing skimming flow (from a 2012 NWSA Annual Conference presentation [44]).	33
Figure 18: A model display of Boundary Dam located inside the dam's visitor center. Spillway 2 is circled, which is the spillway of interest for this research effort.	41
Figure 19: TDG fixed monitoring stations (adapted from Rounds and Orlins [15]).	43
Figure 20: TDG gain summary at Boundary Dam. Categorized by spilled flow as a percentage of total river discharge (from Rounds and Orlins [15]).	44
Figure 21: Plot of TDG flux vs. flow rate; data averaged from spill tests reported by Rounds and Orlins [15]. Note that the curve fit line is only fitted to data at the seven highest flow rates. The error bars represent a standard deviation in the data averaged to calculate each point.	45

LIST OF FIGURES (Continued)

<u>Figure</u>	<u>Page</u>
Figure 22: TDG flux vs. spill discharge. In examining trends, a minimum TDG flux of approximately -6% saturation appears to be reached at spill discharges below 10 kcfs. In addition, this graph illustrates the large amount of scatter present in raw TDG data. (Figure borrowed from a report detailing TDG tests conducted at Boundary Dam in 2002, Columbia Basin Environmental [13]).	46
Figure 23: TDG flux vs. spill discharge when Spillway 2 is in use. A maximum TDG flux of approximately 20% appears to be reached near a spill discharge of 35 kcfs. (The graph includes measurements taken during 2006–2012, and is plotted from data reported by Rounds and Orlins, 2013 [15]).	46
Figure 24: CAD image of Spillway 2 without baffle blocks.	53
Figure 25: a). Current configuration (no blocks) b). Angled blocks (9 blocks) c). Linear blocks (9 blocks) d). Linear no side upstream blocks, or LNSUB (7 blocks).	54
Figure 26: Angled blocks geometry prior to meshing.	55
Figure 27: Images of three mesh sizes for the spillway with a gate opening of 5.93 ft (which equates to a flow rate of 13 kcfs). The number of inflation layers in each mesh, from top to bottom, is 15, 26, and 43.	57
Figure 28: Location of prescribed boundaries.	59
Figure 29: Discharge curve for Spillway 2 (based upon data provided from personal communication with N. Snell, Hatch Engineer).	62
Figure 30: Location of the free surface (denoted by $vofwater = 0.5$) for a flow rate of 13 kcfs. On the exit plane, velocity contours in the water phase are shown.	63
Figure 31: Example residual plot after 5 s of flow time (from a 17.5 kcfs calibration run).	64
Figure 32: Plot of TKE vs. flow time for the calibration case at 13 kcfs. The graph demonstrates that variables of interest become constant after ~4.5 s of flow time, and therefore a total run time of 5 s is sufficient.	65

LIST OF FIGURES (Continued)

<u>Figure</u>	<u>Page</u>
Figure 33: Velocity profiles of the water phase near the center of the spillway outlet (the case shown is for the calibration model at 13 kcfs).....	66
Figure 34: Velocity profile for the 13 kcfs case on the mesh of <i>medium</i> fineness. Discretization uncertainty was computed using Eq. (7) from Celik et al. [57]. A sample of 15 points was used to graph the line and compute uncertainty values, however, the velocity profile is plotted as a thin line for ease of profile visualization.	67
Figure 35: Water volume in spillway for a flow rate of 13 kcfs. Note: the left wall of the spillway is visible while the right wall is removed for viewing purposes.....	72
Figure 36: Volume fraction contours on the exit plane for all four calibration models (1 is all water, and 0 denotes all air). Near the right side of each plot, outlet area of the water phase is reported. From top to bottom the corresponding flow rates are 6, 13, 17.5, and 20 kcfs.....	74
Figure 37: Velocity contours on the exit plane for all four calibration models. Froude (Fr) and specific energy (E) reported. From top to bottom the corresponding flow rates are 6, 13, 17.5, and 20 kcfs.....	75
Figure 38: Turbulence intensity contours on the exit plane for all four calibration models. On the right side of the figure, area-averaged Tu is reported for each case. From top to bottom the corresponding flow rates are 6, 13, 17.5, and 20 kcfs.....	76
Figure 39: Looking down at Spillway 2 comparing turbulence at spillway walls to spillway center. In the image, Spillway 2 discharge is approximately 12 kcfs (Photograph taken 5/13/2013).	77
Figure 40: Wall layer in Spillway 2 compared to CFD model	78
Figure 41: Vortex in the upstream flow caused by the gate-wall geometry configuration. Downstream, the presence of a wall layer is visible.....	79
Figure 42: Calibration curve for specific energy rate, E	81

LIST OF FIGURES (Continued)

<u>Figure</u>	<u>Page</u>
Figure 43: Calibration curve for momentum function, M	81
Figure 44: Time-averaging the mass flow rate at the spillway outlet. The solid line indicates the outlet flow rate at any point in time, and the dashed line is a running average.....	85
Figure 45: Baffle block configurations and prescribed names—view is of spillway outlet, looking upstream.....	85
Figure 46: Free surface profile for all three block cases. From top to bottom, the configurations shown are the linear, LNSUB, and angled.....	87
Figure 47: Outlet velocity contours of the water phase for the three block configurations. Froude number (Fr) and specific energy (E) is reported for each flow. From top to bottom, the configurations shown are the linear, LNSUB, and angled.	88
Figure 48: Turbulence intensity in the water phase at the spillway outlet (linear blocks case shown).....	89
Figure 49: Initial TDG predictions. They y-axis denotes the predicted forebay-to-tailrace TDG flux, and x-axis denotes the different spillway configurations.....	91
Figure 50: Normalized TDG predictions.	92
Figure 51: TDG predictions with the calibration data adjusted to match Hatch's.....	94
Figure 52: The white oval indicates the domain region for the current CFD models. The black, dashed lines indicate the region future work should seek to <i>predict</i> by extrapolating energy and turbulence quantities at the spillway exit.....	99
Figure 53: Comparing the difference between scour hole and plunge pool dissipation (LI et al., [49]).....	110

LIST OF FIGURES (Continued)

<u>Figure</u>	<u>Page</u>
Figure 54: One of the graphs from Rounds and Orlins' report [15]. Data from the "Forebay TDG %" condition of 126% was averaged from this graph (and eleven others like it) to achieve the data plotted in Figure 21.....	113

LIST OF TABLES

<u>Table</u>	<u>Page</u>
Table 1: Hydrolab data sonde measurement parameters [26].....	22
Table 2: Non-dimensional groups presented by Kiger & Duncan [35] which are relevant to air entrainment. Uj is the jet impact velocity, g is gravitational acceleration, L is a single reference length, ρ is density, σ is interfacial tension, μ is dynamic viscosity, u' fluctuation velocity, and l and g are subscripts for liquid and gas, respectively.	30
Table 3: Review of literature related to modeling TDG with numerical methods. Articles are divided by research using (1) CFD and (2) physically based relationships; additionally, they are organized by year, with newest work reported first.....	35
Table 4: Selected flow rates to run calibration models at.....	42
Table 5: Potential parameters of interest for TDG predictions.	48
Table 6: Definition of volume fraction equation variables.....	49
Table 7: Definition of terms for the <i>SST</i> $k - \omega$ transport equations.....	51
Table 8: Specification of boundary conditions.	59
Table 9: Solution methods used in the numerical models. (Underlined solution methods denote settings suggested in ANSYS documentation [60]).	60
Table 10: Mass flux through the domain for calibration models on grids of <i>medium</i> fineness.	64
Table 11: Parameters of interest on the spillway outlet for each of the calibration runs; values reported are from solutions achieved on the <i>medium</i> mesh. GCI measures of discretization uncertainty are tabulated for each parameter.	68
Table 12: Parameters calculated for the LNSUB configuration on the <i>medium</i> mesh.	70

LIST OF TABLES (Continued)

<u>Figure</u>	<u>Page</u>
Table 13: Approximate relative errors for functions of interest in baffle block models.	70
Table 14: Kinetic energy and momentum correction coefficients for calibration models.....	80
Table 15: Inlet turbulence sensitivity analysis for the 13 kcfs case. The maximum difference column compares the maximum and minimum values achieved from the three cases run.	82
Table 16: TDG predictions for operating at a constant spill discharge of 13 kcfs but at two different forebay elevations. *Note: 7.1% is a calibration specified TDG value.	83
Table 17: Kinetic energy and momentum flux correction coefficients for baffle block cases. The specific discharge in each case is 260 ft ² /s.	90
Table 18: Turbulence kinetic energy in water exiting the spillway for all three baffle block cases.	93
Table 19: How data from the “short-term database” was divided for plotting purposes. ...	112

DEFINITIONS AND ACRONYMS

Anadromous fish	Species that live in the sea but migrate up freshwater rivers for breeding
Angled	Baffle block Configuration 4: two rows of blocks arranged at an oblique angle to flow direction
BiOp	Biological opinion
CAD	Computer-aided design
CFD	Computational fluid dynamics
Critical flow	Flow where $Fr = 1$
ESA	Endangered Species Act
FCRPS	Federal Columbia River Power System
FERC	Federal Energy Regulatory Commission
FMS	Fixed monitoring station
GBT	Gas bubble trauma
GCI	Grid convergence index
Hyporheic	Region of streambed important for fish spawning
Linear	Baffle block Configuration 2: two rows of baffle blocks arranged orthogonal to flow direction
LNSUB	Baffle block Configuration 3: Linear no side upstream blocks
NS	Navier-Stokes
NWHA	Northwest Hydroelectric Association
RANS	Reynolds Averaged Navier-Stokes
Sequent depth	Depths of flow up and downstream of a hydraulic jump
Subcritical flow	Flow where $Fr < 1$
Supercritical flow	Flow where $Fr > 1$
Tail water	Water downstream of a hydraulic structure

DEFINITIONS AND ACRONYMS (Continued)

TDG	Total dissolved gas
USACE	U.S. Army Corps of Engineers
USBR	U.S. Bureau of Reclamation
Wall layer	Term used in the present research to describe the aerated flow region containing longitudinal vortices near spillway walls
WQP	Water Quality Plan

VARIABLES AND UNITS

A	Cross-sectional area of flow
cfs	Cubic feet per second
D_h	Hydraulic diameter
E	Specific energy
\dot{E}	Specific energy rate
$E_{transport}$	Energy transport rate of a jet
Fr	Froude number
g	Gravitational acceleration
H	Total energy head
h_{fine}	Representative cell size on the <i>fine</i> grid (for grid convergence study)
kcf/s	Thousand cubic feet per second
KE	Kinetic energy
kWh	Kilowatt-hour (measure of energy)
M	Momentum function
MW	Megawatt (measure of energy per unit time)
P_{atm}	Atmospheric pressure
P_{TDG}	Pressure of in situ dissolved gases
Q	Volumetric flow rate
r	Refinement factor (for grid convergence study)
RMS	Root mean square
s	Seconds
TKE	Turbulence kinetic energy
U	Uncertainty

VARIABLES AND UNITS (Continued)

u'_i	Fluctuating component of velocity in the i^{th} direction
\bar{V}	Average flow velocity
vol_f_q	Volume of fluid of the q^{th} phase
y	Depth of flow
y_c	Critical flow depth
z	Distance from a reference datum
7Q10	7 day flow event that occurs with a frequency of once every 10 years
α	Kinetic energy flux correction coefficient
β	Momentum flux correction coefficient
ε_{ij}	Difference in a variable of interest from the i^{th} to the j^{th} grid during grid refinement (for grid convergence study)
ν	Kinematic viscosity
φ_i	Value of key solution variable on the i^{th} grid (for grid convergence study)

For my Granddad
An inspiration, provider, and avid fisherman

1. INTRODUCTION

1.1. BACKGROUND

Of the many challenges the developed world is currently faced with, the enormity of our energy consumption is certainly of great importance. If one stops to think for a moment about how much “energy” is a part of every action we carry out, it is staggering. In fact it is hard to come up with a single task carried out in day-to-day life that doesn’t require external energy: breakfast in the morning involves milk that is kept cold by an electric refrigerator, a warm shower is made possible by a water heater, the cars we drive consume energy, the computers we work on certainly won’t function if not connected to an energy source... cell phones, manufacturing, entertainment, hospitals, and the list goes on and on. The liberties granted to us by our access to abundant, “cheap” energy are almost unfathomable. Energy provides us the ability to travel to space, store incredible amounts of information, investigate elementary particles that make up our world, and explore the expanses of our universe. All of this adds up to one undeniable truth: the developed world consumes massive amounts of energy.

In 2012 the net electricity generation in the United States totaled nearly 4,504,000,000,000 kilowatt-hours (kWh) [1]—that is 4.5 *trillion* kWh, written in full form for the reader’s benefit. At the beginning of 2012 the population in the U.S. was near 312.8 million people [2]. This means that for every American citizen, 14,400 kWh of electricity were consumed that year.

This value of 14,400 kWh can be made a little more tangible on an individual basis by assuming each person had to generate this energy by pedaling a stationary bicycle—such bicycles have been making their way into gyms so that individuals can generate electricity while exercising. It can be assumed that our human “power plant” can average 0.1 kW of power generation potential [3]. If this were the case, one would have to pedal a bike *continuously* for about 16.5 years just to generate enough electricity for “their consumption” in 2012.

This grossly simplified exercise serves to portray the tremendous quantities of energy that we, the developed world, consume. Sooner or later humans are going to have to confront the issues associated with this reality. Among the many that arise, a few concerns which

stem from our energy practices include environmental impacts, health conditions, the size of our energy reserves, and the cost future generations will have to pay. Due to these concerns surrounding energy generation, consumption, and conservation, a wealth of attention and resources have recently been directed at improving our energy practices.

The current research effort is focused on an issue relating to the generation of electrical energy. While a wide variety of electricity generation methods exist, each different source has potential impacts which must be addressed and mitigated. One technology which has been around in primitive form for many centuries is the use of water flowing under gravitational forces to generate power; today, this approach is most generally referred to as hydropower. Since this method of energy generation has been around for a longer period of time than many other generation techniques, it is a relatively mature industry. Hardware has been developed for a wide variety of flows. Furthermore, applications range from large scale dams such as the Grand Coulee Dam on the Columbia River (which has an installed capacity of 6,809 MW [4]) to small scale systems that can supply modest amounts of energy in a remote locale or to a hydropower hobbyist (for an example of a small hydroelectric configuration, see [5]).

Even though hydropower is a renewable energy source, it has potentially negative impacts—like all energy generation techniques—which must be addressed. One of the main issues facing the hydropower industry today is how facilities can be best operated to ensure minimal impacts on nature. It is important that hydroelectric power plants not only operate efficiently, but also that they do not yield undue harm on the surrounding environment. Issues relating to endangered species, other fish and wildlife, water quality, erosion, and various other impacts can all be of great importance to any given hydropower facility.

Figure 1 shows some of the hydropower projects discussed throughout this thesis.



Figure 1: Columbia River Basin and a few hydropower projects of interest [6].

One currently prominent issue in Northwestern U.S. (and elsewhere) is related to the supersaturation of Total Dissolved Gas (TDG) in river systems. As early as 1965 observations in the Columbia River Basin identified high enough levels of TDG supersaturation to be potentially harmful to fish [7]. Studies carried out in 1966–1967 substantiated that (1) elevated levels of TDG were present throughout the study area (which spanned from Grand Coulee Dam to the mouth of the Columbia River), (2) these concerning levels of TDG were realized during the spring and early summer when high flows required hydropower projects to spill water over their spillways, and (3) elevated surface temperatures combined with a lack of circulation were credited for the fact that supersaturated water did not reach equilibrium very quickly in downstream reservoirs ([5], [8]).

Over the years since the initial discovery of TDG supersaturation in the Columbia River, efforts have been carried out to research and mitigate this issue downstream of hydropower project sites. However, more recently, action regarding TDG supersaturation has resurfaced, and many facilities have been conducting studies and making structural/operational changes for TDG mitigation purposes.

For example, in 2003 the Federal District Court reviewed the *NOAA Fisheries 2000 Federal Columbia River Power System (FCRPS) Biological Opinion (BiOp)*¹. This review originated from the case of *National Wildlife Federation vs. National Marine Fisheries Service (NOAA Fisheries)*. The court determined that NOAA Fisheries “improperly relied on actions that had not undergone Endangered Species Act (ESA) consultation or were otherwise not ‘reasonably certain to occur’” [10]. Essentially this ruling required NOAA Fisheries to re-evaluate the 2000 BiOp to make revisions which would more properly address Columbia River hydropower projects and their effects on the river and surrounding areas.

While the 2000 BiOp addresses a number of issues, TDG concerns are one of the key items on the list. Also introduced with the 2000 BiOp was the *Water Quality Plan for Total Dissolved Gas and Water Temperature in the Mainstem Columbia and Snake Rivers*, USACE [11]. This Water Quality Plan (WQP) “sets forth the Corps’ plan to improve water quality in the mainstem Columbia and Snake Rivers” [11]. A revised BiOp was released in 2004, and Appendix A pertains to the FCRPS WQP. It is stated that the goals of the WQP are to “provide a framework for identifying, evaluating, and implementing reasonable actions for dam operators” as they work to reduce dissolved gas and water temperature influences caused by hydropower projects.

The recent legal attention illustrates that even though dissolved gas issues have been recognized for many decades, there has been a recent re-focusing on how to accurately quantify, address, and improve water quality. Consequently, a large effort is underway in the Northwest, and many hydropower projects have taken, or are in the process of taking action to improve downstream water quality.

¹ A *Biological Opinion* is a document which states the opinion of one federal agency with reference to how actions by another federal agency may (1) jeopardize a threatened or endangered species, or (2) result in the degradation/modification of critical habitat [9].

1.2. PROBLEM STATEMENT AND RESEARCH GOALS

1.2.1. PROBLEM STATEMENT

Figure 2 shows an image of the hydropower project of interest for this research effort. Boundary Dam, which is located in the Northeastern corner of Washington State, is operated by Seattle City Light (SCL). The facility consists of an arch dam and underground powerhouse on the Pend Oreille River. The powerhouse is unique in that it was built inside of the rock face (shown on the right half of Figure 2). Approximately 260 ft of head are available for power generation purposes, and the six generating units present a total installed capacity of 1,068 MW.

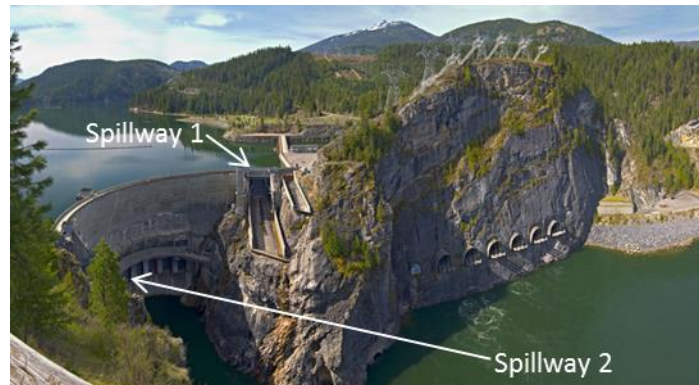


Figure 2: Boundary Dam, located in the Northeastern corner of Washington State (“10 shot stitched photo” credited to Morse-Dayton, 2007 [12]).

During the snow runoff period of late spring, the dam utilizes two chute spillways to pass excess water—each spillway has a maximum capability of passing 54 kcfs. It should be noted that only one spillway can be seen in Figure 2. The smaller chute, visible in Figure 2 next to Spillway 1, is a skimmer not used during normal operations.

When in use, the two spillways create large jets of water which become free falling jets before plunging into the lower reservoir. The falling/impinging jet entrains a substantial amount of air, and concerns surround this process because of the subsequent impact on TDG supersaturation in the river downstream of Boundary Dam.

While TDG has been generally introduced in Section 1.1, the specific concern with elevated levels of TDG is that it can result in Gas Bubble Trauma (GBT) in fish and other aquatic

species. This phenomenon is similar to “the bends” (or decompression sickness) that scuba divers may experience if they come up to the surface too quickly. Rapid depressurization allows bubbles inside one’s anatomy (blood stream, joints, under the skin, etc.) to come out of solution when the ambient pressure is effectively decreased. For humans, symptoms of the bends range from headaches, rashes, and joint pain, to—in extreme cases—death.

Historically, elevated levels of TDG have been identified at Boundary Dam. These levels occur during the high flows of spring runoff and usually last for less than one month in duration [13]. While, to the author’s knowledge, no fish mortalities have been reported in the immediate vicinity of the project, water quality laws place requirements upon all hydropower facilities regardless of local impacts that have, or have not been observed. Therefore, a recent relicensing process has required the dam’s operating entity, SCL, to investigate feasible measures for TDG abatement. These efforts are currently underway, seeking to decrease the levels of TDG introduced at Boundary Dam during high flow periods.

The solution presently under investigation consists of modifying the spillway geometry to dissipate energy *in the spillway chute* itself. The proposed solution involves adding roughness elements to the spillway. The purpose of this installation would be to dissipate energy and accelerate breakup of the falling spillway jet. For visualization, one can image the discharge of water from a fire hose compared to a heavy rain: a fire hose directed at a body of water would plunge far below the water surface while rain drops do not carry sufficient momentum to do the same. Figure 2 provides a visualization of this by comparing the plunging action of a coherent jet to a dispersed jet.

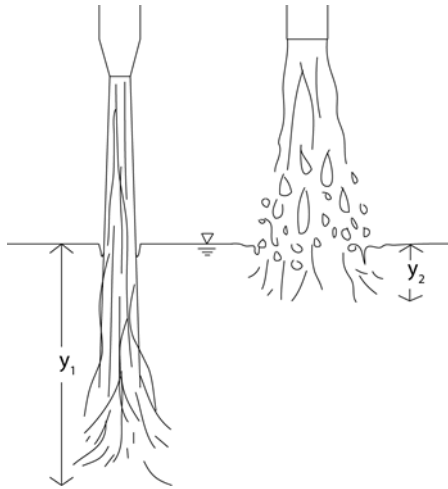


Figure 3: Comparing the impinging action of a coherent water jet vs. a dispersed water jet; in terms of plunging depth, $y_1 > y_2$.

As a result of dispersing the spillway jet, the depth to which water plunges in the lower reservoir will decrease. This is favorable because air entrained by the spillway flow will not experience the same magnitude of overpressures. As a result, TDG supersaturation downstream of Boundary Dam will be decreased.

One challenge in comparing potential TDG abatement alternatives is determining how much TDG generation will be reduced by a given alternative. How can TDG be predicted in a manner that is both time efficient and of acceptable accuracy to justify taking further action by the dam's operator?

1.2.2. HYPOTHESIS

TDG supersaturation is a result of air being exposed to elevated pressures. These elevated pressures are present in a fluid when there is a *source of energy* to drive the increase in pressure. It is well established that spillway flows are a major contributor to the generation of TDG ([8],[14]) because of the excess energy that must be dissipated in a concentrated region of a river. There should exist, then, some correlation between the *physical characteristics of spillway flow* (which produce elevated pressures) and the *amount of TDG that is generated*.

While the generation of TDG is a phenomenon influenced by a wide range of factors, it is well documented that TDG production can be approximately correlated to volumetric

spillway discharge ([13], [15]). Typically, the higher the spill flow, the higher the levels of TDG generated. Therefore, the key spillway flow characteristics that are of interest in this project surround flow velocity, exit water cross-sectional area, and spillway flow depth. These parameters have been identified because they allow for quantification of the energy of spillway flow. Turbulence has also been identified as a parameter of interest because of the role it plays in jet dissipation as well as air entrainment [16].

1.2.3. RESEARCH GOALS

The main goal of this research effort is to identify an efficient numerical methodology which correlates spillway flow characteristics to TDG generation. Current TDG prediction methods do exist, however many provide only limited 2D approximations, while others are restricted by the associated computational expenses.

If successful, the proposed method could pose several benefits to the hydropower community. Most immediately, it could serve to help assess the impact of various proposed spillway modifications at Boundary Dam. Additionally, other hydropower facilities investigating TDG abatement measures could benefit from an efficient methodology for TDG prediction purposes.

Overall, this effort poses to further the ongoing work of utilizing numerical methods to lower environmental impacts introduced by hydroelectric facilities.

2. REVIEW OF RELEVANT TOPICS

2.1. OPEN CHANNEL FLOW

Open channel flow is present in many instances throughout our world. In nature, rivers and streams exist which have irregular cross-sectional shapes; these are termed non-prismatic channels. On the other hand, prismatic channels exist which are characterized by a uniform, regular cross-sectional shape (i.e. rectangular, triangular, parabolic). Examples of such channels may be found in man-made irrigation canals, sewer systems, and dam spillways. Regardless of the cross-sectional shape, however, all open channel flows share one similar attribute: they possess a boundary which is exposed to the atmosphere. This boundary is often called a “free surface.”

Open channel flows are all dealt with in a similar manner when analyzing their physical behavior: most often in terms of specific energy and/or momentum. The energy equation for open channel flow is written in terms of the total energy head, H :

$$H = y + z + \alpha \frac{\bar{V}^2}{2g} \quad (2.1)$$

where y is the depth of flow, z is the elevation from a reference datum, α is the kinetic energy coefficient ($\alpha \approx 1$ for turbulent pipe flow), \bar{V} is the average velocity, and g is gravitational acceleration. (It should be noted that equation (2.1) is achieved by assuming a hydrostatic pressure variation within the fluid [17]).

If the bottom of the channel bed is used as the reference datum, z can be set to zero and the expression for specific energy, E , is achieved:

$$E = y + \alpha \frac{\bar{V}^2}{2g} \quad (2.2)$$

Furthermore, continuity ($V = Q/A$) can be substituted into equation (2.2) which allows for specific energy to be expressed in terms of volumetric flow rate, Q :

$$E = y + \alpha \frac{Q^2}{2gA^2} \quad (2.3)$$

Equation (2.2) provides the foundation for analyzing open channel flows; it states that specific energy is the sum of potential head (the depth of flow) and kinetic head (which results from the velocity of the flow).

When it is reasonable to assume there are no energy losses in a given flow (i.e. for smooth contractions or expansion in channel dimensions) the specific energy remains constant from one cross-section of flow upstream to another cross-section downstream (or vice versa). For instance, suppose a prismatic channel undergoes a smooth contraction in channel width, the specific energy up and downstream of the contraction remains constant ($E_1 = E_2$). Therefore, given knowledge of specific energy at one of the cross-sections, quantities such as flow depth or velocity at the other cross-section can be calculated.

A typical specific energy diagram is shown below in Figure 4. Given a set of flow conditions (such as cross-sectional channel shape and specific energy), it can be seen that for a constant flow rate, Q , there are two possible depths of flow. This is demonstrated in the figure in that fluid flowing in the open channel (at a constant discharge of Q) can be at depth y_1 or y_2 . In both cases the flow would possess the same specific energy, or $E_1 = E_2$.

If the depth of flow y is greater than the critical flow depth, y_c , then the flow is subcritical, and if $y < y_c$ then the flow is supercritical. It is worth noting that critical flow is only possible at one depth for a given set of conditions, for example, flow rate and channel cross-section.

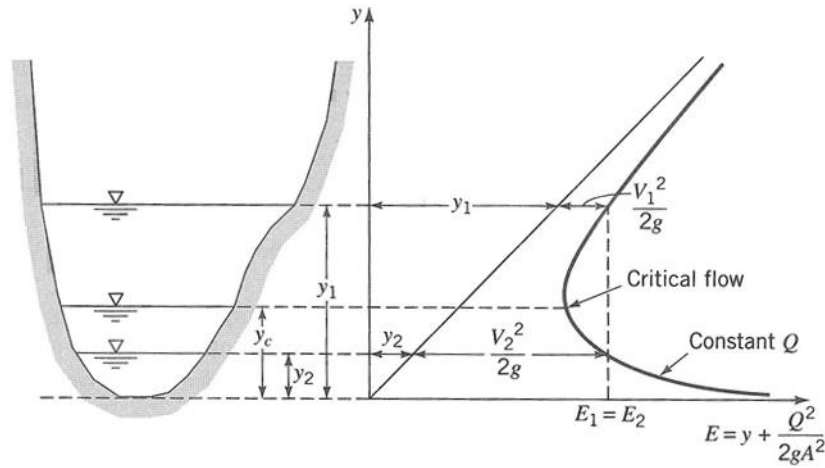


Figure 4: Depth of flow in a channel compared to a specific energy diagram (Fox et al., 2009 [17]).

Similar to the use of Reynolds number to characterize flow regimes (laminar, transitional, or turbulent), open channel flow also has a significant non-dimensional parameter used to classify subcritical, critical, or supercritical flow. This non-dimensional number used for classifying free surface flows is Froude number:

$$Fr = \frac{\bar{V}}{\sqrt{gy}} \quad (2.4)$$

in which \bar{V} is the average flow velocity, y is the flow depth, and g is gravitational acceleration. The physical interpretation of Froude number is the ratio of inertial forces to gravitational forces. General flow behavior can be determined by calculating the value of Froude number. The classifications are as follows:

$$Fr = \frac{\bar{V}}{\sqrt{gy}} \begin{cases} < 1 & \text{subcritical flow} \\ = 1 & \text{critical flow} \\ > 1 & \text{supercritical flow} \end{cases}$$

Common attributes of subcritical flow are flows with larger depths and smaller velocities; in this flow regime gravity is the dominating force. A good example of this would be the lazy river at a water park. On the other hand, supercritical flow is dominated by inertial forces and consists of smaller flow depths with larger velocities. Due to the large velocities present in supercritical cases, disturbances to the flow can only be propagated *downstream* by

means of advection. On the other hand, a flow disturbance in subcritical flow can travel in both the up and downstream directions. For instance, a raindrop falling onto the surface of a slow-flowing reservoir will send ripples both up and downstream; conversely, the ripples from a raindrop landing on water in a typical spillway will only be propagated downstream by the high velocity flow field. The Froude number of water flowing through most standard spillways is in the range of 2 – 8.

2.2. HYDRAULIC STRUCTURES: DAMS, SPILLWAYS, ENERGY DISSIPATION

2.2.1. DAMS

Circumstances in which water is to be utilized for irrigation, recreation, transportation, or hydropower give rise to the need for control structures to harness water for a wide variety of flows. Dams are a common hydraulic structure which allow for greater potential to be harnessed from rivers with variable flows. Responsible implementation of dams can serve a variety of interests: damaging floods can be prevented, energy can be stored, transportation and recreation can be enhanced, and the impact of droughts can be decreased. Of course, dams take on various forms and sizes. They may be managed with one goal in mind, or may have to balance input from dozens of interest groups.

The Three Gorges Dam in China is the largest hydroelectric dam in the world at more than 1.2 miles wide and 600 ft tall [17]. On the other end of the spectrum, small dams may be constructed to divert water for irrigation or small hydropower projects. Often, these smaller structures have limited or no water storage capacity and are therefore “run-of-the-river” arrangements. A run-of-the-river hydroelectric plant is one with little or no water storage capability, and as a result, the power output of the plant varies directly with fluctuations in stream flow [18].

On the left, Figure 5 shows an image of an ogee-shaped spillway with a radial gate control configuration. On the right of Figure 5 is an image of the diversion at Falls Creek Hydropower, which is a ~5MW hydropower facility located in the Cascade Mountain Range of Oregon. For hydropower, larger dams can be advantageous because they provide the ability to store water, but smaller dams typically have fewer negative environmental impacts. That being said, substantial efforts have been, and continue to be made to decrease

the impacts of diversion structures both large and small. For example, Farmers Irrigation District in Oregon developed a fish friendly diversion screen to use for water intakes.² In addition, utilities and federal agencies are continually working to decrease environmental impacts across the board—efforts related to the water quality issue of interest in the current research endeavor will be discussed in Section 2.3.5.

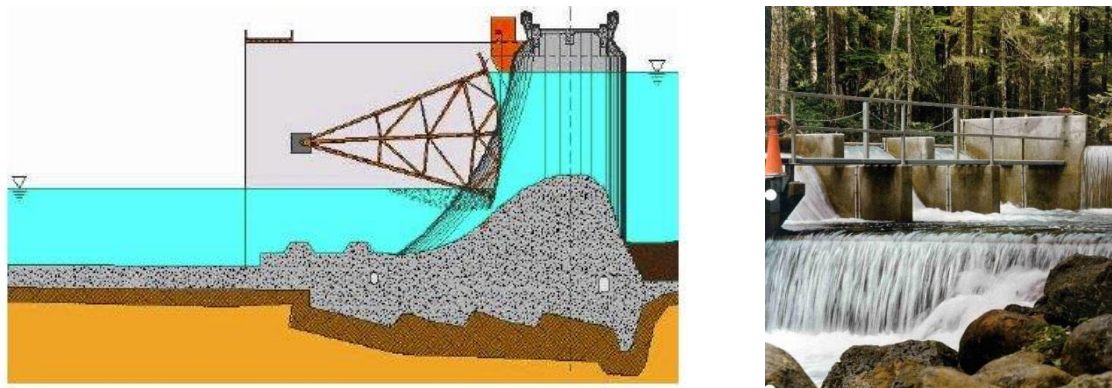


Figure 5: Left: Ogee spillway with a radial gate [19]. Right: Un-gated, overflow diversion structure (Falls Creek Hydropower, Oregon).

2.2.2. SPILLWAYS

Spillways are used in conjunction with dams to pass water flows downstream for a variety of reasons. Spilling water over dams can be necessary during spring runoff, in periods of reduced hydraulic capacity at hydroelectric facilities due to repairs or maintenance, and at certain times when spilling can enhance downstream migration of juvenile fish.

Depending on the type of dam and the surrounding geography, spillways can take on many different forms. Three typical classification systems have been outlined by Khatsuria [20].

In these three systems, spillways may be classified by:

- i) Prominent feature:
 - a. Ogee
 - b. Chute
 - c. Side channel
 - d. Overflow
 - e. Stepped
- ii) Function:
 - a. Service
 - b. Auxiliary

² See <http://farmersscreen.org/> for more information detailing this unique intake design.

- c. Fuse plug/emergency
- iii) Regulation structure:
 - a. Gated
 - b. Un-gated
 - c. Orifice
 - d. Sluice

Figure 6 below shows the main features of common spillways. Each column in the table is devoted to a specific spillway attribute: inlet, regulation control, channel type, and outlet configuration.


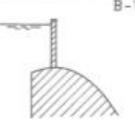
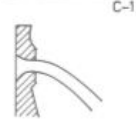
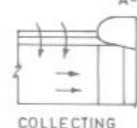

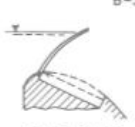
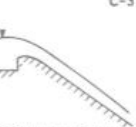
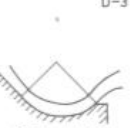
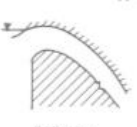



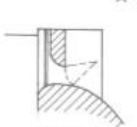
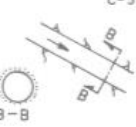
A	B	C	D
INLET	REGULATION	CHANNEL	OUTLET
 <p>A-1 OVERFLOW</p>	 <p>B-1 SLUICE GATE</p>	 <p>C-1 FREE FALL</p>	 <p>D-1 STILLING BASIN</p>
 <p>A-2 COLLECTING CHANNEL</p>	 <p>B-2 RADIAL GATE</p>	 <p>C-2 CASCADE</p>	 <p>D-2 ROLLER BUCKET</p>
 <p>A-3 SHAFT SPILLWAY</p>	 <p>B-3 FLAP GATE</p>	 <p>C-3 SPILLWAY CHUTE</p>	 <p>D-3 SKY JUMP</p>
 <p>A-4 SIPHON</p>	 <p>B-4 FUSE PLUG</p>	 <p>C-4 FREE FLOW TUNNEL</p>	 <p>D-4 PLUNGE POOL</p>
 <p>A-5 ORIFICE</p>	 <p>B-5 UN REGULATED</p>	 <p>C-5 PRESSURE TUNNEL</p>	

Figure 6: Classification of spillways based upon inlet, regulation, channel, and outlet (Khatsuria, 2005 [20]).

As an example, the left spillway shown previously in Figure 5 could be classified by the prominent feature, ogee-shaped, or it could be referred to by the regulation structure which is a radial gate.

One of the issues with dam-spillway configurations is how to maintain reasonable downstream flow velocities. Spillway flows are driven by the elevation difference, known as “head”, between the water surface upstream and downstream of the dam. In many instances, the head and flow rate of water to be passed through spillways represents a substantial amount of energy. Excess energy must be dissipated safely in order to mitigate undesirable effects including erosion, harm to fish, TDG generation, and undermining of the dam’s structural integrity.

2.2.3. ENERGY DISSIPATION

In order to prevent erosion and undermining of dam and spillway structures, it is important to restore water to normal velocities in as short of a distance as possible below spillways [21]. Various mechanisms are implemented to dissipate excess energy, and these energy dissipators have been classified by Khatsuria according to the following categories [20]:

- i) Hydraulic jump stilling basins;
- ii) Free jets/trajectory buckets;
- iii) Roller buckets;
- iv) Dissipation by spatial hydraulic jump; and
- v) Impact energy dissipators.

While items iii) and iv) in the above list are not a focus of this research effort, there is extensive detailing of these dissipation methods in literature—see Khatsuria’s text titled *Hydraulics of Spillways and Energy Dissipators*, 2005 for further information.

Due to their relevance to the current research effort, however, it is worth highlighting components of hydraulic jump stilling basins, free jets, and impact energy dissipators. These categories will be overviewed now.

2.2.3.1. Hydraulic jump stilling basins

Often, stilling basins are designed to utilize a hydraulic jump to dissipate the energy of supercritical flow exiting spillways. A hydraulic jump occurs when supercritical (high velocity, smaller depth) flow transitions to subcritical (low velocity, higher depth) flow. During this process turbulence and a return fluid roller help dissipate energy. Since there are energy losses present in a hydraulic jump, a momentum approach (instead of specific energy) is used to correlate the depths before and after the jump—these depths are called

the up and downstream sequent depths. The momentum function equation for open channel flow can be written as:

$$M = Ah_c + \beta \frac{Q^2}{gA} \quad (2.5)$$

where A is the cross-sectional area, h_c is the distance from the free surface to the cross-sectional area-centroid, β is the momentum flux correction factor, Q is volumetric discharge, and g is acceleration due to gravity.

While hydraulic jumps occur in various flow situations, Figure 7 depicts hydraulic jumps in one common location which is directly downstream of a sluice gate.

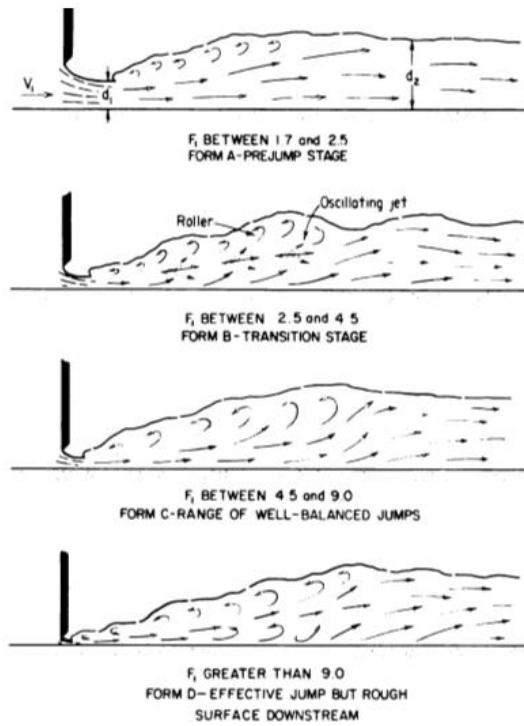


Figure 7: Expression of a hydraulic jump for different ranges of Froude number (USBR, 1987 [22]).

It can be seen that hydraulic jumps take on different forms depending upon the Froude number of the incoming flow. Accordingly, different percentages of energy are dissipated as shown in Figure 8. If the incoming supercritical flow has a Froude number greater than ~ 5 , over 50% of the flow's energy can be dissipated in a hydraulic jump. Due to the fact that

hydraulic jumps are able to dissipate large percentages of energy, they are a desirable feature to utilize for the purpose of energy dissipation in hydropower stilling basins.

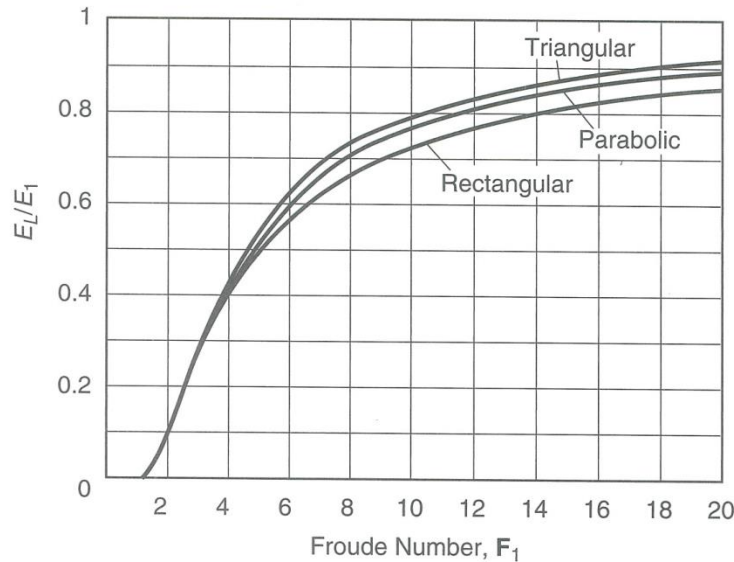


Figure 8: Hydraulic jump energy losses vs. the Froude number of incoming flow—shown for channels with rectangular, parabolic, and triangular shaped cross sections (Sturm, 2010 [21]).

The goals of a hydraulic jump stilling basin are to maintain the hydraulic jump within the basin, match the downstream sequent depth with that of the downstream river height, and achieve a velocity roughly equal to that of the natural downstream river flow. The United States Bureau of Reclamation (USBR) has generalized designs for stilling basins which can be found in texts such as *Design of Small Dams*, 1987 [22].

It is worth noting that stilling basins are found at the *base* of spillways. As water flows down the spillway, potential energy (head) changes into kinetic energy. The role of a stilling basin is to safely dissipate excess kinetic energy and restore the water to a reasonable velocity before it exits into the lower reservoir. Figure 9 shows a USBR Type III stilling basin. This design incorporates baffle blocks, which are a type of impact energy dissipator which will be discussed now.

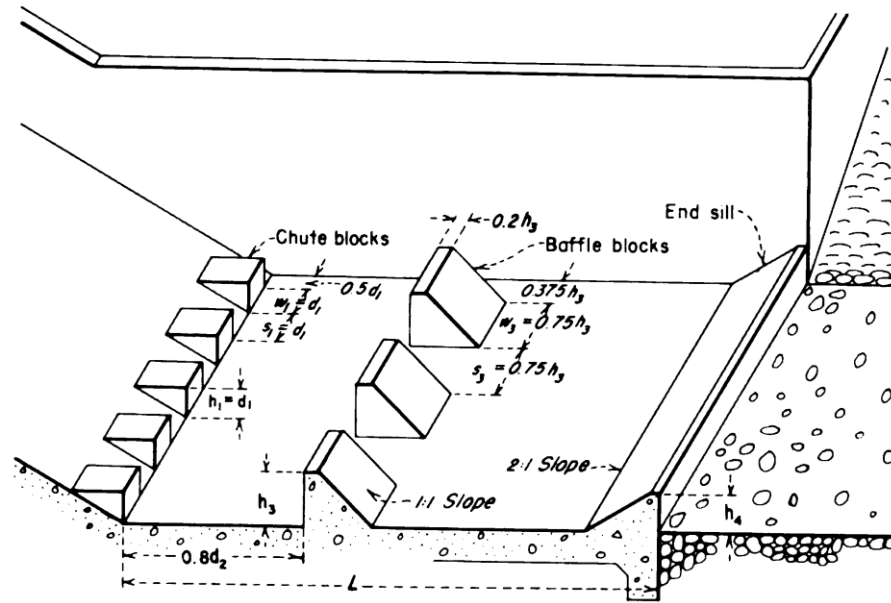


Figure 9: Type III Stilling basin for Froude numbers greater than 4.5 and incoming velocity ≤ 60 ft/s (USBR, 1987 [22]).

2.2.3.2. Impact dissipators

Impact energy dissipators are formed by placing an object directly in the path of high velocity flow. The desire of this configuration is to use drag force and induced turbulence to dissipate unwanted energy. Impact dissipators can be effective, however, the application of them is somewhat limited due to apprehension of cavitation and the danger of overly excessive drag forces [20].

Even though there are a variety of configurations of impact type energy dissipators, they all operate based on the same principal mentioned, and that is by placing an obstruction directly in the path of flowing fluid. Some designs induce tumbling in which the flow alternates between subcritical and supercritical states; such a design is shown on the left in Figure 10. On the right in the same figure, a baffled apron is shown which may be used to prohibit high flow velocities from occurring.

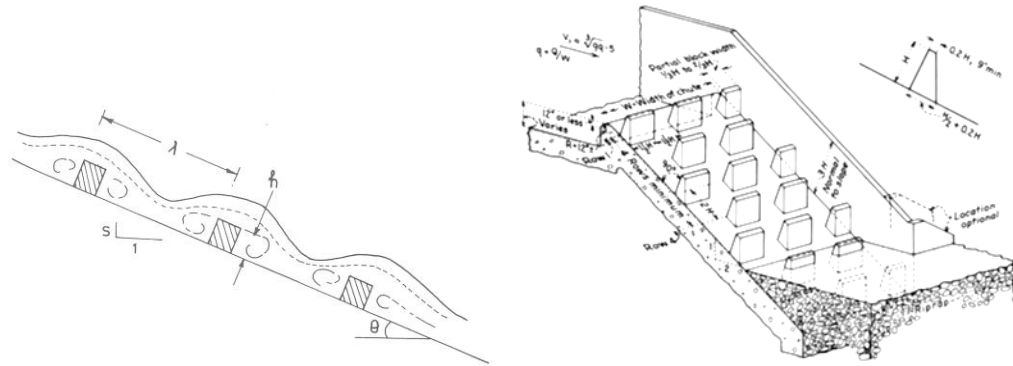


Figure 10: Impact energy dissipation. Left: Induced tumbling flow (Khatsuria, 2005 [20]). Right: baffled apron (USBR, 1987 [22]).

A special advantage of impact dissipators is that they do not require tail water in order to function. For instance, hydraulic jumps (discussed earlier in Section 2.2.3.1) require tail water in order to effectively dissipate energy.

2.2.3.3. Free jets

The final energy dissipation devices to be considered are free jets. Free jets are formed when water is issued into the atmosphere or directly into a downstream reservoir via a submerged outlet. Plunging jets play a central role in the current research effort. In this configuration, water is released from a higher elevation and then free falls in air for some distance before finally striking the lower reservoir. Figure 11 shows a schematic of a free jet issuing from a hydraulic structure.

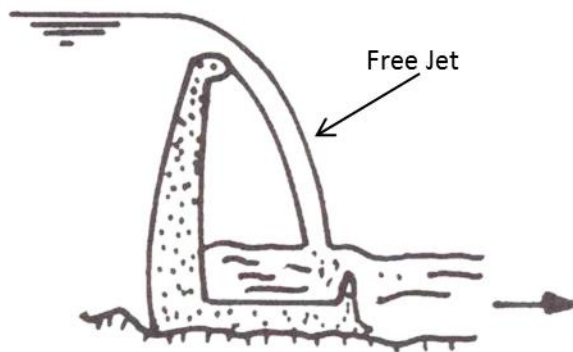


Figure 11: Schematic of a free, plunging jet (adapted from Ervine et al., 1997 [23]).

In the alternative configuration, submerged outlets employ a closed conduit to transport water from the upper to lower reservoirs. As implied by the name, the outlet terminates below the surface of the lower reservoir.

Typically the choice to use a free jet is dictated by local geography and geology, and both types of free jets are often used in high head dams such as arch dams. Concerns that surround the use of free jet dissipation include scour that can occur from a high velocity jet plunging into the lower reservoir and the impact forces in the case where the free jet impacts a stilling basin floor [20]. While fluid jets have been investigated and implemented in many different circumstances, Khatsuria ([20], pg. 234) states that the characterization of designing free jet releases for dams remains highly empirical in nature due to the number of factors which influence free jet behavior.

As mentioned in Section 1.2.1, the facility of interest in this research effort, Boundary Dam, utilizes two chute spillways that terminate ~180 ft above the lower reservoir [24]. When water is spilled from the dam, a high amount of energy is associated with the release as water flows through the spillways, free falls, and plunges into the lower pool. The free falling jets gain kinetic energy and entrain substantial quantities of air as a result of the impinging action on the lower reservoir.

Overall, dissipating excess energy at hydraulic control structures is an important task to be carried out correctly. Excess energy that is not dissipated adequately can result in a variety of problems ranging from erosion and dam failure, to water quality issues. While standardized energy dissipation designs for dams and spillways do exist, Khatsuria notes that “site specific conditions, economy in construction, and urge for innovation have often led to the evolution of unconventional design of energy dissipators” ([20], pg. 531). It is also stated that unique solutions to energy dissipation challenges are, in most cases, developed from model studies because generalized design procedures have not been established. In examining possible ways of safely dissipating excess energy at Boundary Dam, this claim certainly holds true. The ongoing TDG studies at Boundary Dam have been, and are pioneering new territory for the use of impact dissipation devices to help improve water quality; generalized design procedures for this task do not exist.

2.3. TOTAL DISSOLVED GAS

For the purpose of this thesis, it is appropriate to present an overview of TDG to give the reader a deeper understanding of the physical phenomenon involved. However, it is also important to note that, to the best of the author's knowledge, negative effects on fish species have *not* been documented immediately downstream of Boundary Dam. TDG abatement efforts at the project have been required by the Federal Energy Regulatory Commission (FERC) as part of a relicensing of the dam. Furthermore, while political components of dam licensing are outside of the scope of this effort, it is worth noting that the legislation is not well suited to adapt to the differences of each individual hydropower project.

2.3.1. WHAT EXACTLY IS TOTAL DISSOLVED GAS (TDG)?

Essentially TDG is air that is “dissolved” into water. When an air bubble trapped in water is exposed to high enough pressures, the air can be forced from a gas phase into the water solution. A good illustration of this is to consider a soft drink. If you examine Sprite in a closed 2-liter bottle, there are typically few bubbles visible. However, once you twist open the top, the sound of pressure releasing can be heard and the fluid inside is then exposed to atmospheric pressure. At this lower pressure, carbonation within the fluid (which is initially at a higher pressure) is able to come out of solution, and, as a result, one can observe bubbles forming and rising to the surface.

TDG generation is essentially the *reverse* of this process. Initially air bubbles are present in the water, and if certain conditions exist—namely elevated pressure—then bubbles can be forced into solution. Supersaturation of TDG occurs when the dissolved gas pressure in the aqueous solution is elevated above normal conditions. High enough levels of TDG supersaturation in river systems can yield harmful results on fish species and other organisms; a discussion highlighting these effects is included in Section 2.3.4.

The quantification of TDG is expressed as a ratio of dissolved gas pressure to the local atmospheric pressure:

$$TDG \text{ (\% of surface saturation)} = \frac{P_{TDG}}{P_{atm}} * 100 \quad (2.6)$$

where P_{TDG} is the in situ dissolved gas pressure and P_{atm} is the local atmospheric pressure. The measure of each pressure is reported in a standard pressure measurement scale, for example mm of mercury (mm Hg).

A typical river system in equilibrium with the atmosphere would exhibit a TDG level of 100% saturation. This would mean that gases dissolved located near the water's surface are at the same pressure as the local atmosphere. Under normal circumstances, Federal and Washington State's water quality laws require that hydropower projects do not generate TDG levels in exceedance of 110% [25], however, a few exceptions do exist. For instance, when total river discharge surpasses the highest flow rate which occurs with a duration of 7 consecutive days and a frequency of 10 years (the "7Q10" flow), this water quality law is waived. For Boundary Dam, the 7Q10 flow is 108 kcfs [24]. An additional exception when the standard of 110% may be adjusted for hydropower projects is if the facility is spilling water to aid the downstream migration of anadromous fish species.

TDG monitoring can be carried out by sensors such as the water quality data loggers (sondes) provided by Hydrolab (Loveland, CO). While field measurements were not conducted in direct coordination with this research, sensors used in previous TDG studies at Boundary Dam have had the range and accuracy presented in Table 1.

Table 1: Hydrolab data sonde measurement parameters [26].

Sensor	Range	Accuracy	Resolution
TDG (Total Dissolved Gas)	400 to 1,400 mmHg (7.7 to 27.1 psi)	± 1.5 mmHg	1.0 mmHg
Temperature	-5 to 50° C	$\pm 0.10^\circ$ C	0.01° C

2.3.2. MECHANISMS OF GENERATION

In order to successfully address TDG generation at hydropower facilities it is important to understand the mechanisms which cause supersaturation. As with most processes of interest, the mechanisms at play are numerous. Furthermore, it is often difficult or even impossible to isolate individual parameters when collecting/analyzing field data.

An examination of previous work has revealed a variety of components important to the supersaturation of TDG in river systems. The following factors have been highlighted:

- i) Supersaturation is caused by air entrainment, bubbles carried to depth, and highly turbulent and energetic flows [27].
- ii) Elevated TDG originates from the higher pressures which bubbles experience in stilling basins [28].
- iii) TDG concentration relies heavily on spillway geometry, flow behavior in the stilling basin, the bubbly flow region immediately downstream of spillways, and hydraulic operating conditions ([29], [28]).
- iv) Small bubbles are expected to have the strongest effect on TDG generation [30].
- v) Dissipation structures and spill rate heavily influence TDG [31].
- vi) Air entrainment on the spillway face and where the jet impacts the downstream pool, bubble breakup and coalescence, and degasification at the water surface play significant roles in TDG production [32].
- vii) Dissolution of dissolved gases can take a substantial amount of time in reservoirs because of the lower velocities, reduced surface area, and large depths often found in river-reservoir flows [28].
- viii) And, a few other items of importance include water temperature, local atmospheric pressure, proportion of water flowing through turbines compared to spill flow, and forebay TDG pressures.

Some of the most important items in this list will be discussed in greater detail below.

First, it is intuitive that air entrainment is a necessary contribution for increased TDG pressures. Initially, air must be present within a high pressure region in the fluid in order for mass to transfer from the gas phase to the fluid. Air entrainment is a difficult process to mitigate in most spillway configurations. Both ogee-crested spillways with stilling basins and free jet discharges have regions with high velocity gradients and mixing. Figure 12 depicts both of these hydraulic structures and their expected locations of air entrainment.

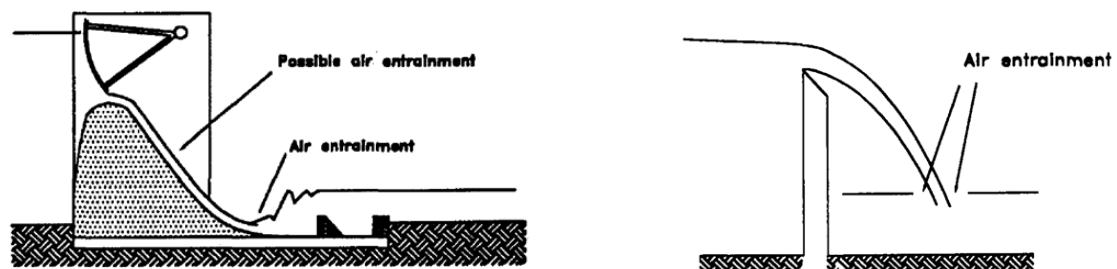


Figure 12: Left: air entrainment at an ogee-crested spillway. Right: location of air entrainment at a free jet (Gulliver et al., 1998 [33]).

Another important component needed for the generation of TDG is an energetic, turbulent flow. Some consideration leads to the possible respective roles of bulk energy and turbulent fluctuations. It would appear that turbulent energy is necessary to entrain air and also shear larger air volumes into smaller bubbles. While, on the other hand, it seems the cause of bubbles becoming exposed to elevated pressure is due to the bulk energy of spillway flow. This reasoning is supported by a previous investigation on air entrainment at liquid, plunging jets, “We found that, without disturbances [turbulence], the jet does not entrain air even when its Reynolds and Froude numbers exceed the thresholds reported by earlier investigators” [34]. The study referenced here made use of a precisely-manufactured, smooth nozzle in order to create water jets which were free of disturbances. The results of their investigation support the notion that turbulence (or a “disturbance”) plays an important role in entraining air, and is therefore critical for TDG production.

Following this reasoning, it appears possible to predict TDG generation by examining the bulk energy along with turbulent energy. One form of energy turbulence kinetic energy (TKE) serves to mix air in with the water (while also influencing jet behavior), and the other energy source (the bulk flow energy) provides the necessary power to either (1) increase pressure through an impinging action, or (2) provides sufficient energy to carry bubbles to depth such that increased hydrostatic pressures can force them into solution. Overall, it appears that one of the key requirements for TDG supersaturation is the presence of excess energy.

2.3.3. PLUNGING JETS AND AIR ENTRAINMENT

Plunging jets are found in many instances throughout nature and industrial processes. For example, the impact of physics associated with plunging jets can be found at waste treatment facilities, in fermentation processes, naval hydrodynamics, the casting of polymers or glass, and in natural water systems [18, 19]. With relation to hydropower, hydraulic structures such as spillways often employ turbulent water jets for energy dissipation purposes [36].

Extensive research efforts have studied the characteristics of free jets as well as the mechanisms associated with air entrainment in liquid plunging jets. In the studies encountered during the current investigation, a majority of the work appeared focused on

jets issuing from a circular nozzle in a laboratory setting. While the Boundary Dam spillway jets are rectangular at the point of issuance, it has been reported that rectangular jets deform in a manner similar to circular jets for cross-sectional length-to-width ratios less than 10 [37]. The spill configuration of interest at Boundary Dam has a length-to-width ratio on the order of 10. Additionally, since the fall distance at high head dams is typically long, the cross-sectional shape of a spillway jet often tends toward a circular shape the further the jet falls [37]. For these reasons, a review of the work related to circular, liquid plunging jets has been beneficial to gain a better understanding of the physics associated with spillway jets at Boundary Dam.

When examining jet behavior, key parameters which allow for estimation of jet trajectory and energy include jet velocity, air drag, and initial jet geometry; to gain a more complete description, however, information about a jet's turbulence is necessary [37]. This is because turbulence plays a significant role on how a jet deforms as it falls through the air.

Turbulence intensity, Tu , is a common quantification of turbulence and is defined as:

$$Tu = \frac{u'}{U} \quad (2.7)$$

where u' is the root mean square (RMS) of the instantaneous axial velocity and U is the average axial velocity of the flow. It has been reported that turbulence intensities of 4 – 8% are expected in gated spillways with ski-jump outlets [37]. It is also worth noting that the inclusion of additional energy dissipation devices such as baffle blocks would increase turbulent fluctuations above the range expected in a standard spillway, as is the intent at Boundary Dam [24].

With respect to turbulence, it has been highlighted by previous researchers that the expression of turbulence on a Froude-scaled model is not representative of the physics associated with prototype-scale spillway jets. An article by Ervine and Falvey [36] shows jets of similar turbulence intensities (5 and 7%), yet the model jet (issuing at 5 m/s) expresses well-rounded surface vortices while the prototype-scale jet (issuing at 25 m/s) has two length scales of associated vortices (a smaller length scale serving to create

droplets at the jet surface, as well as a larger scale which expresses medium-sized surface undulations similar to the model jet).

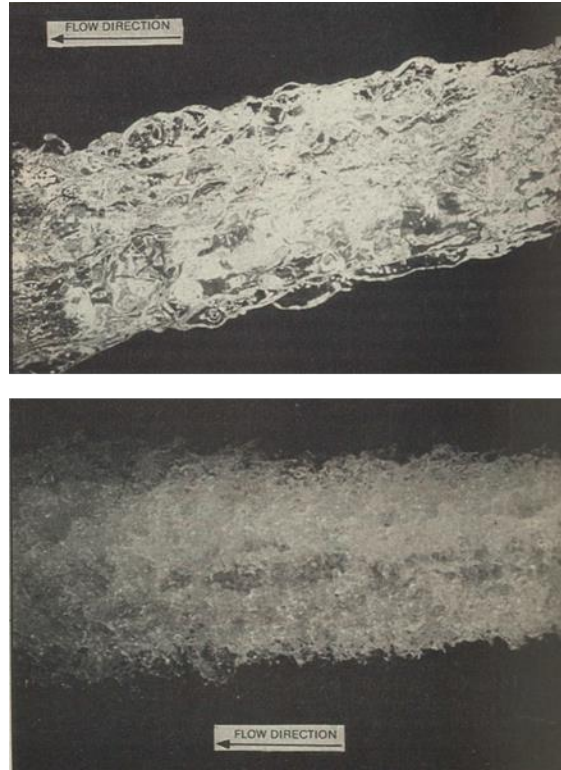


Figure 13: Comparison of jets with similar turbulence intensities but issuing at substantially different velocities. Top: jet flowing at 5 m/s with a Tu of 5%. Bottom: jet flowing at 25 m/s with a Tu of 7% (Ervine & Falvey, 1987 [36]).

The turbulence level at the issuing point of a free jet plays a key role in energy dissipation, lateral jet spreading, and general jet decay as well ([36], [37]). It has been reported that the length required for the eventual breakup of a free jet is given by L/d (fall length to jet diameter) from 50 – 100 depending upon the turbulence present in the jet ([36], pg. 303). At Boundary Dam, a sufficient distance for full jet decomposition, based on the aforementioned estimate, does not exist in the current structural geometry. Therefore, a coherent jet core does impinge the lower reservoir. This jet core not only entrains air, but also contains substantial momentum which carries entrained air bubbles deep into the lower reservoir.

In addition to jet behavior in the atmosphere, it is important to understand the gas entrainment mechanism as it is related to TDG supersaturation. It is also essential to

recognize, however, that there is not a linear relationship between air entrainment and downstream TDG supersaturation. For instance, in considering air entrapped on the spillway face it has been reported that a relatively large difference in entrapped air (10%) leads to only modest TDG variations downstream (1.4% and 3.1% for low and high flow situations respectively) [29]. From this, Urban et al. conclude that “the expected maximum range of air ejected or entrapped at the plunge point causes relatively minor changes in peak TDG concentrations” [29].

Politano et al. [38] postulate a similar point in that, in comparison to the actual volumes of air entrained at spillway jets, only 3% of the total gas volume entrained is required (if the bubbles are small) to achieve TDG levels which are measured in the field. This illustrates that over 90% of air actually entrained at spillways plays little, or no direct role in causing TDG supersaturation. The reason for this is that large bubbles have a “very short life and overpressure” [38]. Larger bubbles rise quickly and potentially coalesce to create big volumes of air which ascend to the surface and escape. In another article, Politano et al. again iterate that their model “predicts that the amount of air that needs to be dissolved to reach the levels of TDG measured downstream of spillways is much smaller than the air entrained in the spillway itself” [39].

When considering gas entrainment at a liquid plunging jet, characteristic behavior can be divided according to the prominent physics present. For the current research effort, the category of interest surrounds jets of high velocity and associated energy/turbulence. At Boundary Dam, the outer edge of the spillway jet disintegrates into distinct water droplets while the core of the jet remains intact throughout the fall.³ This information is of interest because discrete droplets entrain air in a slightly different manner than a continuous plunging jet.

To highlight the fundamentals of gas entrainment at a liquid plunging jet, Figure 14 is provided. Attention should be directed to images (c) and (d) within the figure, as these depict entrainment conditions for relative low-viscosity and large amplitude disturbance instances respectively. These two types of entrainment are most relevant to the physics present at Boundary Dam.

³ See SCL’s Facebook page to view a video of Boundary Dam’s spillways in operation [40].

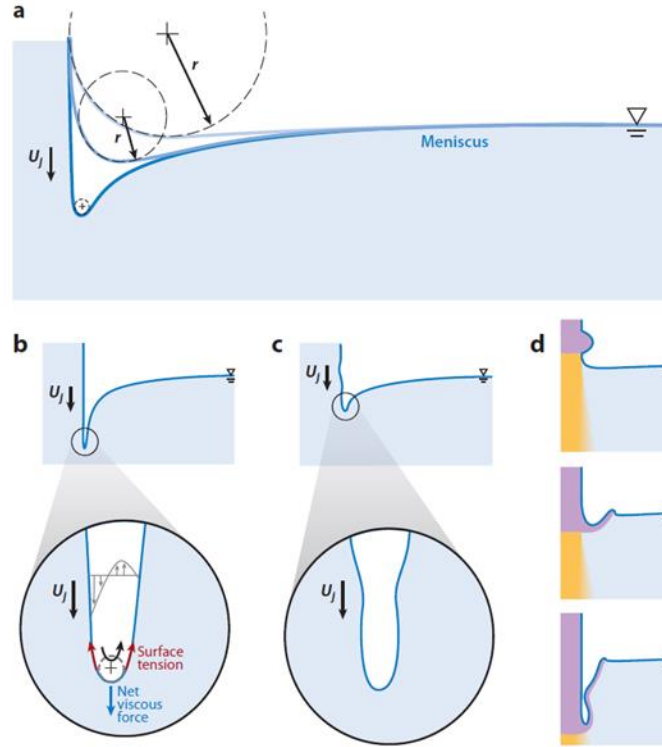


Figure 14: Schematic of liquid plunging jets: (a) evolution of the meniscus with increasing impact velocity, U_j (the minimum radius of curvature of the meniscus, r , is indicated by the dashed circle), (b) incipient conditions for shear-dominated viscous entrainment, (c) incipient conditions for low-viscosity, low-disturbance level, and (d) entrainment by large-amplitude disturbances. (Figure borrowed from Kiger & Duncan, 2012 [35]).

As demonstrated in Figure 14, the process of air entrainment at a plunging jet begins with an air cavity growing into the plunge pool's free surface. The air cavity can be caused by various mechanisms including viscous forces, a single jet disturbance, continuous turbulent fluctuations, or a single droplet. Provided there exists sufficient jet velocity, the cavity grows such that jet momentum pushes the air boundary layer far enough below the free surface for instabilities to occur. Consequentially, the water "walls" surrounding the air cavity collapse and air becomes trapped below the free surface. (For additional detailing of jet hydrodynamics and entrainment processes, refer to a review article by Bin [16]).

Once captured below the free surface, the fate of entrained air depends on the nature of the impinging jet. In the case of Boundary Dam, the high energy of the plunging jets carries entrained air bubbles well below the water surface. Furthermore, the relatively large area of

jet impingement (when compared to laboratory scale investigations) serves to entrain substantial quantities of air.

Figure 15 provides an image of Boundary Dam spillways discharging a combined total of approximately 24 kcfs. The river immediately downstream of the impinging jets appears white, which indicates a large volume of air present in the river. Further downstream (at the top of the picture) it can be seen that the river is a darker color; this indicates air within the river reduces quickly as bubbles rise to the free surface and escape.

In terms of turbulence, Figure 15 can be compared to the water jets shown in Figure 13 (on page 26). Figure 15 illustrates that spillway jets at Boundary Dam resemble the prototype jet at a velocity of 25 m/s more than the model jet at a velocity of 5 m/s. The jet surface at Boundary Dam breaks up into small droplets, which is behavior not likely to be observed on a Froude-scaled physical model of the spillway flow.



Figure 15: View of spillway jets from the top of Boundary Dam. Immediately downstream of the spillway jets the flow is white because of the large volume of air entrained by spilled flow. Further downstream (at the top of the image) it can be seen that a substantial amount of entrained air has escaped from the flow, as the river is a darker color (Photograph taken 5/13/2013).

In Kiger and Duncan's recent article [35], non-dimensional groups relevant to air entrainment were highlighted. These groups are summarized below in Table 2.

Table 2: Non-dimensional groups presented by Kiger & Duncan [35] which are relevant to air entrainment. U_j is the jet impact velocity, g is gravitational acceleration, L is a single reference length, ρ is density, σ is interfacial tension, μ is dynamic viscosity, u' fluctuation velocity, and l and g are subscripts for liquid and gas, respectively.

Name	Symbol	Expression
Primary Groups		
Froude number	Fr	$\frac{U_j^2}{gL}$
Weber number	We	$\frac{\rho_l U_j^2 L}{\sigma}$
Capillary number	Ca	$\frac{\mu_l U_j}{\sigma}$
Density ratio	γ	$\frac{\rho_g}{\rho_l}$
Viscosity ratio	M	$\frac{\mu_g}{\mu_l}$
Fluctuation intensity	Tu	$\frac{u'}{U_j}$
Alternate Groups		
Reynolds number	Re	$\frac{We}{Ca} = \frac{\rho_l U_j L}{\mu_l}$
Ohnesorge number	Oh	$\frac{Ca}{\sqrt{We}} = \sqrt{\frac{Ca}{Re}} = \frac{\mu_l}{\sqrt{\rho_l \sigma L}}$
Bond number	Bo	$\frac{We}{Fr} = \frac{\rho_l g L^2}{\sigma}$

While not all of these parameters are of interest for bulk TDG predictions, it is useful to examine each of the individual variables to help understand what quantities influence air entrainment. Some of the individual terms including jet velocity, a characteristic length, and turbulence will be of interest for TDG production.

With regards to the “Alternate Groups” of numbers, it is mentioned that Reynolds number is typically only useful in distinguishing between laminar and turbulent regions; the Ohnesorge number is used for correlating turbulent viscous jets; and the Bond number is employed in describing a static meniscus away from the region of entrainment [35]. Consequentially, these parameters are not likely to be of greatest interest for predicting TDG at Boundary Dam.

At the end of this brief overview on free, turbulent, plunging jets, important conclusions include:

- i) Air entrainment, though not linearly correlated to, is critical for TDG supersaturation;
- ii) Initial jet velocity, a length scale, and turbulence are important physics which help characterize jet behavior;
- iii) At Boundary, a coherent jet impinges the lower reservoir (as opposed to a fully decayed jet); and
- iv) Increasing turbulence in the spillway would help promote jet decay during the fall; ultimately, this which would decrease the depth to which entrained air plunges in the tailrace.

2.3.4. EFFECTS ON RIVER SYSTEMS

Issues relating to the supersaturation of TDG in the Columbia River Basin were identified as far back as the 1960s [41]. While research and modifications to dams have been ongoing since the initial discovery of TDG effects, more recently the topic has re-emerged as an item in need of attention. This is due in part to public demand for environmentally friendly energy practices, and attention can also be attributed to dam relicensing efforts which have been ongoing in recent years.

Both current and previous research has indicated that short-term exposure of aquatic species to TDG levels up to 120% does not yield significant negative health effects when compensating⁴ water depths are available [41]. A 2006 report by Pacific Northwest National Laboratories (PNNL) does, however, identify five areas in which harmful effects to fish may be realized at TDG levels below 120% [41]:

- i) Sensitive and vulnerable species or life stages;
- ii) Long-term, or multiple exposure;
- iii) Vulnerable habitats and river reaches;
- iv) Incubating fish in hyporheic habitats; and
- v) Community and ecosystem impacts.

Due to the fact that these five points have been highlighted by PNNL, they are key areas of interest when assessing the impacts that dams have on TDG generation. For instance, TDG levels in the lower Columbia may not be excessively high at certain times of the year, but

⁴ Compensating water depths refers to the existence of sufficient water depth for TDG to exhibit saturation pressure, see Figure 16.

concerns may still exist because of long term exposure of fish as they pass multiple hydraulic structures on their migration route.

Another important consideration is that the effect of TDG is greatest in the top portion of the water column. Figure 16 demonstrates the reason for this: hydrostatic pressure is higher at greater depths, therefore, the equilibrium pressure of bubbles in solution increases along with water depth. Due to this relationship between water depth and pressure, fish at lower depths are not in danger of GBT. For illustration, if the TDG pressure is at 130% saturation near the water surface, ~3m down the TDG pressure will be at 100% saturation, and bubbles will not come out of solution at that depth. In this example fish near the surface may be in danger of GBT, while fish swimming 3m down will not experience bubbles coming out of solution.

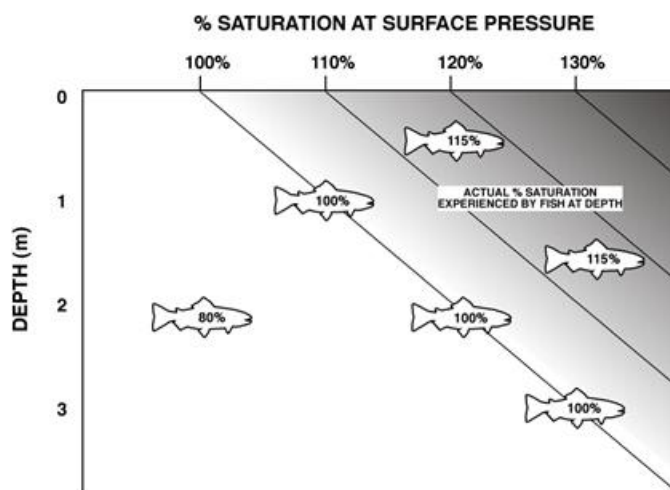


Figure 16: TDG variation with depth and surface saturation (Weitkamp, 2008 [42]).

In extreme cases of GBT, fish mortality may occur. For instance, in 2011 a fish farming operation downstream of the Grand Coulee Dam claimed to be losing 100,000 fish per day due to elevated levels of TDG [43]. High flows in the Columbia River—stemming from a heavy spring runoff—caused increased spilling at Grand Coulee Dam which was the source for TDG pressures reaching as high as 144%. This illustration serves to demonstrate the basis for water quality restrictions, but it is important to emphasize this occurrence was *not related to spill at Boundary Dam*.

2.3.5. MITIGATION MEASURES TO DATE

One method that has been adopted at dams along the Columbia River for TDG abatement purposes is the installation of surface deflectors—see Figure 17 for a representative schematic. These deflectors are installed at the base of a dam to direct energetic spillway flow along the top of the downstream reservoir. The associated skimming action of water on the lower reservoir surface can reduce TDG generation downstream of hydropower facilities.

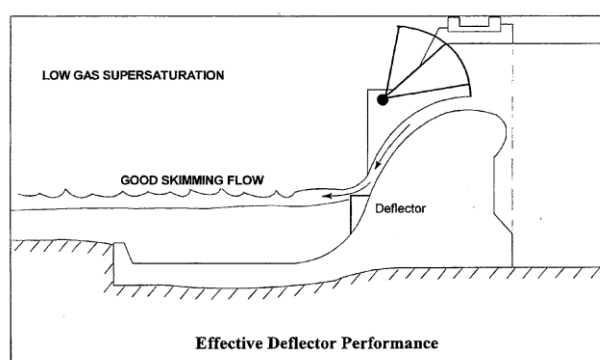


Figure 17: Spillway deflector schematic showing skimming flow (from a 2012 NWA Annual Conference presentation [44]).

On the United States Army Corps of Engineers (USACE) website it states that they have installed spillway deflectors on 5 of the 8 lower Columbia & Snake River dams [45]. While other abatement measures are under investigation, operational changes and spillway flow deflectors have been the most commonly used tools for TDG abatement. As recently as 2009, spillway deflectors were installed on a USACE-operated dam (Chief Joseph Dam).

While spillway deflectors have proven useful for large dams such as those found on the Columbia River, they are not suited for all facilities. For instance, it may not be effective (or even feasible) to use spillway deflectors at hydropower projects that use other spillway configurations. This is true for the spillways present at facilities such as Boundary Dam and Cabinet Gorge.

Cabinet Gorge is a hydropower facility on the Clark Fork River in Idaho which shares similarities with Boundary Dam in regards to spillways and TDG. In January of 2013, Avista (the company that owns and operates Cabinet Gorge) completed an installation of baffle

blocks on one of the spillways. Spill tests conducted in February and also during the spring runoff of 2013 will provide the first set of data portraying how the prototype installation performed. If the baffle blocks perform favorably, Avista says they will retrofit one or two more spill bays in 2013 with installation on all remaining spillways planned for dates further in the future [46].

2.4. COMPUTATIONAL WORK RELATED TO TDG

Numerical models have proven to be robust and valuable when used responsibly in combination with other engineering techniques such as proven theory, physical models, experimental data, etc. It is a branch of engineering that is continually evolving; as modern day computers keep improving, the size and complexity of problems that can be tackled continue to grow as well.

Computational Fluid Dynamics (CFD) is one branch of numerical modeling used to aid engineers in many different circumstances ranging from research to design in industry. CFD is commonly used in the aerospace, automotive, energy, and maritime industries (just to name a few). While the benefits of numerical models are vast, it is important to recognize the limitations of them as well. In the hands of an inexperienced user numerical techniques have potential to be greatly misleading, and in certain cases the misinterpretation of numerical results can be disastrous.

Once a numerical solution is achieved, it is easy to prematurely draw conclusions from the broad amount of information that can be gained through simple clicks of a computer mouse. Flow features including velocity profiles, temperatures, pressures, and many other parameters can easily be exported. The danger of an inexperienced user is that accurate numerical solutions depend upon the correct specification of boundary conditions, appropriate selection of numerical models and discretization schemes, and also temporal, spatial, and iterative convergence.

Key points to keep in mind when working with numerical models include:

- i) It takes a considerable amount of work to correctly set up the model (an introductory CFD book states that “over 50% of the time spent in industry on a CFD project is devoted to the definition of the domain geometry and grid generation” [47]);

- ii) There are various sources of error that must be recognized (incorrect boundary conditions or solvers/schemes, round-off, iteration, discretization, etc.); and
- iii) Convergence is not achieved simply because a program claims that it has converged on a solution (due diligence must be carried out by the CFD user to ensure solutions of acceptable accuracy have been achieved).

Previous computational work related to the prediction of TDG has included two dimensional models ([38],[39], [48]); three-dimensional models ([30], [32]); placing buoyant particles in regions of air entrainment and monitoring a time series of pressures experienced by the particles as they move throughout the domain ([24]); and transporting bubbles through the domain via advection and diffusion, and accounting for gas transfer through defining mass transport equations between bubbles and water ([48]).

A review of previous work demonstrates a distinct truth that the generation of TDG is a difficult phenomenon to capture with its wide array of influencing factors. That said, numerous approaches have been attempted, with varying degrees of predictive success achieved. Table 3 summarizes the key articles related to the prediction of TDG at hydropower structures. Each work has presented some form of advancing TDG modeling efforts; however, only a few of the efforts have *direct* relation to the hydraulics present at Boundary Dam.

Table 3: Review of literature related to modeling TDG with numerical methods. Articles are divided by research using (1) CFD and (2) physically based relationships; additionally, they are organized by year, with newest work reported first.

<i>Predictive models that employ CFD</i>		
Article Title	Focus of Research	Findings
<i>A multiphase model for the hydrodynamics and total dissolved gas in tailraces</i> (Politano et al., 2009 [32])	A 3D, anisotropic, two-phase CFD model for predicting water entrainment, gas volume fraction, bubble size, and TDG concentration at Wanapum Dam.	Suppression of turbulence by bubbles plays an important role in predicting the flow field downstream of spillways and TDG distribution. TDG predictions reach "fairly good" agreement with field data.
<i>A multidimensional two-phase flow model for the dissolved gas downstream of spillways</i> (Politano et al., 2007 [39])	A 2D, two-phase CFD model is presented to calculate gas volume, density, and the velocity of bubbles downstream of Wanapum Dam. A two-phase mass transport equation is used to model gas transfer and predict TDG.	Bubble size distribution is significant for TDG generation. Small and medium sized bubbles are most important for gas transfer because larger bubbles have a larger rise velocity (therefore they reach the free surface quicker) and a smaller surface area/mass ratio.

Table 3 (Continued)

<i>Prediction of total dissolved gas downstream of spillways using a multidimensional two-phase flow model (Politano et al., 2005 [30])</i>	The commercial software ANSYS Fluent was used to construct a 3D CFD model to make TDG predictions downstream of Wanapum Dam. A transport equation for TDG was solved considering the absorption and dissolution of air bubbles.	Predictions were compared to field data. The model could capture the main flow features, but "considerable" discrepancies existed in the diffusion of TDG between the model and experimental observation. The CFD model predicted much sharper gradients than were observed in field data.
<i>Prediction of the total dissolved gas downstream of spillways using a two-phase flow model (Politano et al., 2004 [38])</i>	A 2D, two-phase CFD model is presented to calculate gas volume fraction and velocity of bubbles for TDG prediction at Wanapum Dam.	Presents the results of the model TDG predictions compared with TDG field data. The percent difference between the two appears to range from approximately 3.7% to 18%. Furthermore, the amount of dissolved air needed to reach downstream TDG levels measured in the field is much smaller than the actual amount of air entrained on the spillway—this implies a majority of entrained air escapes before mass transfer occurs.
<i>Dissolved gas supersaturation downstream of a spillway II: computational model (Orlins et al., 2000 [48])</i>	A physical model was used to obtain hydrodynamic data. This measured data was then used for input into a 2D CFD model. The computational model used mass transport equations combined with data from the physical model to predict TDG downstream of Wanapum Dam for different spillway deflector designs.	Using a physical model to obtain inputs for the numerical model allowed for selection of the spillway modification which best met TDG reduction goals. However, obtaining necessary measurements on the physical model proved difficult and was therefore a source of error in the computational model. The 3D nature of flow observed on the physical model could not be captured by the 2D numerical simulations.
<u>TDG predictions that use physically-based relationships</u>		
Article Title	Focus of Research	Findings
<i>Prediction for supersaturated total dissolved gas in high-dam hydropower projects (Ran et al., 2009 [49])</i>	Focused on high head dams in China with ski jump energy dissipation (employing either a scour hole or plunge pool downstream of the spillway). Developed equations for TDG prediction based on hydrodynamic pressure and water depth.	One equation for TDG prediction in scour holes and a similar equation for plunge pools are presented. Predictions from the model equation are calibrated to match field data within 5%. The model equation is applied to a dam that was not yet constructed to predict downstream TDG supersaturation.
<i>Modeling total dissolved gas concentration downstream of spillways (Urban et al., 2008 [29])</i>	Presents a model which simulates the physical processes of gas transfer using a two-layer, steady-state model. Field measurements from Ice Harbor Dam on the Snake River are used to calibrate the model.	Peak TDG concentrations are only weakly dependent upon the "maximum range of air ejected or entrapped at the plunge point." For dam configurations of interest in the study, tail water depth plays an important role on TDG generation.

Table 3 (Continued)

<i>Predictive capabilities in oxygen transfer at hydraulic structures</i> (Gulliver et al., 1998 [33])	Twelve equations from literature are compared to field data for <i>oxygen</i> transfer at four types of hydraulic structures (spillways, weirs, sills, and conduit outlets). Each equation is assessed for its accuracy in prediction.	The most successful equations for predicting <i>oxygen</i> transfer at ogee-crested spillways and sharp-crested weirs are presented; the standard errors were 0.16 and 0.17 respectively (these values are ~equivalent to uncertainty to the 68% confidence interval). The equation presented for weirs is dependent upon a Froude and Reynolds number for the jet/nappe. It is suggested that the presented equations may be used for predicting transfer of other compounds, but verification on this belief was not conducted. Equations are provided in terms of transfer efficiency.
<i>Modeling dissolved gas supersaturation below spillway plunge pools</i> (Geldert et al., 1998 [28])	Field data from three dams (Ice Harbor, The Dalles, and Little Goose) were used to fit coefficients for a predictive TDG relationship.	An equation for mass transfer across bubble and free surface interfaces is discussed. The equation presented relies on physical flow and design parameters as well as established theory for mass transfer. Further field data and analysis are needed to assess if the coefficients reported remain constant, or if they are dependent upon other changing variables.

The review of relevant literature demonstrated that TDG prediction efforts over the past 15 or so years have focused on hydropower projects that have typical ogee-shaped spillways terminating in stilling basins—Figure 17 on page 33 shows a configuration of this type. In the literature, only a few *CFD modeling* efforts have been presented which seek to develop TDG predictions. Of the efforts that have been presented, CFD models have been coupled with field measurements and/or physical model studies in order to seek TDG relationships for hydropower projects. These numerical efforts have resulted in interesting discoveries relating to dissolved gas phenomenon and numerical methods. However, as previously mentioned, all of these CFD studies have been related to dams that do not consist of a free falling water jet. While the core mechanism of TDG generation remains constant, the differences in flow features between various classes of spillways and energy dissipation structures are substantial. Furthermore, while methods for predicting TDG are in need of further study across all hydropower configurations, the area of high head dams with free jet discharges is one *specific* field of study heavily lacking in research and available information.

It has been proposed by Urban et al. [29] that TDG predictive techniques can be divided into the following two categories:

- i) Operational models based on data fitting; and
- ii) Conceptual models which describe gas transfer processes and fit coefficients to available field data.

A majority of recent TDG modeling efforts have focused on the second category. The currently investigated TDG predictive effort for Boundary Dam, however, falls under category i) above. Specifically, the desire is to use CFD modeling to correlate TDG field data to spillway hydrodynamics.

One previously developed TDG prediction method of particular interest is the one the engineering firm Hatch is currently using. This methodology is of interest because the predictions from their model are used to assess the validity of the currently sought TDG prediction method. A selection from *Hydraulic Design of Total Dissolved Gas Mitigation Measures for Boundary Dam* provides a description of the TDG prediction method currently employed by Hatch:

The second approach is considerably simpler in nature, and similar to a technique developed and used on other studies to simulate TDG transfer, that has provided reasonable estimates of TDG performance.

This technique involves the “sprinkling” of a representative number of history particles within the air entraining area of a jet. These particles are given a buoyancy equivalent to a standard air bubble, and then their position is tracked as they move throughout the computational domain. The CFD model tracks time, pressure, air entrainment fraction, and velocities experienced by these “bubbles” as they move through the mesh.

This information is then exported from the CFD model, and imported into a special spreadsheet model to estimate gas transfer. This spreadsheet estimates the amount of gas transfer which might occur for each bubble based on the pressure and velocity hydrographs experienced by each. The gas transfer associated with each bubble is then integrated to determine a total TDG percentage for the main flow field. (Sweeney et al., 2009 [27])

The approach described above was developed by Professor Gulliver at the University of Minnesota [24].

One important item to highlight is the cost associated with some of the more recent CFD efforts aimed at making TDG predictions downstream of hydropower projects. For instance, an ANSYS Fluent model developed by Politano et al. [32] for TDG predictions downstream of Wanapum Dam (which is located on the Columbia River) made use of a 128-processor Linux cluster (with 2GB of memory per processor). With this configuration, and with zero velocity and turbulence used throughout the domain for the initial condition, it took a total of 67 days of wall-clock time to complete their two-step approach for TDG predictions. User defined scalars and user defined functions were developed within the architecture of Fluent, and transport equations were solved throughout the domain (which consisted of $1.7\text{E}+06$ nodes and extended $\sim 3,280$ ft downstream of the dam). A strength of solving a TDG transport equation, provided that sufficient accuracy and calibration is achieved, is the wealth of knowledge that can be gained with regards to the flow field and TDG distribution throughout the three dimensional space downstream of hydropower project. On the other hand, when considering optimization of possible structural alternatives to a given hydropower project, the 60+ day computational expense poses certain limitations. For this reason, a new approach to make initial TDG predictions has been sought during the current research effort. The approach is discussed in the following section.

3. METHODS: A NUMERICAL APPROACH

As outlined in Section 2.4, previous TDG prediction efforts have utilized empirical relationships from field data, theoretical-based mass transfer relations, physical models, and also numerical methods. The current research effort aims to use a numerical approach to make TDG predictions. The desire is to study fluid dynamics at the spillway exit to relate flow characteristics to downstream TDG. This method is unique compared to previous efforts in that the plunging jet, air entrainment, and bubble mass transfer are not directly evaluated, nor is the flow field in which the mass transfer takes place modeled. This is advantageous because it allows for the use of a smaller model domain.

The major benefit of using a smaller model domain is the decrease in associated computational expenses. As previously mentioned, the model developed by Politano et al. [32] took a total of 67 days to achieve statistically steady solutions. As their methodology is further refined, the robust approach has potential application in a variety of circumstances. Even so, computational cost limitations do pose as one major drawback.

If successful, the approach proposed in the current effort could be used to analyze a variety of TDG abatement alternatives in a more timely manner. The anticipated methodology could serve as an initial step in the design process for future engineering efforts. For instance, the fluid dynamics for a variety of spillway modifications could be evaluated; the evaluations could be used to make initial TDG predictions at the project of interest; then, the most promising few configurations could be examined on a larger CFD/physical model combination to more accurately assess TDG performance. If proven to be a sound approach, the method would be applicable to spillway structures that employ free, plunging jets, and also in instances when only alterations to the flow *in* the spillway are being considered.

While Boundary Dam has two spillways, the present study focuses exclusively on Spillway 2. Below, Figure 18 shows a display model of Boundary Dam located in the dam's visitor center. Spillway 2 is located on the left side of the figure.

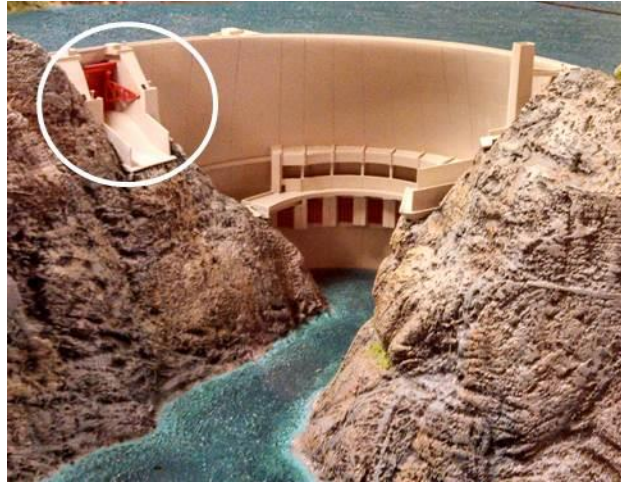


Figure 18: A model display of Boundary Dam located inside the dam's visitor center. Spillway 2 is circled, which is the spillway of interest for this research effort.

In order to make TDG predictions for proposed spillway modifications, a two-step modeling approach is adopted. *Phase I* of the project is the calibration step, while *Phase II* consists of evaluating spillway modifications for the purpose of making TDG predictions. Below a high-level overview of the methodology is provided:

Phase I:

- i) Draft a CAD model of the current spillway configuration
- ii) Within ANSYS Design Modeler, parameterize the spillway gate opening such that the spillway can be modeled at different discharge rates
- iii) Mesh the geometry
- iv) Within Fluent, set up the boundaries, models, solvers, and solution methods
 - a. These specifications are outlined in Sections 3.4 and 3.5, with further detail provided in "Appendix C: Modeling details"
- v) Run the current spillway configuration at different flow rates of interest (low, medium, and relatively high flows)
- vi) Upon achieving a solution at each flow rate, form a calibration curve which relates physical flow quantities at the spillway exit to historical TDG generation observed at Boundary Dam
 - a. Physical flow quantities of interest are discussed in Section 3.3

Phase II:

- i) Create a CAD model of the spillway *with proposed geometric modifications*
- ii) Mesh the new geometry
- iii) Repeat Step iv) from *Phase I*
- iv) Run the model at a single target flow rate of 13 kcfs

- v) Compute the physical flow quantities at the spillway exit, and utilize the calibration curve achieved in Step vi) from *Phase I* to make TDG predictions
- vi) Repeat *Phase II*, Steps i) – v) for all proposed spillway modifications of interest

3.1. PHASE I: CALIBRATION

In the first step, the CFD model is run with the current spillway configuration at various flow rates. The four flow rates selected for this step are reported below in Table 4. The flow rate of 13 kcfs was selected because it is desired to reduce TDG at Boundary Dam at this spill condition. The other flow rates chosen are both lower and higher than the target discharge to allow for characterization of fluid dynamics at these lower and higher ranges.

Table 4: Selected flow rates to run calibration models at.

Spill Gate Opening (ft)	Flow Rate (cfs)	TDG Flux (% Sat)
2.49	6,000	0.1
5.93	13,000	7.0
8.87	17,500	8.5
11.00	20,000	8.7

The main purpose of *Phase I* is to correlate spillway flow characteristics (such as water velocity, energy, and momentum) to the resulting TDG which has been observed at the project historically. In Table 4, “TDG Flux” denotes the margin by which TDG pressures increase—from forebay to tailrace—when water is being spilled at Boundary Dam. The values listed in the table were achieved by filtering historical data, and since this is an important step of the project it will be discussed in further detail now.

TDG monitoring at Boundary Dam has been ongoing for over a decade. The purpose of these observations has been to build a database which identifies TDG behavior at the project for various operational/flow conditions. A report prepared for SCL by Rounds and Orlins [15] was consulted for the data of interest in the current research. It should be noted that a large amount of scatter is present in the field data, and this is typical of TDG measured across hydropower projects ([13], [24], [33], [38], and [48]). In order to effectively deal with the fact that there are many variables which influence TDG supersaturation, assumptions had to be made; a tabulation of these assumptions is presented in Section 3.6.

TDG data reported by Rounds and Orlins [15] was collected at the fixed monitoring stations (FMS) shown in Figure 19.

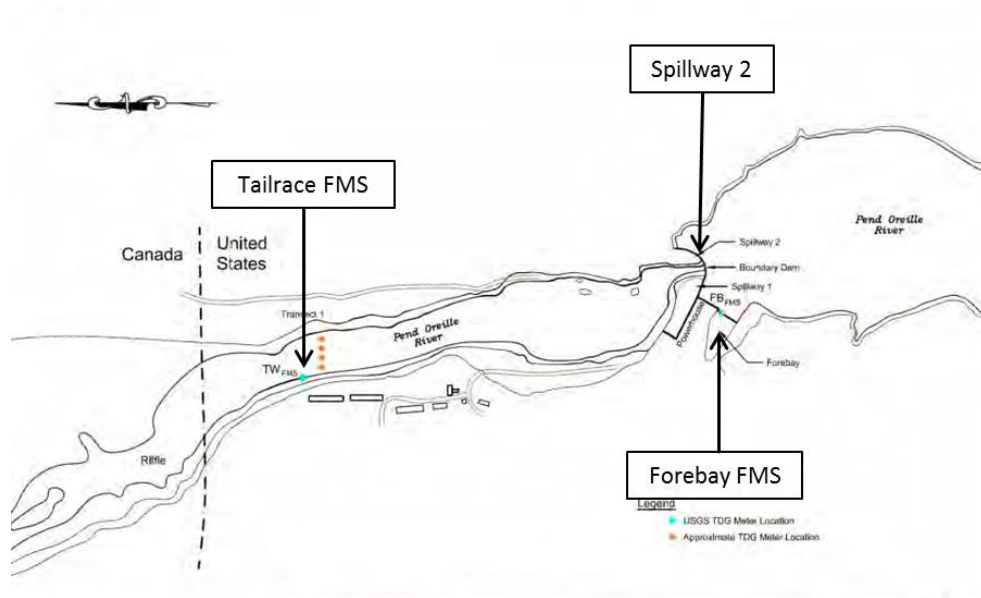


Figure 19: TDG fixed monitoring stations (adapted from Rounds and Orlins [15]).

Data provided by Rounds and Orlins contains 580 tests during which the spill settings were maintained constant for at least four hours. In the report, these test data were evaluated to build a series of graphs which contain the spill rate, forebay TDG, and TDG flux observed at Boundary Dam. These field measurements were collected from 2006–2012, and a summary of the data is shown in Figure 20.

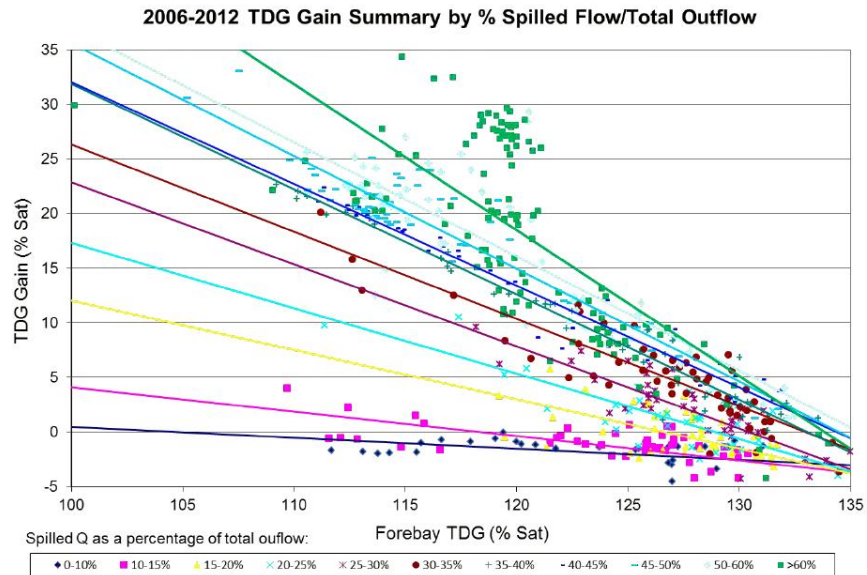


Figure 20: TDG gain summary at Boundary Dam. Categorized by spilled flow as a percentage of total river discharge (from Rounds and Orlins [15]).

Following communication with engineers at Hatch, it was determined that the flow condition of current modeling interest is when forebay TDG is at 126% saturation. In examining Figure 20 it can be seen that the TDG flux at this condition ranges from approximately -2 to 11% saturation (when considering the curve fit lines).

Taking into account the assumptions of Section 3.6, data from Rounds and Orlins [15] were averaged to arrive at a TDG flux vs. flow rate graph for the conditions of interest—the result is provided in Figure 21. The standard deviation in TDG flux shown in Figure 21 ranges from 0.38% to 2.75% saturation. The corresponding minimum and maximum *percent deviations* are 14% and 190%, respectively. These modest to high standard deviations exhibited in the field data demonstrate how much scatter is present in evaluating TDG production at any given hydropower project. It is worth noting, however, that the standard deviation of 190% is at a lower flow condition; this is relevant because TDG flux is typically small at low flows, and therefore not of greatest concern.

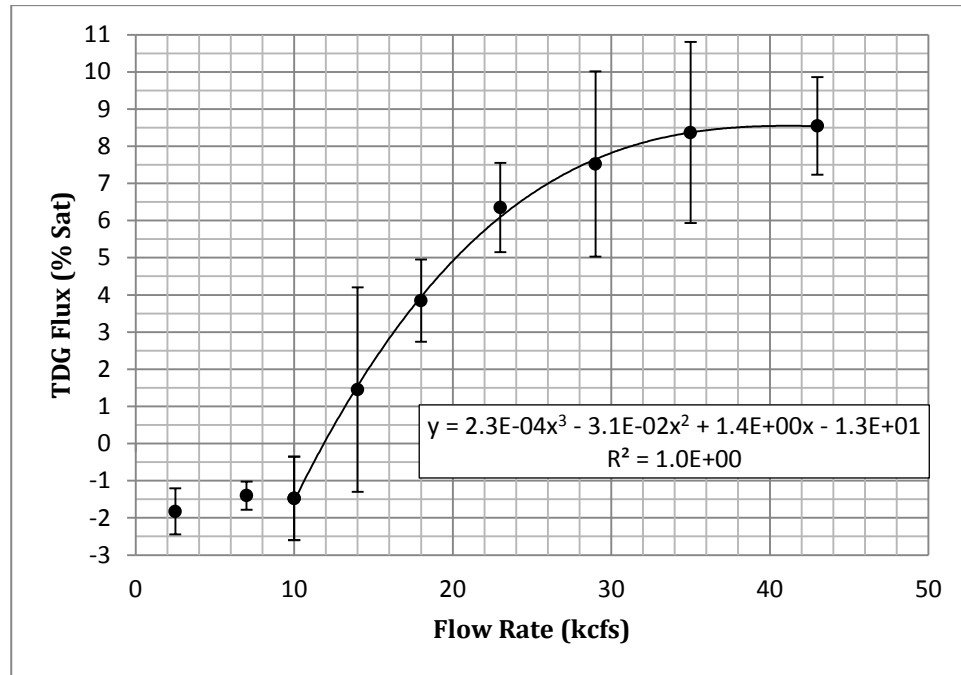


Figure 21: Plot of TDG flux vs. flow rate; data averaged from spill tests reported by Rounds and Orlins [15]. Note that the curve fit line is only fitted to data at the seven highest flow rates. The error bars represent a standard deviation in the data averaged to calculate each point.

The coefficient of determination (R^2) for the curve fit indicates a third order polynomial fits the averaged data points well. It should be pointed out that the curve fit shown in Figure 21 is only fitted to the points at the seven highest flow rates. This is because it has been observed that there are relative minimum and maximum values of TDG generation. For example, in Figure 21, spill rates lower than ~10 kcfs all exhibit similar TDG behavior; on the other end of the range, TDG flux at spill rates above ~35 kcfs appears to asymptotically approach a maximum value. Figure 22 and Figure 23 are provided to further demonstrate this point. In Figure 22, an average minimum TDG flux of approximately -6% is achieved at flow rates less than 10 kcfs.

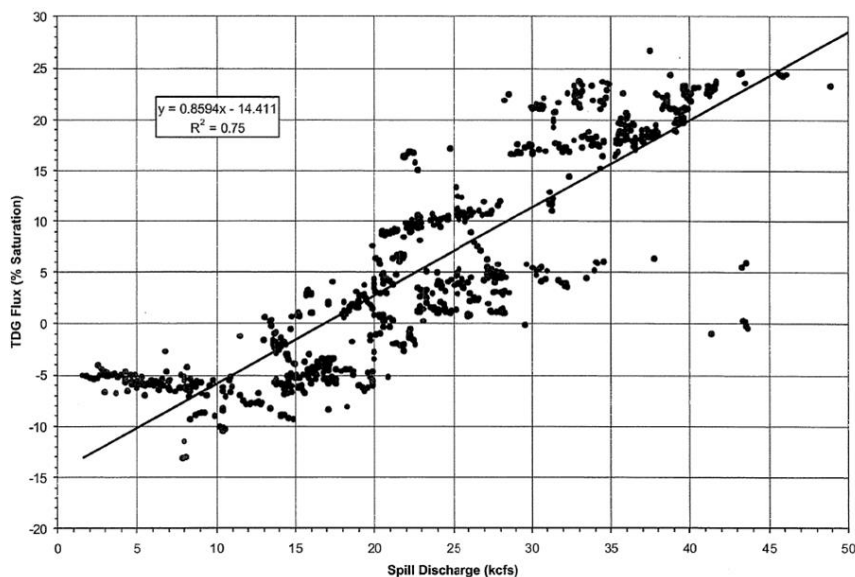


Figure 22: TDG flux vs. spill discharge. In examining trends, a minimum TDG flux of approximately -6% saturation appears to be reached at spill discharges below 10 kcfs. In addition, this graph illustrates the large amount of scatter present in raw TDG data. (Figure borrowed from a report detailing TDG tests conducted at Boundary Dam in 2002, Columbia Basin Environmental [13]).

Figure 23 demonstrates that at the higher end of spill rates there appears to be a maximum TDG flux. In the figure, a maximum flux of ~20% is exhibited at flow rates of 35 kcfs and higher.

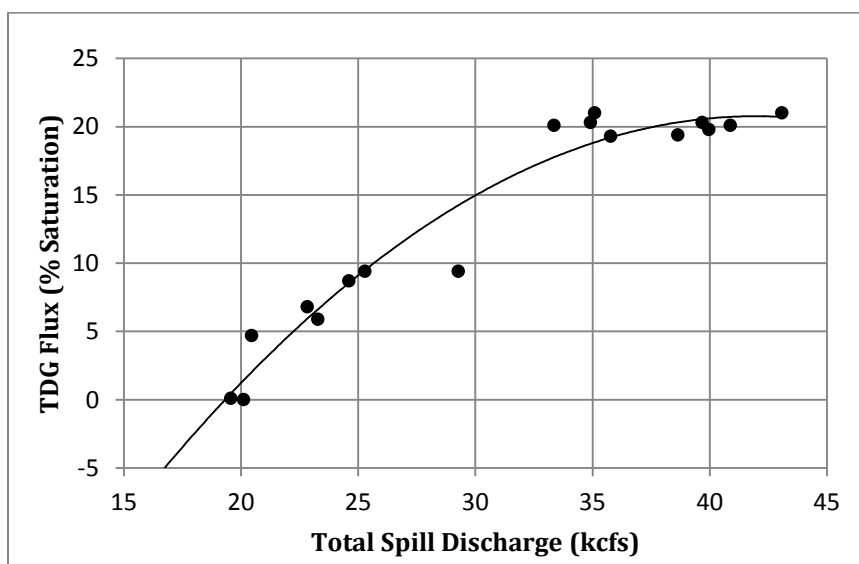


Figure 23: TDG flux vs. spill discharge when Spillway 2 is in use. A maximum TDG flux of approximately 20% appears to be reached near a spill discharge of 35 kcfs. (The graph includes measurements taken during 2006–2012, and is plotted from data reported by Rounds and Orlins, 2013 [15]).

It should be noted that Figure 22 and Figure 23 are provided only to demonstrate the idea that there are minimum and maximum values of TDG flux, which occur at low and high flow rates respectively. The region between these minimum and maximum values, where TDG flux increases along with increasing spill discharge, contains the spill conditions of highest interest for this research effort.

Once the process of correlating historical TDG to spill discharge was completed, CFD model results could be used to relate fluid dynamics at the spillway exit to TDG flux data. The result of forming these relations are calibration curves. As previously mentioned four CFD models were used for this step, and the flow rates selected for the models are shown in Table 4 on page 42. For further details regarding calibration model settings, refer to Sections 3.3 – 3.5.

3.2. PHASE II: MAKING TDG PREDICTIONS

In the second phase of this research, a model of the spillway with proposed modifications is developed. In the case of Boundary Dam, the modifications consist of installing impact energy dissipation devices in the spillway. Once this numerical model was developed, then the flow characteristics at the spillway exit could be compared to the calibrations runs of *Phase I*. Based upon this comparison TDG predictions are estimated for proposed spillway geometry modifications.

Unlike the calibration step—which consisted of modeling the spillway at various flow rates—all *Phase II* models were run at a single spill discharge of 13 kcfs. Section 3.5 contains details about the specific geometries and settings used for *Phase II* models.

3.3. PARAMETERS OF INTEREST

As established in Section 2.4, it has been recognized that spilled water is a key factor in producing elevated levels of TDG supersaturation. Furthermore, it has been established that there is a general correlation between the magnitude of spillway discharge and the level of TDG supersaturation—as spill discharge increases, so do downstream TDG pressures. However, even though these observations have been made, the complexity of TDG phenomenon makes it difficult to isolate exact quantities that most heavily influence TDG production. Consequentially, several parameters have been selected for correlation to downstream TDG.

The quantities listed in Table 5 were selected for their relation to describing flow physics, and potentially TDG production. A review of literature covering (1) plunging jets/air entrainment, and (2) dissolved gas issues at hydropower projects was carried out to help inform the selection of parameters of interest.

Table 5: Potential parameters of interest for TDG predictions.

Parameter	Description	Influence on TDG
$E = y + \alpha \frac{Q^2}{2gA^2}$	Specific energy: sum of depth and velocity head (or “the height of the energy grade line above the channel bottom” [21])	Energy is necessary to transport bubbles to greater water depths at which the bubbles experience elevated pressure
$M = Ah_c + \beta \frac{Q^2}{gA}$	Momentum function: “force plus momentum flux divided by the specific weight of the fluid, [...] this quantity is conserved across [a] hydraulic jump” ([21] pg. 73)	The momentum of spillway flow will influence the depth to which the plunging jet carries entrained air
$TKE = \frac{1}{2} (\overline{(u'_1)^2} + \overline{(u'_2)^2} + \overline{(u'_3)^2})$	Turbulence kinetic energy: root mean square (RMS) of velocity fluctuations in turbulent flow	Turbulent energy serves to enhance jet breakup and entrain air
$E_{transport} = \frac{1}{2} \alpha \rho Q \bar{V}^2$	Energy transport rate of a plunging jet [50]	The rate of energy transport could correspond to the rate of tailrace dissolved gas generation
Non-dimensional Numbers		
$Fr = \frac{\bar{V}}{\sqrt{gy}}$	Froude number: ratio of inertia to gravitational forces	This expression provides a description of bulk flow characteristics
$Re = \frac{\bar{V} D_h}{\nu}$	Reynolds number: ratio of inertial to viscous forces	This ratio yields insight into the relative magnitude of turbulence in the spillway flow, which is important for air entrainment, bubble transport, and jet decay

Specific energy, momentum, and turbulence are the parameters of greatest interest for the current effort. That being said, Froude and Reynolds numbers will also be investigated for potential correlation to downstream TDG.

3.4. SOFTWARE AND MODELS USED

For this effort commercially available software is employed for numerical calculations. ANSYS Workbench v14.5 was used, and within the Workbench architecture Fluent was selected for CFD calculations.

In determining appropriate settings for the model, both the Fluent User’s Guide and literature relevant to the topics at hand were considered. These two sources of information

were consulted to help determine meshing characteristics, models, discretization schemes, and boundary conditions.

In order to capture the key features of spillway flow, it is necessary to model *two-phase, turbulent* flow. The following models were activated within Fluent in order to resolve these physics of interest.

3.4.1. TWO PHASE MODEL

The Volume of Fluid (VOF) model was selected to resolve water and air within the spillway. The VOF model calculates the fraction or “volume of fluid” of the phases within each computational cell. Cells can be full of air ($vo f_{air} = 1$), full of water ($vo f_{air} = 0$), or be a mix of water and air in the interface region between the two phases ($0 < vo f_{air} < 1$) [51].

Since an implicit scheme was used for time discretization, the volume fraction equation takes on the following form when considering the q^{th} phase [51]:

$$\frac{vo f_q^{n+1} \rho_q^{n+1} - vo f_q^n \rho_q^n}{\Delta t} V + \sum_f (\rho_q^{n+1} U_f^{n+1} vo f_{q,f}^{n+1}) = \left[S_{vo f_q} + \sum_{p=1}^n (\dot{m}_{pq} - \dot{m}_{qp}) \right] V \quad (3.1)$$

The terms of equation (3.1) are defined in Table 6:

Table 6: Definition of volume fraction equation variables.

Variable	Quantity
n	Index for previous time step
$n + 1$	Index for current time step
$vo f_{q,f}$	Face value of the q^{th} volume fraction
V	Cell volume
U_f	Volume flux through face
ρ_q	Density of the q^{th} phase
Δt	Time step
$S_{vo f_q}$	Source term (zero by default)
\dot{m}_{pq}	Mass transfer from phase p to q

In addition, the volume fraction is not solved for the phase designated as the “primary phase.” Therefore since air was set as the primary phase for all models, the following relation was employed:

$$\sum_{q=1}^n \text{vol} f_q = 1 \quad (3.2)$$

3.4.2. TURBULENCE MODEL

The set of Navier-Stokes (N-S) equations provide basis for analysis of flowing fluid. Any introductory fluid mechanics text will provide the reader with information regarding the formulation and use of N-S equations, therefore such a discussion is not provided in this thesis (for example, see Fox et al. [17]).

One of the most common ways of resolving the N-S equations for turbulent flows is by Reynolds averaging them. In decomposing velocity into a mean and fluctuating component, a set of equations can be formulated that depend only on the mean velocities and “Reynolds stresses” (which are time-averaged, fluctuating velocity components). In three-dimensional flows, a total of nine Reynolds stresses are introduced, and these terms are modeled in order to capture turbulent flow behavior. This formulation results in so called Reynolds-averaged Navier-Stokes (RANS) equations, which are commonly utilized in CFD applications. RANS equations provide a description of the effects of turbulence on mean flow properties, which are often of greatest interest in engineering. The turbulence closure selected for the current project is based upon RANS modeling. (For further details on N-S and RANS equations, see Versteeg & Malalasekera [47]).

While the benefits of various RANS models range from solution expediency to solution accuracy, three of the more popular two-equation, RANS-based turbulence models are the $k - \varepsilon$, $k - \omega$, and the Shear Stress transport (SST) $k - \omega$. It has been reported that all three models offer a compromise between accuracy and computational effort and can be used for a wide range of flows ([52],[53]). In terms of literature reviewed during the current effort, the $k - \varepsilon$ model has been one of the most widespread used models for capturing the mean effects of turbulence at hydropower projects. In this model k is turbulence kinetic energy, and ε is turbulence dissipation rate.

While the $k - \varepsilon$ model was considered for use, information provided in the Fluent User's Guide led to the investigation of the $k - \omega$ turbulence model for the current numerical work. It has been reported that this model exhibits a more robust capability, when compared to the widely used $k - \varepsilon$ turbulence closure, of modeling highly strained flows with adverse pressure gradients and separation ([51], [54]). As in the $k - \varepsilon$ model, k represents turbulence kinetic energy, while ε is replaced with ω which is specific dissipation rate; ω can be thought of as the ratio of ε to k . The transport equations for k and ω are formulated as [51]:

$$\frac{\partial}{\partial t}(\rho k) + \frac{\partial}{\partial x_i}(\rho k u_i) = \frac{\partial}{\partial x_j} \left(\Gamma_k \frac{\partial k}{\partial x_j} \right) + \tilde{G}_k - Y_k + S_k \quad (3.3)$$

$$\frac{\partial}{\partial t}(\rho \omega) + \frac{\partial}{\partial x_j}(\rho \omega u_j) = \frac{\partial}{\partial x_j} \left(\Gamma_\omega \frac{\partial \omega}{\partial x_j} \right) + G_\omega - Y_\omega + D_\omega + S_\omega \quad (3.4)$$

where the individual terms are defined in Table 7:

Table 7: Definition of terms for the *SST* $k - \omega$ transport equations.

Variable	Quantity
ρ	Fluid density
k	Turbulence kinetic energy
u_i	Velocity in the i direction
Γ_k	Effective diffusivity of k
\tilde{G}_k	Generation of turbulence kinetic energy due to mean velocity gradients
Y_k	Dissipation of k
S_k	User-defined source term
D_ω	Cross-diffusion term

While $k - \omega$ has demonstrated increased accuracy over $k - \varepsilon$, one downside to the standard $k - \omega$ closure is its sensitivity to free stream conditions. For this reason, the Shear Stress Transport (*SST*) $k - \omega$ model was considered for use. The *SST* variation blends accuracy of $k - \omega$ in the near-wall region with the free stream independence of $k - \varepsilon$ in the far field [51].

Menter's work [54] demonstrates that the *SST* $k - \omega$ model achieves "significant improvement for all flows involving adverse pressure gradients", and also that the model

has proven very stable, even in complex applications. Furthermore, it has been reported that *SST* $k - \omega$ consumes “only insignificantly more computing time” compared to the standard $k - \omega$ closure [54]; therefore, the potential for an increase in accuracy is not accompanied by a detriment to solution expediency.

A study by Kang & Sotiropoulos [55] used the *SST* $k - \omega$ turbulence closure on a model for simulating three-dimensional, free surface flows. Research findings concluded that their model was able to accurately predict the free surface location for flows over complex hydraulic structures. In the investigation, numerical results were validated by experimental measurements taken on a laboratory flume.

In another free surface flow investigation carried out by Rahimzadeh et al. [56], the results of a *SST* $k - \omega$ turbulence model appeared to match experimental velocity and free surface profile data for flow over a circular-crested spillway. Overall, due to the potential for increased accuracy without any major drawbacks, the *SST* $k - \omega$ turbulence model was selected for all numerical simulations run during the current research effort.

3.5. SETUP OF SPILLWAY 2 COMPUTATIONAL MODEL

The following sections outline the domain and boundary conditions used in the present effort. For further details of the specific quantities used within the models, refer to “Appendix C: Modeling details”.

3.5.1. DOMAIN

The domain is limited to the flow of water and air within the spillway itself. A CAD image of the spillway geometry is provided in Figure 24. In the figure, the “current configuration” of the spillway is shown—that is, there are no baffle blocks on the spillway face.

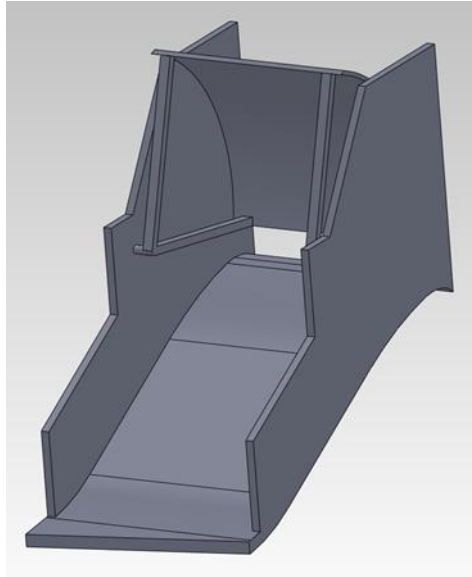


Figure 24: CAD image of Spillway 2 without baffle blocks.

For the purpose of reducing downstream TDG pressures at Boundary Dam, it has been proposed by a TDG study team [24] that impact energy dissipators (baffle blocks) be installed on the face of the spillway. While the design of block dimensions and determination of the most desirable block configuration were not a part of this research effort, it is worth highlighting the need for evaluation of various baffle block designs.

In the interest of dissipating the greatest amount of energy, it is desirable to have baffle blocks in a line orthogonal to the flow direction. For this project, blocks arranged perpendicular to the flow has been termed the linear blocks alternative. However, this configuration has certain limitations at Boundary Dam because there is a drain underneath the concrete near the end of the spillway. This drain presents certain problems when considering anchoring the blocks. For this reason, an angled blocks design is also being explored. In this configuration the blocks run parallel to the drain to mitigate anchoring challenges. While this alternative is feasible from an anchoring perspective, baffle block effectiveness diminishes when they are oriented at an oblique angle to oncoming flow. Therefore, a final configuration is considered: linear blocks without two upstream side blocks. During the current research effort, this arrangement has been designated as “Linear, No Side Upstream Blocks” or LNSUB. Images of the current spillway configuration (without blocks) and the three proposed modifications are shown below in Figure 25.

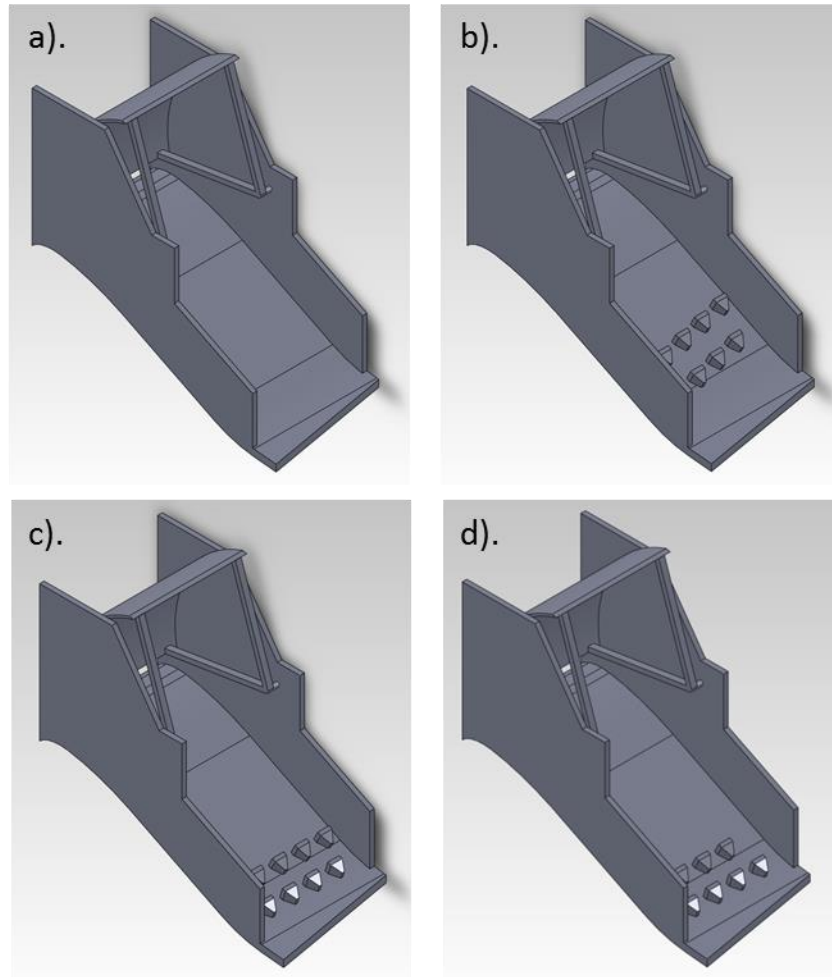


Figure 25: a). Current configuration—no blocks b). Angled blocks—9 blocks c). Linear blocks—9 blocks d). Linear no side upstream blocks, or LNSUB—7 blocks.

After each of the four CAD geometries were drafted (using SolidWorks), they were imported into ANSYS Workbench and set as the first component in a Fluent fluid flow analysis project.

ANSYS Design Modeler was then used to parameterize the spillway gate opening. In doing so, the height of the water inlet (which is equivalent to spillway gate opening) could easily be changed in Workbench at a later time. An image of the angled blocks geometry ready for meshing is shown in Figure 26.

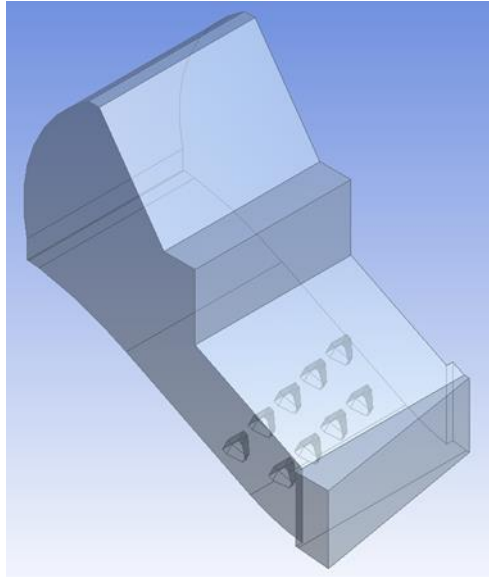


Figure 26: Angled blocks geometry prior to meshing.

As portrayed in Figure 26, it should be emphasized that the extent of the domain spans from where the water passes under the radial spillway gate to where the spillway terminates, and water enters a free fall.

3.5.2. *MESHING*

Tetrahedral cells were selected for meshing the spillway due to their ability to conform to irregular-shaped boundaries. ANSYS provides the option for meshing with hexahedral cells (or a mix of cell shapes), however, an acceptable mesh could not be achieved for the baffle block cases with these settings. Therefore, for consistency, tetrahedral cells were selected for all models run during this project.

In order to assess the impact of mesh cell size on the achieved solution, the grid convergence index (GCI) method outlined by Celik et al. [57] was used. This method requires that calculations be run on three different sized meshes. Figure 27 shows the spillway with a gate opening of 5.93 ft, which corresponds to a flow rate of 13 kcfs. A solution was achieved on each of the displayed meshes, and instructions in the referenced article were followed to achieve a GCI for variables of interest in this case.

Size functions were used on the water inlet and outlets to achieve a finer mesh in these regions. This was especially important on the outlet, as variables of interest were monitored

at this location. On the spillway outlet for the 13 kcfs models (which includes the baffle block models), the specified element size was 0.45 ft for the *fine* grid and 1.31 ft for the *coarse* grid. In the 13 kcfs cases, the average representative cell size throughout the entire domain was 0.61 ft for the *fine* grid and 0.88 for the *coarse* grid. For additional details of mesh settings and the size of mesh elements on the spillway outlet, refer to “Appendix C: Modeling details.”

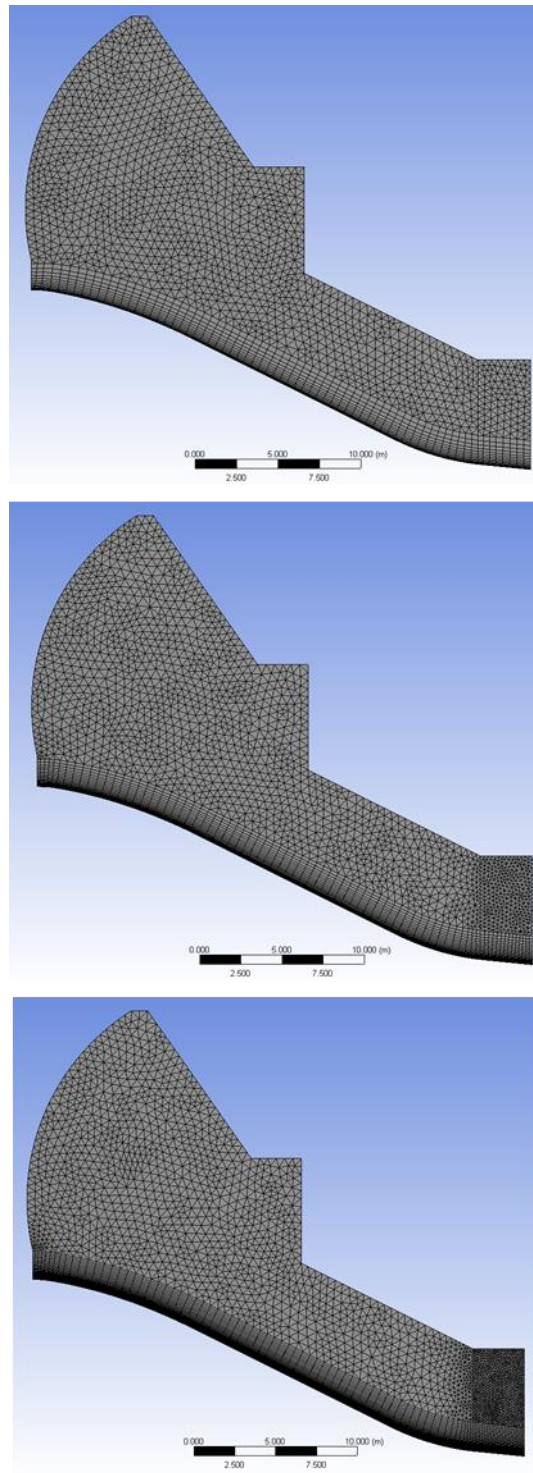


Figure 27: Images of three mesh sizes for the spillway with a gate opening of 5.93 ft (which equates to a flow rate of 13 kcfs). The number of inflation layers in each mesh, from top to bottom, is 15, 26, and 43.

In seeking a balance between accuracy and required simulation time, *inflation layers*⁵ were used within ANSYS Meshing to accommodate for finer cell sizes near the bottom wall of the spillway. From a physical perspective, it is necessary to have finer cells near no-slip walls in order to accurately resolve the boundary layer region, and the gradients present therein. For initial mesh guideline settings, the ANSYS User's Guide was consulted [51]. This documentation states that it is important to ensure there are at least 10 cells covering the boundary layer. It is also stated that the region of structured cells should extend beyond the boundary layer thickness to avoid restricting boundary layer growth. These guidelines were used as a *starting point* for setting mesh parameters, and, as previously mentioned, a grid convergence study was carried out to evaluate final solutions in terms of discretization uncertainty.

In computing spillway solutions on three different grids, it was ensured that the finer two grids contained greater than 15 wall-normal cells in the boundary layer region. For an initial estimate, the boundary layer thickness was computed by running a model and examining the height at which the eddy viscosity was greatest—twice this value was assumed to be the thickness of the boundary layer, as eddy viscosity is maximum at the middle of the boundary layer ([51], [54]). In addition, the structured mesh region was inflated sufficient distance to cover the entire water phase in the calibration models; in doing so (1) this region of interest could be successively refined during the grid convergence study, and (2) it was also ensured that boundary layer growth was not limited by the interface between structured and unstructured cells.

3.5.3. BOUNDARY CONDITIONS

Table 8 and Figure 28 detail the location and specification of boundaries. Water enters at Boundary 1, and, for the inlet conditions used, the Reynolds number based upon the gate opening ranged from $9.9\text{E}+06$ to $3.3\text{E}+07$ for the lowest and highest flow rates respectively.

Water exits at Boundaries 2 and 3, and it should be mentioned that Boundary 3 is located on both sides of the spillway, but in Figure 28 is only annotated on the viewer's side of the

⁵ Inflation controls provided by ANSYS allow for finer, structured cells to be generated in user-specified locations.

image. Similarly, Boundary 8—the spillway walls, are on both sides of the spillway but only one side is annotated in the figure.

Table 8: Specification of boundary conditions.

Corresponding Number in Figure 28	Location	Boundary Specification	Value
1	Spillway water inlet	Mass flow inlet	Varied, hydrostatic pressure specification
2	Spillway water outlet	Pressure outlet	Zero gauge pressure
3	Spillway water outlet (two sides)	Pressure outlet	Zero gauge pressure
4	Top of the spillway, upstream section	Pressure inlet	Zero gauge pressure
5	Top of the spillway, downstream section	Pressure outlet	Zero gauge pressure
6	Radial gate	Wall	No slip
7	Spillway face	Wall	No slip (specified roughness, $k_s = 2.49 \times 10^{-3} \text{ ft}$ [58])
8	Spillway sides (two faces)	Wall	No slip (specified roughness, $k_s = 2.49 \times 10^{-3} \text{ ft}$ [58])
9	Baffle block faces	Wall	No slip (specified roughness, $k_s = 2.49 \times 10^{-3} \text{ ft}$ [58])

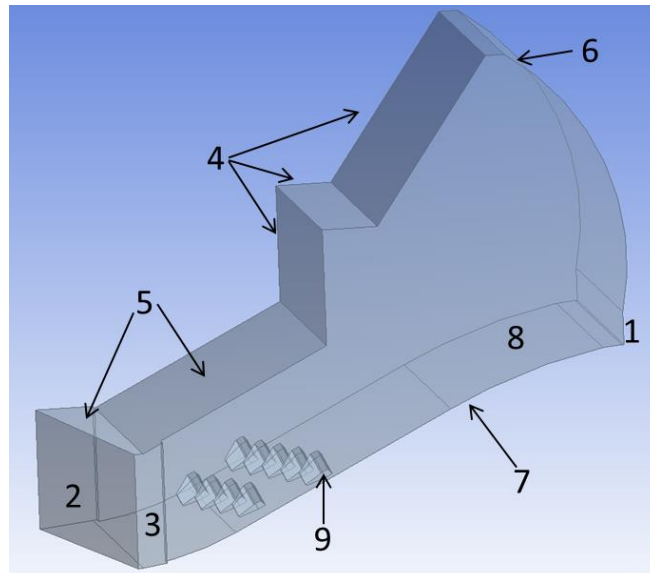


Figure 28: Location of prescribed boundaries.

The turbulence intensity was specified as 2% at Boundary 1 and 5% at Boundaries 2 and 3 for the initial condition. These specifications were based off of information regarding previous investigations on turbulent spillway jets ([36], [37], [59]).

3.5.4. NUMERICAL METHODS

The following methods were selected for numerical modeling. In Table 9, the underlined parameters were selected as per guidance of ANSYS training documentation. Furthermore, other researchers which used the same methods are referenced in the table.

Table 9: Solution methods used in the numerical models. (Underlined solution methods denote settings suggested in ANSYS documentation [60]).

Parameter	Solution Method
Pressure-velocity coupling scheme	<u>PISO</u> ([39], [56], [61])
Gradient (spatial discretization)	Green-Gauss Cell Based
Pressure (spatial discretization)	<u>PRESTO!</u> ([56])
Momentum (spatial discretization)	Second Order Upwind
Volume Fraction (spatial discretization)	<u>Compressive</u>
Turbulence Kinetic Energy (spatial discretization)	Second Order Upwind
Specific Dissipation Rate (spatial discretization)	Second Order Upwind
Transient Formulation	First Order Implicit, Adaptive Time Marching ([32], [61])

Similar to previous CFD models of other hydropower projects [32], a transient formulation was utilized in the current research. For the adaptive time marching approach used, the initial time step size was specified as 1.0E-03 s for the calibration cases and 1.0E-04 s for the block cases. All following time step sizes were computed automatically within Fluent by enforcing a Global Courant number of 2. The following equation was used to do so:

$$\Delta t_{global} = \frac{CFL_{global}}{\max \left(\sum \frac{outgoing\ fluxes}{volume} \right)} \quad (3.5)$$

Here, Δt_{global} is the calculated time step value, $\sum \frac{outgoing\ fluxes}{volume}$ is a ratio calculated for each cell, and CFL_{global} is the global Courant–Friedrichs–Lewy number. The ANSYS default value of 2 was used for the Global Courant Number and not changed during any of the calculations. As a result, the time step size observed during computations varied from 1.0E-04 s to approximately 3.0E-03 s.

3.5.5. CONVERGENCE & MONITORING SOLUTION DATA

For convergence, it was required that all normalized residuals decrease three orders of magnitude (i.e. 1.0E-03). This criteria is not the most stringent, but sufficient for the current

exploratory endeavor. Celik et al. [57] state that this criterion is acceptable in determining iterative convergence; additionally, previous CFD investigations appear to have achieved acceptable accuracy with this standard ([32], [62]).

The second requirement for convergence was to ensure mass conservation throughout the domain. This was established by comparing the mass leaving the domain to the mass entering the domain. If the difference was under 1%, convergence was presumed.

The final convergence measure was that time-fluctuations present in the model stabilize to a steady value, or that sufficient time-averaging of parameters of interest be carried out to achieve a representative average. This is especially true for the baffle block cases, as the blocks induced time-dependent fluctuations on the mean flow field. Within Fluent, time-averaging was carried out using the *Data Sampling for Time Statistics* option. In order to monitor solution data using this time-averaging option, Custom Field Functions had to be used. Therefore, field functions for flow rate, average velocity of the water phase, turbulence kinetic energy at the outlet, and turbulence intensity were implemented.

3.6. ASSUMPTIONS

The following assumptions were used for all models run as a part of the current research effort (unless specified otherwise):

- Even split spill between Spillway 1 and 2 for determination of TDG values for calibration runs;
- Constant forebay TDG of 126% saturation;
- Constant forebay elevation of 1990 ft;
- Constant tailrace elevation of 1736 ft;
- Constant powerhouse flow rate of 48 kcfs;
- Gate opening vs. discharge obeys the discharge curve shown in Figure 29;
- $\text{vof}_{\text{water}} = 0.5$ denotes the location of the free surface level [62];
- Uniform flow at the mass flow inlet;
- Flow enters normal to the inlet boundary; and
- Wall roughness of k_s equal to 2.49×10^{-3} ft. for the spillway bottom, blocks, and side walls [58].

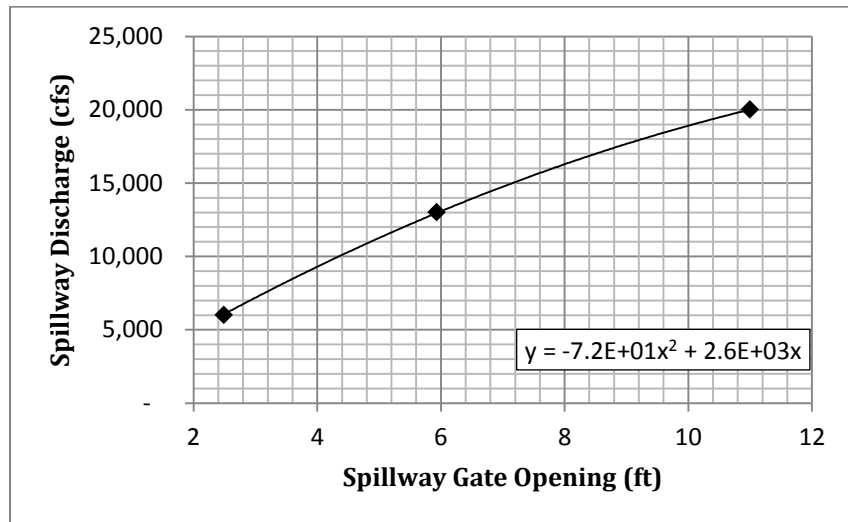


Figure 29: Discharge curve for Spillway 2 (based upon data provided from personal communication with N. Snell, Hatch Engineer).

4. RESULTS & DISCUSSION

Results achieved from carrying out the methods of Section 3 are presented in the following pages. When examining figures it is important to keep in mind that:

- i) The spillway is not symmetric about the center plane, therefore the results on the outlet exhibit differences from the left to right side; and,
- ii) The side walls do not extend all the way to the spillway outlet.

Figure 30 illustrates these two points, and also shows the location of the free surface for a calibration flow rate of 13 kcfs.

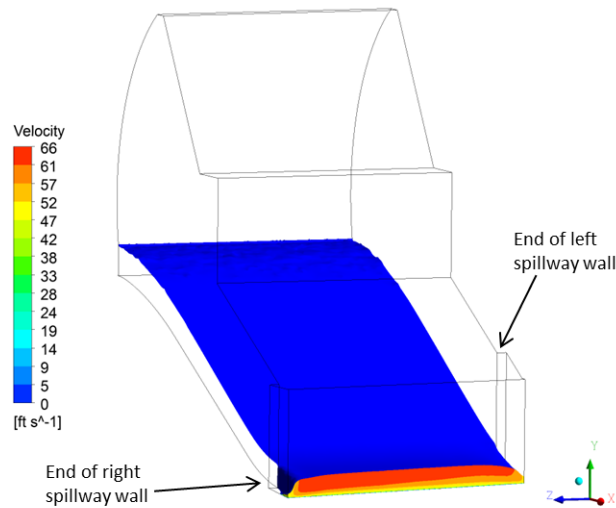


Figure 30: Location of the free surface (denoted by $\text{vol}_{\text{water}} = 0.5$) for a flow rate of 13 kcfs. On the exit plane, velocity contours in the water phase are shown.

4.1. ASSESSING CONVERGENCE AND ACCURACY OF NUMERICAL SIMULATIONS

4.1.1. CALIBRATION MODELS

Prior to formulating calibration curves for making TDG predictions, it was first necessary to establish confidence in the “converged” simulations run during *Phase I*.

As outlined in Section 3.5.5, convergence criteria included three main components:

- i) Residuals decrease by 1.0E-03;
- ii) Mass must be conserved throughout the domain; and
- iii) Time fluctuations in variables of interest reach steady-state (or change by less than 0.5% with additional time-steps).

For all of the calibration models, it was determined that running for a total flow time of 5 s was acceptable to satisfy the above convergence criteria. Figure 31 shows a residual plot for one of the model runs. As portrayed in the figure, after running for a total flow time of 5 s the residuals were below the required criterion of $1.0\text{E-}03$.

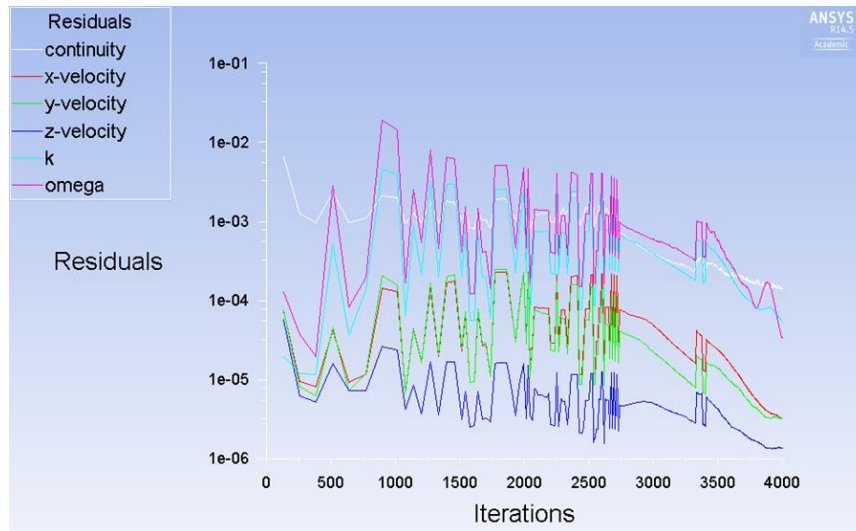


Figure 31: Example residual plot after 5 s of flow time (from a 17.5 kcfs calibration run).

Table 10 shows mass flux results gathered to inspect the second convergence criterion. It can be seen that the average mass flux is well below 1%, and therefore it is concluded that conservation of mass is satisfied.

Table 10: Mass flux through the domain for calibration models on grids of *medium* fineness.

Flow Rate (cfs)	Mixture (water and air)		
	Inflow (lbm/s)	Flux (lbm/s)	Percent Mass Flux
6,000	3.75E+05	-2.57E+01	-0.01%
13,000	8.11E+05	-6.26E+02	-0.08%
17,500	1.09E+06	3.04E+02	0.03%
20,000	1.25E+06	3.32E+02	0.03%

Finally, Figure 32 is provided to demonstrate that 5 s is sufficient time for variables of interest to converge to a steady value. It can be seen that after approximately 4.5 s the TKE on the outlet reaches a steady solution. To confirm this, a few of the calibration models were

run longer than 5 s to see if any changes in the solution occurred—no further changes were observed.

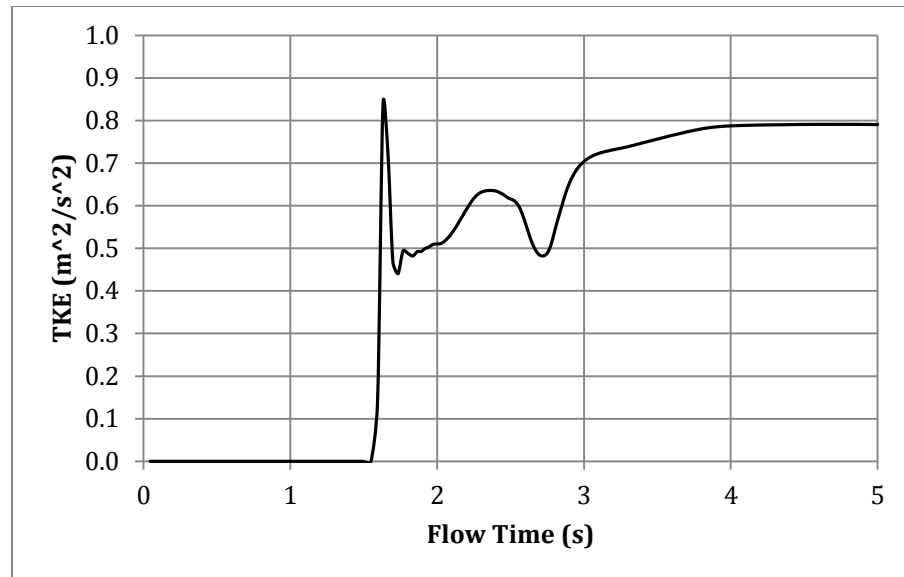


Figure 32: Plot of TKE vs. flow time for the calibration case at 13 kcfs. The graph demonstrates that variables of interest become constant after ~ 4.5 s of flow time, and therefore a total run time of 5 s is sufficient.

After the models ran for 5 s of flow time and all of the convergence criteria were met, it was necessary to ensure the solutions were physically reasonable. This step was important because even though some of the model runs would reach a simulation flow time of 5 s and satisfy all convergence criteria, the results were later realized to be physically unreasonable. For instance, when using the *Open Channel Flow* outlet boundary setting combined with the selection to determine the outlet pressure using the *From Neighboring Cell* option, the velocity of the flow in the air phase would become un-physically high. All other variables (flow depth, outlet water area, etc.) appeared reasonable when these settings were used, but the velocity field in the air phase would increase well above the water velocity. For this reason, zero gauge pressure was specified at the outlet instead, and physically reasonable solutions were attained.

Once converged, physically realistic solutions were achieved in a temporal space, it was necessary to evaluate what influence the physical discretization had on numerical results. As previously mentioned, the method used for assessing discretization uncertainty is the one outlined by Celik et al. [57]. For this process it was necessary to run each CFD model on

three different sized grids, for example a *coarse*, *medium*, and *fine* grid. Therefore, for the calibration step a total of twelve models were run: the spillway at discharges of 6, 13, 17.5, and 20 kcfs; and each of these were run on a *coarse*, *medium*, and *fine* grid. During grid refinement, Celik et al. state that a refinement factor $r = h_{coarse}/h_{fine}$ greater than 1.3 is required (here, h is the representative cell size). On average, the refinement factor used for each of the GCI studies in the calibration step was 1.9.

The purpose of a grid convergence study is to examine how an important parameter of interest varies with a change in mesh size. Therefore, since velocity is one of the main parameters of interest in this study, velocity profiles were examined to see what effect changing the mesh size had on them.

In Figure 33 velocity profiles of water near the spillway exit are plotted. It can be seen that the profile changes only a small amount from one grid to the next. This qualitatively demonstrates that an acceptable mesh has been achieved, and the numerical solutions are independent of mesh size.

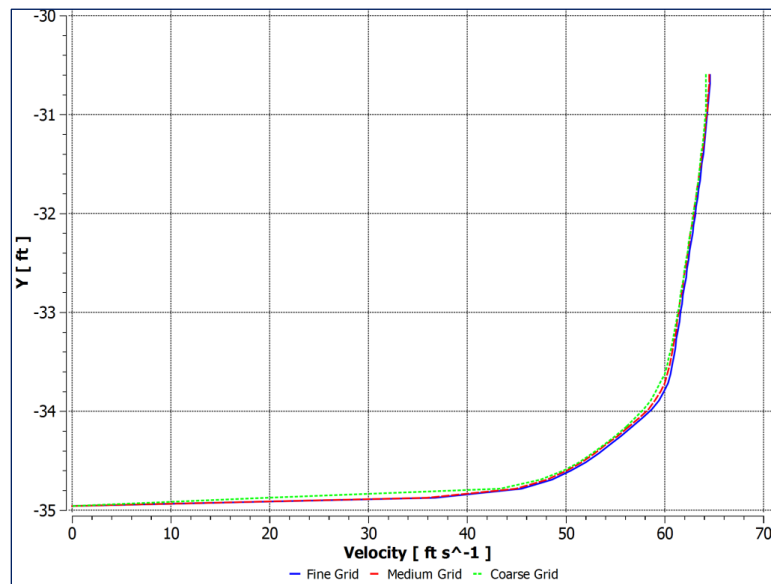


Figure 33: Velocity profiles of the water phase near the center of the spillway outlet (the case shown is for the calibration model at 13 kcfs).

Once convergence of a velocity profile was qualitatively established, the next step was to compute a grid convergence index (GCI). In doing so, quantitative measure of uncertainty due to discretization error could be established.

The three sets of grids run for the 13 kcfs calibration case had $2.61\text{E}+05$, $3.88\text{E}+05$, and $7.75\text{E}+05$ cells. Analysis of the velocity profile for the calibration run on the *medium* grid is shown in Figure 34. To plot the figure, a sample of 15 points from the water phase were taken along a vertical line near the spillway exit. For these 15 points, the GCI measure of uncertainty ranges from 0.01% to 6.56%. The average GCI measure of uncertainty for a selection of 50 points (taken along the same vertical line) was calculated to be 2.57%. For the same sample of 50 points, the average apparent order of accuracy, p_{ave} , was computed to be 2.84, with a range of 0.07 to 10.12.

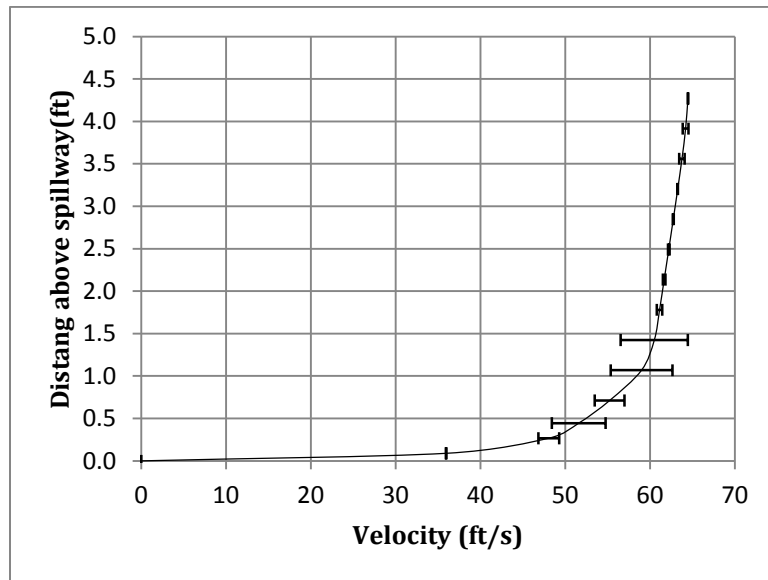


Figure 34: Velocity profile for the 13 kcfs case on the mesh of *medium* fineness. Discretization uncertainty was computed using Eq. (7) from Celik et al. [57]. A sample of 15 points was used to graph the line and compute uncertainty values, however, the velocity profile is plotted as a thin line for ease of profile visualization.

Similar to the above analysis of the velocity profile, measures of discretization uncertainty are reported in Table 11 for parameters of interest on the spillway outlet.

Table 11: Parameters of interest on the spillway outlet for each of the calibration runs; values reported are from solutions achieved on the *medium* mesh. GCI measures of discretization uncertainty are tabulated for each parameter.

		Spillway Discharge (kcfs)			
		6	13	17.5	20
Flow Depth, y	Value (ft)	1.9	4.1	5.7	6.9
	Discretization Uncertainty (%)	0.2	2.1	3.3	4.8
Area-averaged Velocity, V	Value (ft)	59.4	59.5	58.1	56.0
	Discretization Uncertainty (%)	0.4	3.1	3.5	2.5
Water Area, A	Value (ft ²)	100.3	223.4	310.0	371.9
	Discretization Uncertainty (%)	0.2	2.1	3.3	4.8
Area-averaged Water TKE, k	Value (ft ² /s ²)	9.7	5.2	3.7	3.3
	Discretization Uncertainty (%)	22.6	2.3	1.2	6.7
Area-averaged Water Turbulence Intensity, Tu	Value (%)	4.7	3.7	3.1	2.7
	Discretization Uncertainty (%)	0.1	5.3	2.0	0.3

A point worthy of discussion is the calculated uncertainty for area-averaged TKE in the 6 kcfs case. This high value of uncertainty, 22.6%, can be explained by referring to the guidelines of Celik et al. [57]. It is stated that the procedure for calculating discretization uncertainty does not work if either $\varepsilon_{32} (= \varphi_3 - \varphi_2)$ or $\varepsilon_{21} (= \varphi_2 - \varphi_1)$ are “very close” to zero. (Here φ_i represents the value of a key solution variable on the i^{th} grid). In the point of concern listed above, ε_{32} and ε_{21} are both 0.009 ft²/s². Since these values are the same and both small numbers, the GCI uncertainty calculation is likely not valid. Celik et al. state that such results “might be an indication of oscillatory convergence, or in rare situations, it may indicate that the exact solution has been attained” [57]. While no further investigation was made, it can be noted that the *approximate relative error*⁶ for the 6 kcfs area-averaged TKE is on the order of 1.0%. In the instance mentioned above, the approximate relative error of 1.0% is likely more accurate than the GCI computed uncertainty of 22.6%.

In examining Table 11, a general trend emerges that uncertainty on the calibration run of 6 kcfs is less than that for the same parameter on the 20 kcfs calibration run. This can be

⁶Approximate relative error is calculated by $e_a^{21} = \left| \frac{\varphi_1 - \varphi_2}{\varphi_1} \right|$ [57]. Here, φ_i is a variable of interest (such as TKE) on the on the i^{th} grid, and the superscript “21” indicates approximate relative error from grid 2 compared to grid 1.

explained by the fact that “similar” boundary layer mesh settings were used for each of the calibration cases. By similar settings, it is meant that *approximately* the same number of wall-normal layers covered the inlet water phase in each calibration case. Therefore, since the water depth changes from case to case, so does the cell density covering the water phase. On average, in the direction normal to the bottom of the spillway, the 6 kcfs case had ~ 9 cells/ft while the 20 kcfs had ~ 4 cells/ft.

Due to this, ultimately the results of the 6 kcfs model are more precise than the 20 kcfs model. That being said, the discretization uncertainties listed in Table 11 for the 20 kcfs calibration run are of acceptable magnitude for the current effort. The justification for this is that the present research seeks to investigate a TDG prediction *method*, and is therefore more focused on trends than achieving precise predictions. For the calibration model of 20 kcfs the average uncertainty of all the parameters of interest is only 3.8%; this is compared to 0.4%, 3%, and 2.7% for the 6, 13, and 17.5 kcfs cases respectively. An average discretization uncertainty of 3.8% is well within the acceptable range, especially when one considers the scatter present in observed TDG field data used for calibration.

4.1.2. BAFFLE BLOCK MODELS

Analysis of discretization uncertainty on the baffle block models proved to be less clearly conclusive than for the calibration runs. As a result of introducing baffle blocks into the domain, the height of the water flow was increased, and therefore the water phase extended up into the unstructured, “non-inflated” cell region in certain locations throughout the domain. Since these cells were not as fine as the structured region of inflated cells, the discretization uncertainty is expected to be higher. However, an unexpected result was realized in attempting to carry out a grid convergence study, and that was that oscillatory convergence was experienced. For illustration, Table 12 is provided. It can be seen that from the *coarse* to *medium* mesh the specific energy decreases, while from the *medium* to *fine* mesh the specific energy increases.

Table 12: Parameters calculated for the LNSUB configuration on the *medium* mesh.

	Mesh			GCI
	Coarse	Medium	Fine	
Specific Energy	29.76	28.88	30.48	8%
Momentum Function	1.68E+04	1.65E+04	1.70E+04	5%
α	1.46	1.47	1.43	2%
β	1.16	1.16	1.15	1%

Celik et al. [57] state that values of $\varepsilon_{32}/\varepsilon_{21} < 0$ indicate oscillatory convergence, which is the case for the data reported in Table 12. Due to the oscillatory nature of baffle block results, a more qualitative approach was taken in examining discretization uncertainty, and the magnitude of approximate relative errors were examined.

Table 13 lists the approximate relative errors calculated from the *coarse* to *medium* grids in each of the baffle block cases. The bottom two rows in the table report the approximate relative errors for the specific energy and momentum values utilized in making TDG predictions; it can be seen that these values range from 0.3% – 6.3%. As previously highlighted, errors in this range are sufficiently low to investigate the trends of interest in the current study.

Table 13: Approximate relative errors for quantities of interest in baffle block models.

	Linear	LNSUB	Angle
Specific Energy	5.3%	5.3%	8.6%
Momentum	3.5%	3.1%	5.1%
α	11.3%	3.0%	7.0%
β	4.7%	1.4%	1.2%
Specific Energy Corrected with α	1.3%	3.5%	3.7%
Momentum Corrected with β	0.3%	1.9%	6.3%

An additional point of interest is the approximate relative error for α in the linear blocks case. The difference in α obtained from the *coarse* to *medium* grid was an increase of 11.3%. From the *medium* to *fine* grid (which is not shown in Table 13), the value of α decreased by approximately the same amount. This is of interest because solutions computed on the *medium* grids were used for making TDG predictions, and, as will be seen later in Section 4.4, a high value of “specific energy rate corrected with α ” for the linear blocks model resulted in a higher than anticipated TDG prediction for this case. The influence of a higher

approximate relative error for the linear blocks could be one factor which caused these elevated TDG predictions.

In terms of the current study, it appears as though oscillatory convergence may be experienced for two reasons. First, the presence of time-dependent flow fluctuations in the baffle block models was a phenomenon not encountered in the calibration models. The effect of time-dependent fluctuations could have some influence on creating oscillatory convergence behavior. A second possible explanation is the existence of lower quality mesh elements in the block models because of the irregular-shaped baffle blocks. If the desire of the current study was to seek precise TDG predictions, it would have been worth developing a higher quality mesh—either through further adjusting parameters within ANSYS Meshing, or by using a third party meshing software. However, in the current study the range of approximate relative errors is acceptable because (1) observing general trends is of greatest interest, and any trends of interest should be captured with the above ranges of approximate relative error, and (2) the substantial scatter in TDG field data does not warrant further reduction of approximate relative error at this stage of analysis.

4.2. CALIBRATION MODEL RESULTS

Figure 35 shows the calibration run at 13 kcfs. The water phase in the spillway is displayed, which is denoted by cells where the $\text{vof}_{\text{water}} \geq 0.5$. It is worth noting that this is the same criterion use when delineating quantities for calculations. In the figure, the locations of the three water outlets are annotated. As logic would suggest, a majority of water flows out of the domain through the main outlet located at the downstream end of the spillway. However, at larger flow rates and for the baffle block cases water does exit through both the left outlet as well as the right outlet. In all calculations of specific energy and momentum, water mass exiting through the left and right outlets was accounted for.

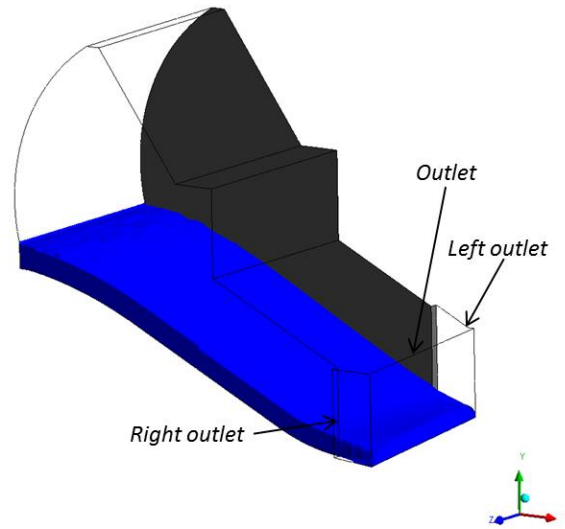


Figure 35: Water volume in spillway for a flow rate of 13 kcfs. Note: the left wall of the spillway is visible while the right wall is removed for viewing purposes.

The figures on the following pages are provided for the reader to visualize the differences from one calibration case to another (i.e. the *Phase I* models). Figure 36 shows volume fraction contours of water, Figure 37 shows velocity contours, and Figure 38 shows contours of turbulence intensity in the water phase. Each calibration model was run using the same initial conditions except for (1) the height of the inlet gate opening and (2) the associated mass flow rate.

As was discussed in Section 4.1, the calibration run at a flow rate of 6 kcfs had the highest density of mesh elements in the water phase. As a result, it can be seen that there is less numerical diffusion exhibited in this model. Figure 36 demonstrates this in that there is a sharper air-water interface in the 6 kcfs model than in the other cases. Figure 36 is also useful to visualize the cross-sectional area of water exiting the spillway. As expected, the water outlet area increases along with discharge. This cross-sectional area was computed by summing the area of each cell on the outlet boundaries where $\text{vof}_{\text{water}} \geq 0.5$.

In addition to outlet area, velocity is another parameter of importance. For this reason, Figure 37 is provided. It should be noted that each model has a different maximum velocity, with the case of 6 kcfs exhibiting the highest velocity. As shown near the right side of each contour plot, flow velocity directly influences Froude number and specific energy. While all

of the calibration runs exhibit supercritical flow throughout the entire spillway, the 6 kcfs case is the flow most dominated by inertial forces (with $Fr = 7.7$) while the 20 kcfs case (with $Fr = 3.8$) is still dominated by inertia, but not as heavily so. Even though the 6 kcfs case exhibits the highest velocity (and Froude number), the calibration data of Table 4 (page 42) shows that it also yields the lowest downstream TDG pressures. Therefore, it is concluded that water velocity alone is not what increases TDG supersaturation; the magnitude of mass flow has a more important effect on transporting energy to yield elevated TDG levels.

Finally, turbulence was monitored as it plays an important role in jet breakup/dissipation. In Figure 38, contours of turbulence intensity in the water phase are shown, and two expected phenomenon become apparent. First, it can be seen that the turbulence intensity is greatest near the boundary layer on the channel bottom. This boundary layer region—which contains high velocity gradients—is an anticipated location of shear production and therefore exhibits a higher level of turbulence [63]. Second, it can be seen that the effect of sidewalls is persistent to some degree in that the sides of the spillway jet exhibit higher turbulence intensities than the middle. This is not surprising since the spillway walls do not end very far upstream of the outlet plane.

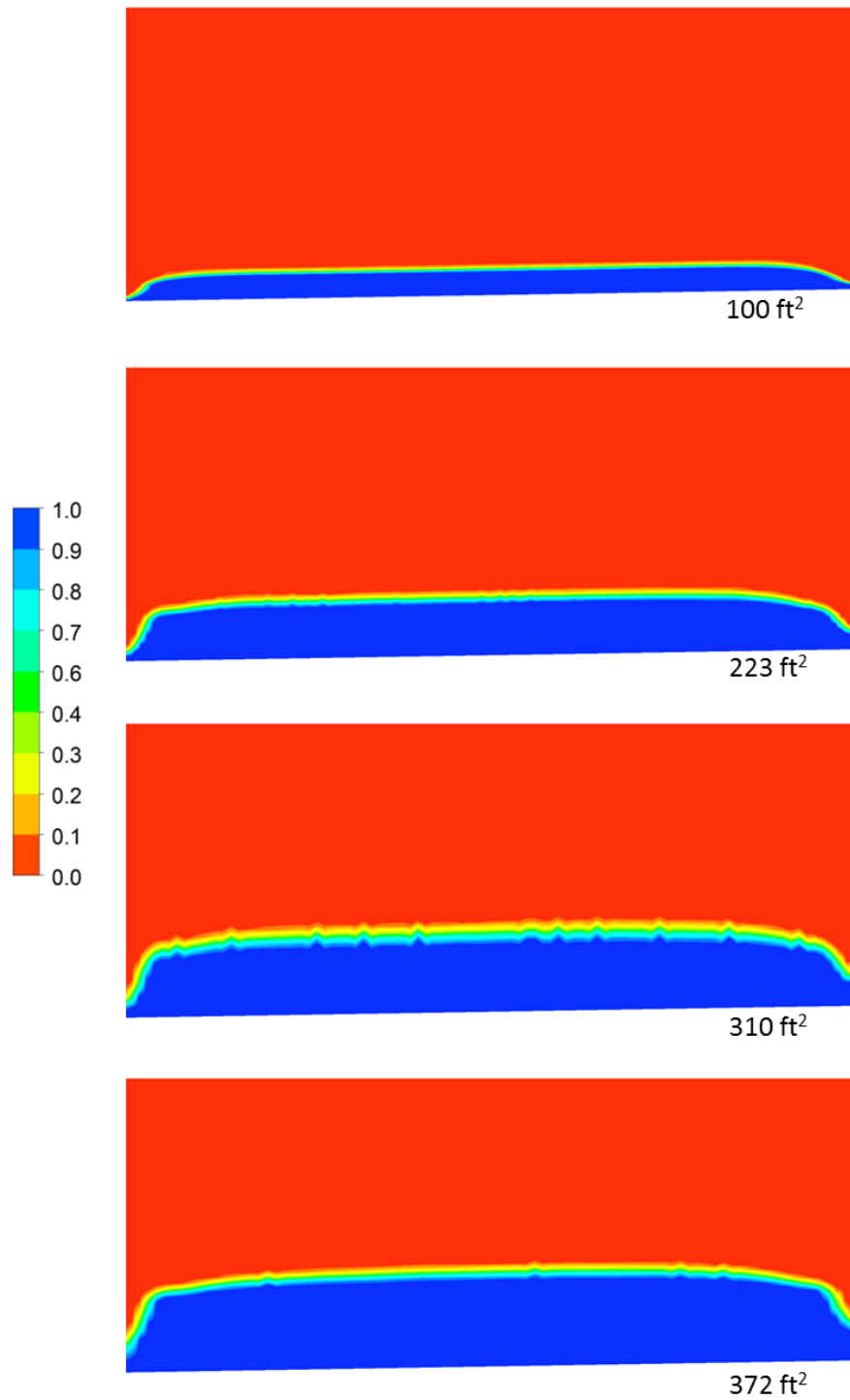


Figure 36: Volume fraction contours on the exit plane for all four calibration models (1 is all water, and 0 denotes all air). Near the right side of each plot, outlet area of the water phase is reported. From top to bottom the corresponding flow rates are 6, 13, 17.5, and 20 kcfs.

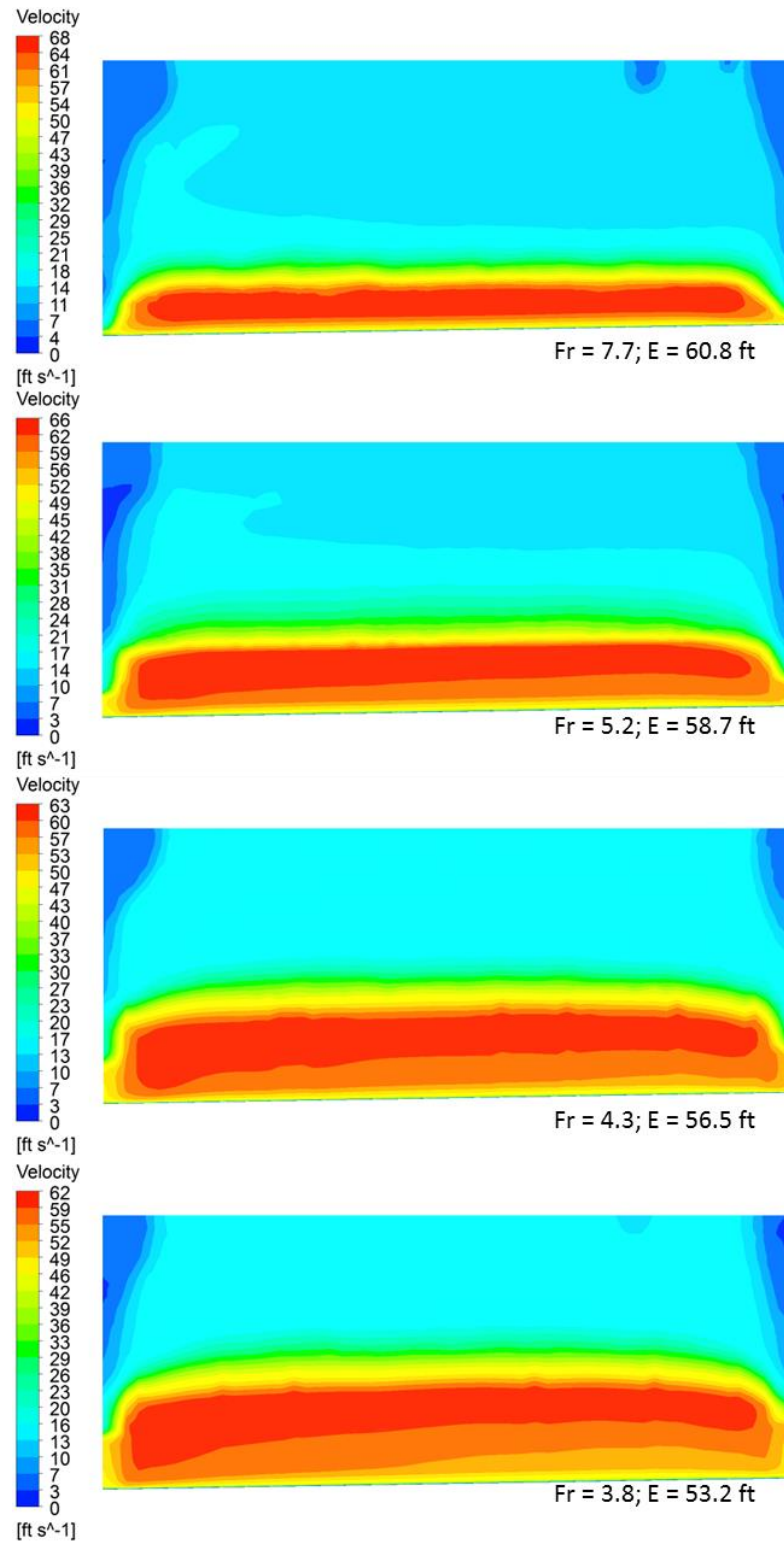


Figure 37: Velocity contours on the exit plane for all four calibration models. Froude number (Fr) and specific energy (E) are reported. From top to bottom the corresponding flow rates are 6, 13, 17.5, and 20 kcfs.

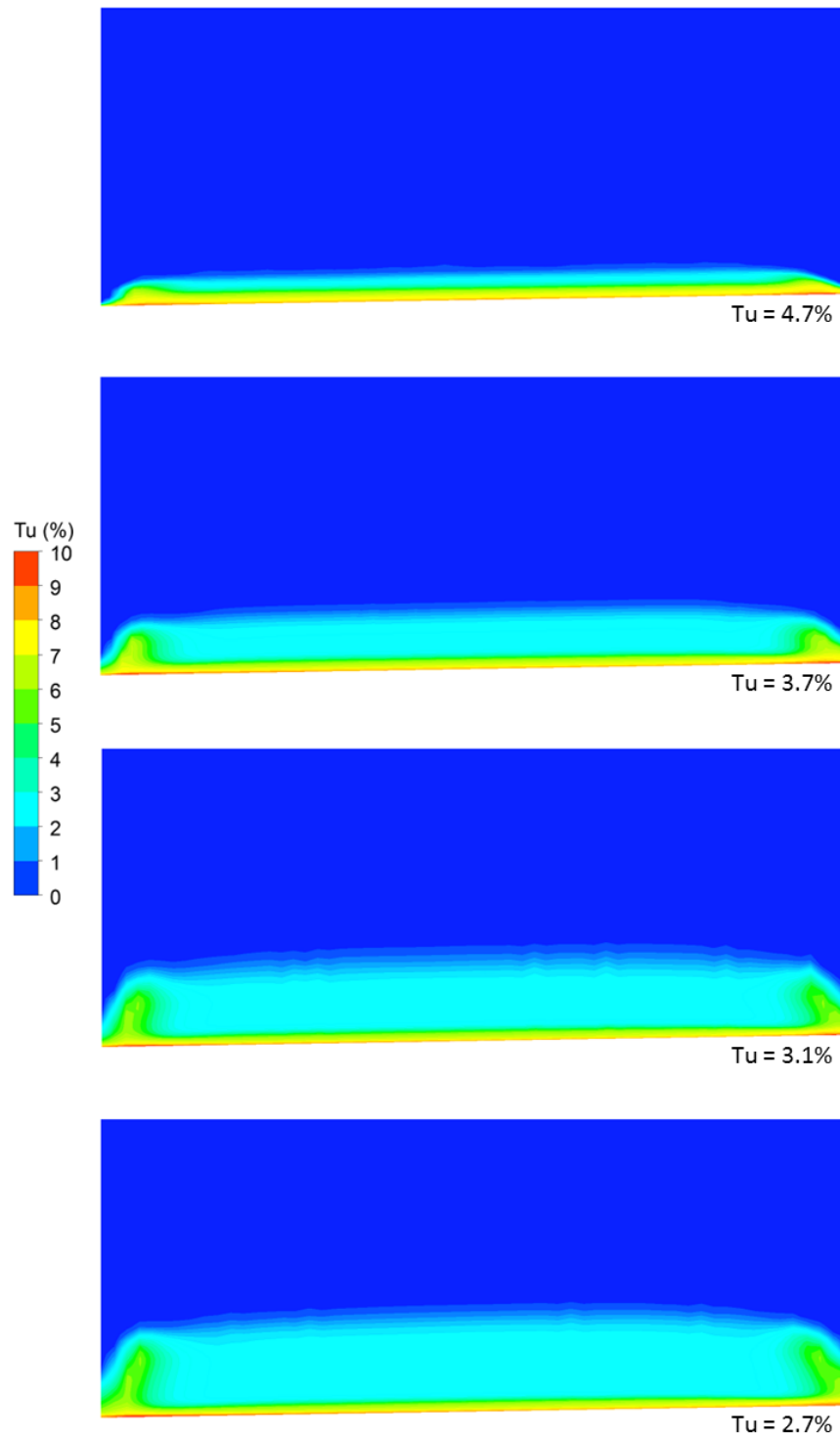


Figure 38: Turbulence intensity contours on the exit plane for all four calibration models. On the right side of the figure, area-averaged Tu is reported for each case. From top to bottom the corresponding flow rates are 6, 13, 17.5, and 20 kcfs.

With regards to jet breakup, it is interesting to compare the turbulence contour plots of Figure 38 to an image of the actual spillway flow. Figure 39 shows an image of Spillway 2 at Boundary Dam with a discharge of approximately 12 kcfs. It can be seen that the sides of the jet appear to breakup more quickly than the spillway-center region of the jet. Wall induced turbulence is likely *one* reason for this to occur.

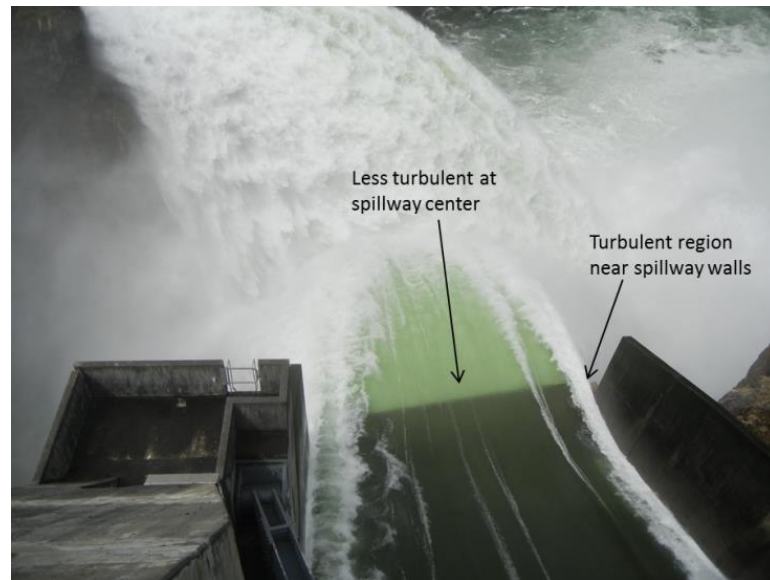


Figure 39: Looking down at Spillway 2 comparing turbulence at spillway walls to spillway center. In the image, Spillway 2 discharge is approximately 12 kcfs (Photograph taken 5/13/2013).

One of the biggest discrepancies observed between the calibration models and actual spill flow at Boundary Dam is the presence of an aerated wall layer at the dam which is not captured in the CFD models. Figure 39, shown above, displays one angle of this. The term “wall layer” is used to refer to the regions near both of the spillway walls that exhibit different behavior than flow at the center of the spillway. Two key differences include that (1) the wall layer is aerated and (2) it appears to be more turbulent than flow in the middle of the chute. It is also worth noting that the wall layer is different from the left to ride side of the spillway as seen above in Figure 39.

In Figure 40, an additional view is provided to compare Spillway 2 flow to the CFD model. It can be seen that, in the left image, an aerated wall layer is present at the side of the chute for almost the entire length of the spillway. On the right side of Figure 40, it can be seen that the CFD model does not capture the wall layer flow behavior.

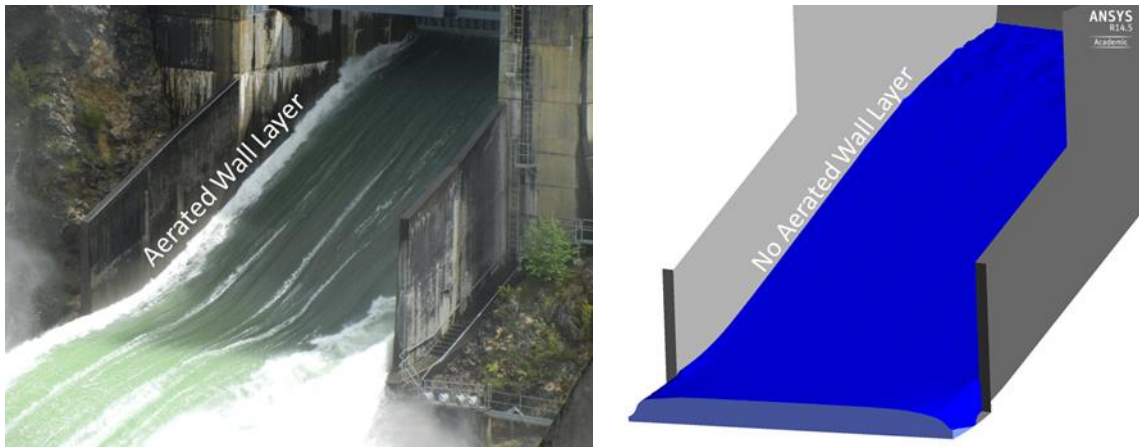


Figure 40: Wall layer in Spillway 2 compared to CFD model.

One possible explanation for aerated flow behavior near the spillway walls was observed on a trip to Boundary Dam. Figure 41 shows an image of the radial gate which controls flow in the spillway. Upstream of the gate (on the right side of the image) it can be noticed that a vortex is present near the wall. It is possible that air becomes entrained in the flow due to this vortex. Furthermore, since this aeration occurs near the turbulent wall region, the effect is that a white, aerated wall layer forms. The reason then, this phenomenon is not captured in the CFD model is due to the inlet conditions specified in the model. At the inlet, a uniform level of turbulence was specified, the flow was assumed to enter normal to the boundary, and also the inflow was considered to consist entirely of the water phase (i.e. no aeration).

While the lack of wall layers in the CFD model is a source of error in comparison to actual spillway physics, it is not of great concern in this initial investigation for two reasons. First, the bulk energy of the spillway flow (which is captured in the CFD models) is much larger than that of the wall layer energy. This is relevant because bulk spillway energy is the quantity of greatest interest in the current TDG prediction effort. Secondly, the absence of a wall layer is consistent for all of the models run during the present research. Therefore, since the CFD models (1) do resolve the major spillway hydrodynamics and (2) exhibit consistent wall behavior from one model to another, model-to-model comparison is still expected to yield reasonable results.



Figure 41: Vortex in the upstream flow caused by the gate-wall geometry configuration. Downstream, the presence of a wall layer is visible.

After running all calibration models and observing differences between actual spillway flow and the models, calibration curves could be formulated. For each calibration model, the following equations were used to compute quantities of interest. Variables required in calculations were taken on the exit plane (which is shown in Figure 36 through Figure 38).

- i) For specific energy rate [21]:

$$\dot{E} = \left(y + \alpha \frac{(\dot{m}/\rho)^2}{2gA^2} \right) \dot{m} \quad (4.1)$$

in which y is flow depth, α is the kinetic energy flux correction coefficient, \dot{m} is mass flow rate, ρ is water density, g is gravity, and A is outlet cross-sectional area. For all calculations, y was computed by taking the outlet cross-sectional area and dividing by 54 ft (which is the spillway width of the end sill). Furthermore, the kinetic energy flux correction coefficient was computed by:

$$\alpha = \frac{\int_A v_s^3 dA}{\bar{V}^3 A} \quad (4.2)$$

where v_s is the point velocity and \bar{V} is the average velocity at the cross section.

- ii) In the case of a rectangular channel, the momentum function equation takes on the form of [21]:

$$M = \frac{by^2}{2} + \beta \frac{(\dot{m}/\rho)^2}{(gby)} \quad (4.3)$$

where b is channel width and β is the momentum flux correction coefficient, which is computed using:

$$\beta = \frac{\int_A v_s^2 dA}{\bar{V}^2 A} \quad (4.4)$$

The above relations for kinetic energy and momentum flux correction coefficients yielded the values reported below in Table 14.

Table 14: Kinetic energy and momentum correction coefficients for calibration models.

Discharge per Unit Width (ft ² /s)	Froude	α	β
120	7.7	1.06	1.02
260	5.2	1.04	1.01
350	4.3	1.02	1.01
400	3.8	1.03	1.01

The values of α and β reported in Table 14 are in the expected range for a chute spillway. For turbulent flow in prismatic channels, it is expected that: $1.0 \leq \alpha \leq 1.1$, and for β not to vary significantly from unity ([21],[37]).

Using equations for \dot{E} and M , these quantities at the spillway exit were correlated to historically observed TDG production at Boundary Dam. Results of this analysis are shown in the calibration curves of Figure 42 and Figure 43. In these figures, four points are plotted (one for each calibration model) and a curve fit is displayed which relates TDG to each function. It can be seen that a second order curve fit matches the data very well.

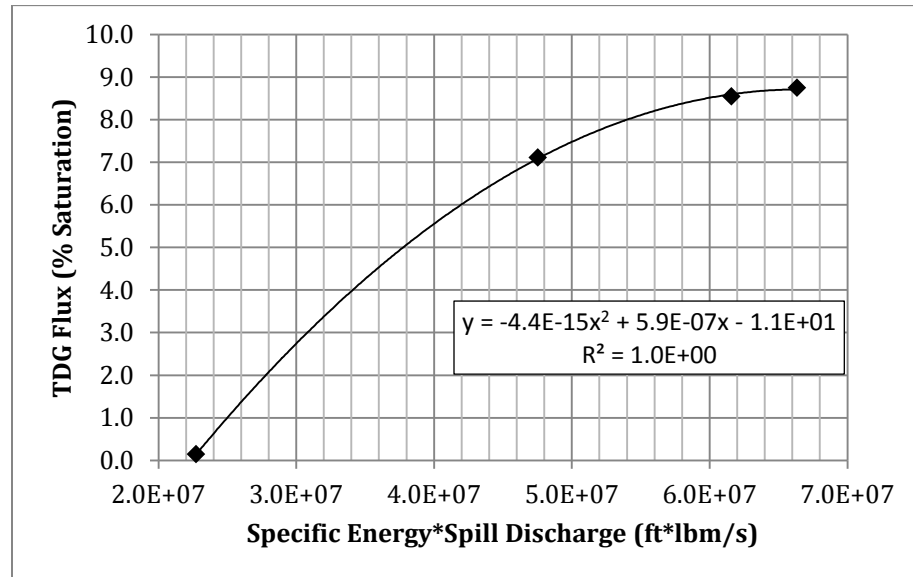


Figure 42: Calibration curve for specific energy rate, \dot{E} .

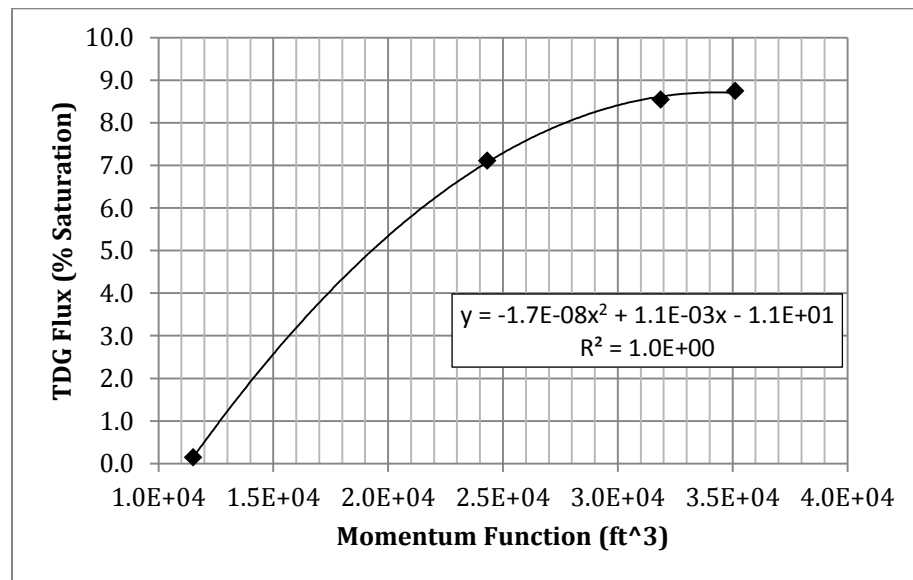


Figure 43: Calibration curve for momentum function, M .

Now that \dot{E} and M are correlated to historical TDG performance at Boundary, baffle block TDG predictions can be made using the curve fit equations achieved in Figure 42 and Figure 43. Baffle block results are discussed in Section 4.2.2, and TDG predictions in Section 4.4.

4.2.1. SENSITIVITY ANALYSIS

Of all the initial conditions, the turbulence intensity at the inlet has one of the higher levels of uncertainty. An investigation into literature regarding turbulent spillway jets led to the specification of a 2% turbulence intensity ([36], [37], [59]). This is a relatively low level of turbulence, and while field data is not available for Boundary Dam, the inlet turbulence is likely in this lower range. Even so, due to the uncertainty in this specification, a sensitivity study was conducted. In this process, the 13 kcfs calibration model was run at two additional inlet turbulence intensities, 0.5% and 5%. Table 15 below shows the results of this investigation.

Table 15: Inlet turbulence sensitivity analysis for the 13 kcfs case. The maximum difference column compares the maximum and minimum values achieved from the three cases run.

		Inlet Tu Specification			Maximum Difference
		0.5%	2.0%	5.0%	
Parameters of Interest on The Outlet	Momentum (ft ³)	2.399E+04	2.398E+04	2.396E+04	0.1%
	Energy Transport Rate (ft ³ lbm/s)	1.436E+09	1.435E+09	1.432E+09	0.3%
	Area-averaged Tu (%)	2.6	3.7	5.1	66.1%

It is readily noticeable that only very slight changes in the parameters sought for TDG predictions (momentum and energy transport rate) are realized. The maximum change for these two parameters occurs in the energy transport rate, and is a value well below 1%.

The outlet-to-inlet turbulence sensitivity, on the other hand, is substantially higher. For a tenfold increase in specified turbulence intensity at the inlet, an approximate 66% increase was realized for area-averaged turbulence intensity at the spillway outlet. While this demonstrates moderate sensitivity of spillway outlet turbulence to inlet conditions, this parameter was not used for making TDG predictions in the current study.

Overall, these findings substantiate that parameters of interest in the model are not highly sensitive to specified inlet turbulence. This discovery is of value in the current investigation because of the uncertainty in the specified inlet turbulence conditions.

4.2.2. OBSERVED POTENTIAL FOR TDG REDUCTION FROM OPERATIONAL CHANGES

During the process of setting up CFD models of the spillway, it was realized that the specific energy at the spillway inlet is a function of forebay elevation. The higher the forebay elevation above the spillway crest, the greater the head present to force water under the radial gate. Consequentially, the spillway gate opening to achieve a flow rate of 13 kcfs when there is 44 ft of head on the spillway is smaller than when there is 34 ft of head.

While a validated discharge curve for Spillway 2 which relates spillway discharge to forebay elevation was not obtained during the current project, an investigation was conducted to examine how the specific energy at the spillway exit would vary with forebay elevation. This was carried out by assuming that, given a forebay elevation decrease of 10 ft, the spillway gate would have to be opened to 6.93 ft (compared to 5.93 ft) to maintain a constant flow rate of 13 kcfs. Table 16 reports the results of this investigation.

Table 16: TDG predictions for operating at a constant spill discharge of 13 kcfs but at two different forebay elevations. *Note: 7.1% is a calibration specified TDG value.

	Forebay Elevation Above Spillway Crest (ft)	Spillway Gate Opening (ft)	Specific Energy (ft)	Momentum Function (ft ³)	Estimated TDG based on \dot{E} (%)	Estimated TDG based on M (%)
	44	5.9	58.7	2.4E+04	7.1*	7.1*
	34	6.9	54.2	2.3E+04	6.4	6.7
Percent change	-22.7%	16.9%	-7.7%	-4.1%	-9.9%	-5.6%

In the table, it can be seen that an approximate 8% reduction in outlet specific energy is realized if the spillway is operated at 34 ft of head instead of 44 ft. Using the calibration curve Figure 42, the specific energy rate method results in a predicted decrease in TDG flux of ~10%. Based upon a momentum analysis, a ~6% reduction is predicted.

While these reductions in predicted TDG flux are not tremendous, the achieved results do imply that downstream TDG pressures may be reduced by operating the spillways when the forebay is at a lower elevation. Furthermore, at higher spill rates, the difference in energy at the spillway exit will be greater for different forebay conditions; therefore it is predicted that a greater reduction in TDG would be realized.

While this discovery is unlikely to yield sufficient downstream TDG reduction for all spill discharges at Boundary Dam, there are certain conditions under which it may allow the facility to operate within water quality laws, when it otherwise may have not been able to. The author does recognize, however, that changing the forebay elevation by 10+ ft may not be feasible at all times, as the upstream stretch of the Pend Orielle River serves other purposes in addition to power generation at Boundary Dam.

4.3. BAFFLE BLOCK RESULTS

To run baffle block cases, a similar approach was used to that of setting up the calibration models. All initial conditions were the same except, as previously mentioned, baffle block cases were only run at a single flow rate of 13 kcfs.

One important difference in obtaining numerical solutions for the baffle cases, however, was the need for calculating time averages of all quantities. The incorporation of baffle blocks into the spillway created time-dependent fluctuations in the domain downstream of the blocks. Therefore, the models were run until a quasi-steady-state was reached (for example, a state in which the outlet flow rate would exhibit fluctuations around a mean value), then the following quantities were time-averaged for 30 s:

- i) Velocity;
- ii) Turbulence kinetic energy;
- iii) Turbulence intensity;
- iv) Volume fraction; and
- v) Mass flow rate.

Figure 44 is a plot of the mass flow rate at the spillway outlet for one of the block cases—also plotted in the figure is the running average of outlet mass flow rate. By 30 s, it can be seen that the average exit mass flow rate becomes relatively constant. It was determined that averaging for 30 s would yield results that were within 0.5% of the value if it were averaged over a period twice as long. Based on this minimal level of difference, it was concluded that averaging for 30 s would sufficiently resolve any time-dependencies. In computing parameters of interest for the block cases (i.e. specific energy or momentum) the time-averaged values of variable were used.

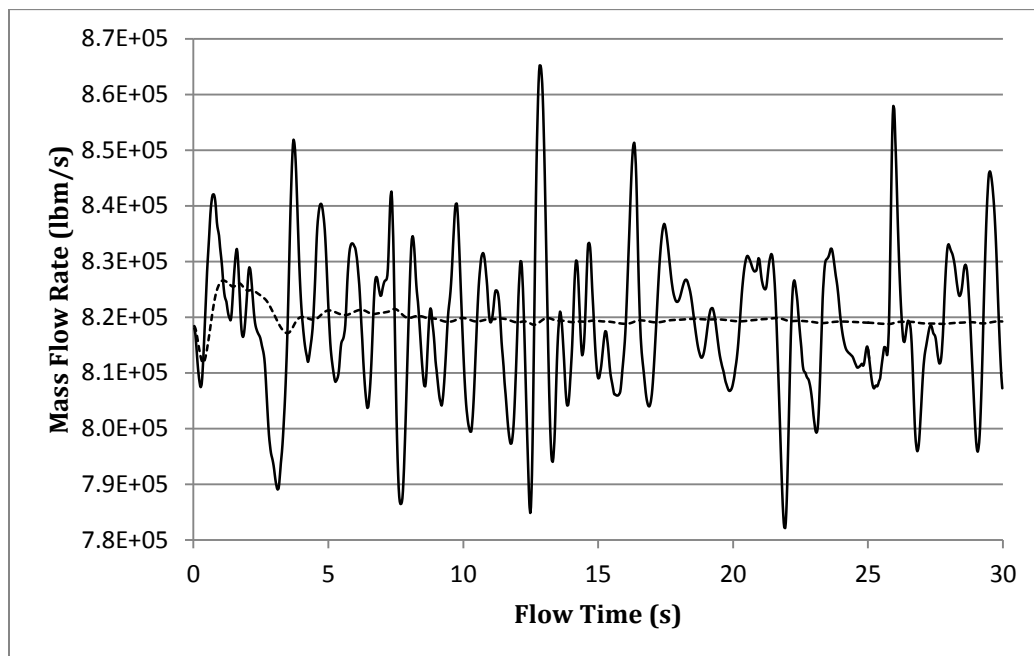


Figure 44: Time-averaging the mass flow rate at the spillway outlet. The solid line indicates the outlet flow rate at any point in time, and the dashed line is a running average.

To refresh the reader's memory, the following figure is provided to relate baffle block configurations to the terminology used.

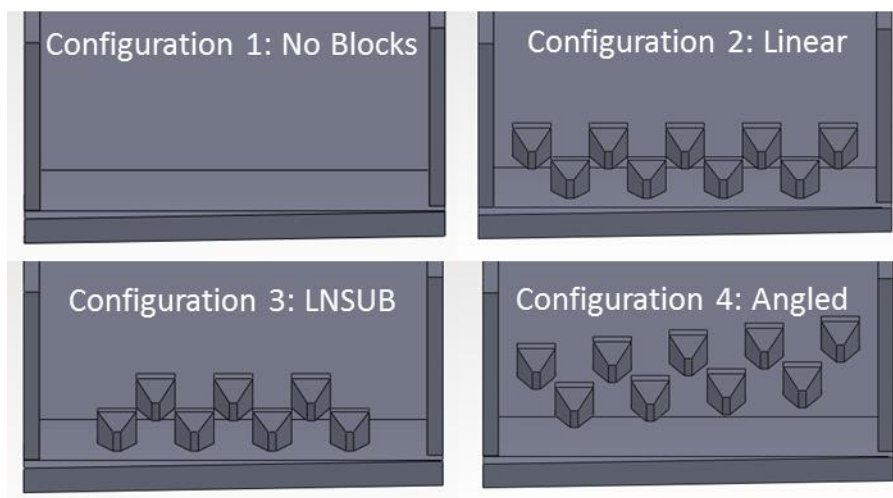


Figure 45: Baffle block configurations and prescribed names—view is of spillway outlet, looking upstream.

In the next three figures, images are provided for visual representation of baffle block results. As previously described, all of the images shown are the result of time-averaging

numerical solutions for 30 s. Additionally, a wireframe outline of the domain remains visible for the viewer's reference.

Figure 46 shows water surface profiles for all three of the baffle block cases. These images provide representation of how baffle blocks influence the location of the free surface in the spillway. In each case, cross-sectional area of the water phase at the exit plane is increased over the 13 kcfs calibration run shown previously in Figure 36. Since the flow rate is the same, continuity suggests the average outlet velocity must decrease by the introduction of blocks into the spillway. This is both expected and desirable.

Figure 47 displays velocity contours on the exit plane for each of the block cases. Also displayed in this figure is the calculated specific energy for each configuration. It can be seen that the specific energy for the linear blocks case is 7% and 15% less than the angled and LNSUB configurations, respectively. It will be seen later that this directly results in a lower predicted TDG flux for the linear configuration.

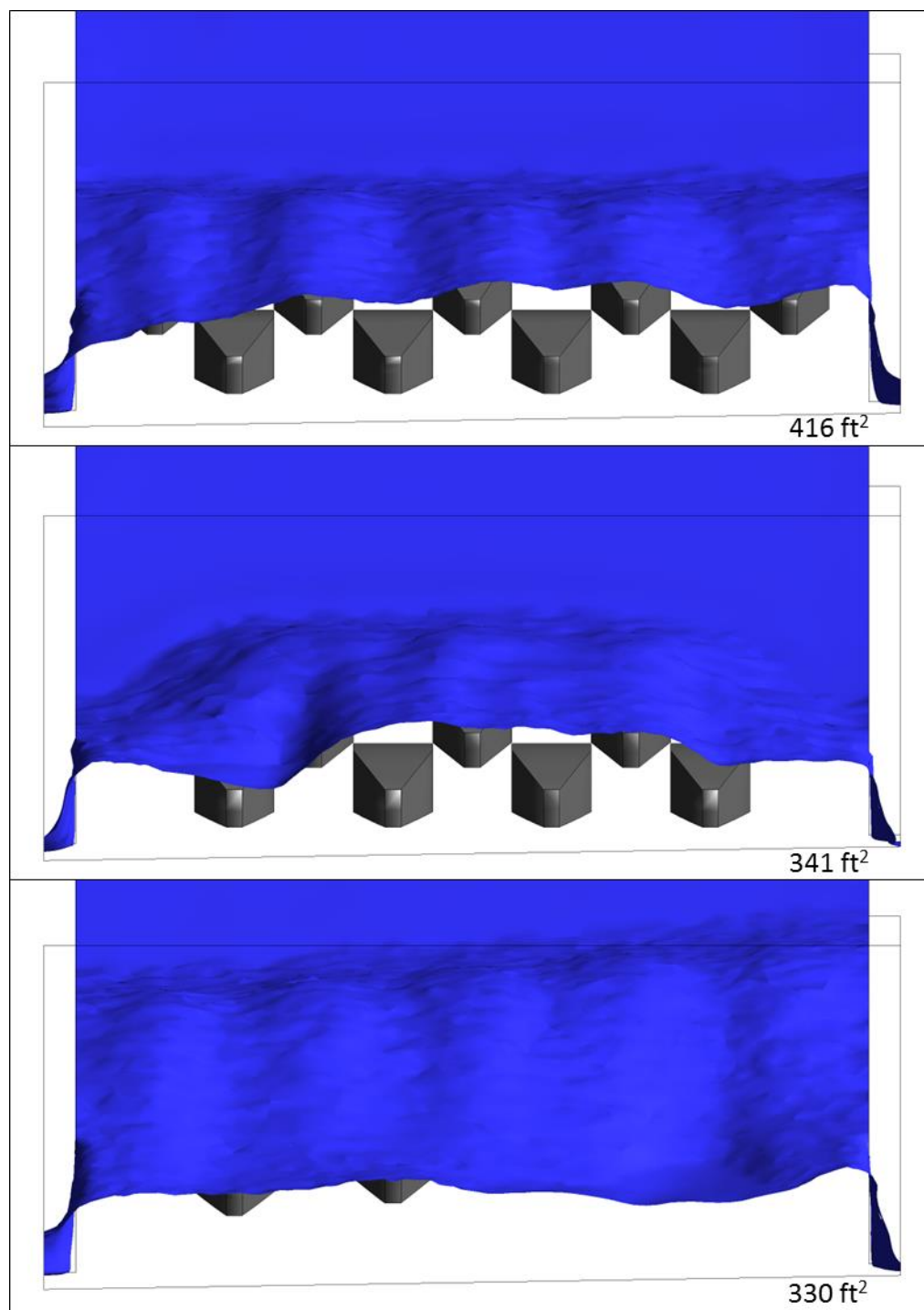


Figure 46: Free surface profile for all three block cases. From top to bottom, the configurations shown are the linear, LNSUB, and angled.

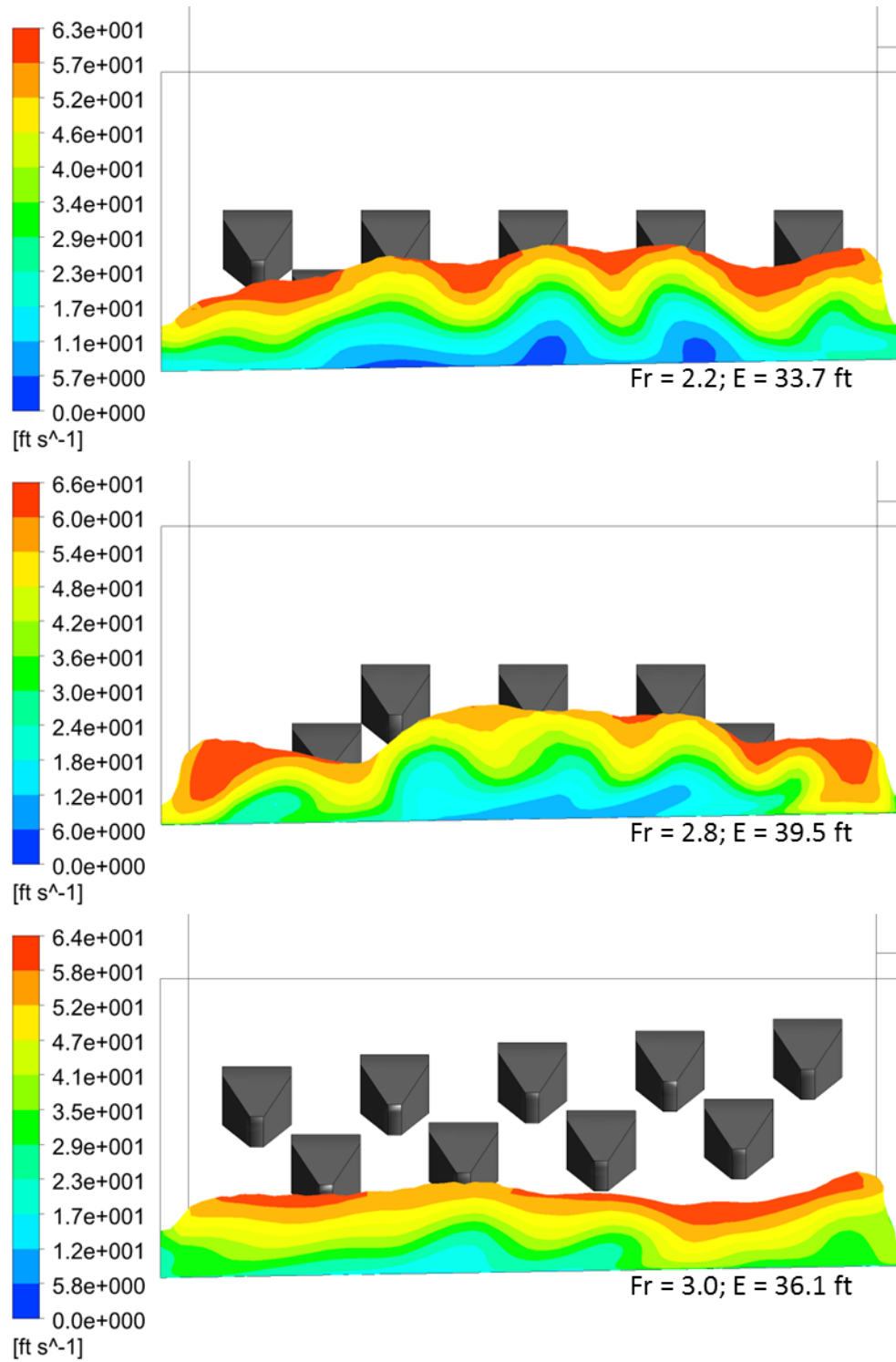


Figure 47: Outlet velocity contours of the water phase for the three block configurations. Froude number (Fr) and specific energy (E) is reported for each flow. From top to bottom, the configurations shown are the linear, LNSUB, and angled.

The final image provided of baffle block results is shown below in Figure 48. This image demonstrates that the turbulence intensity after baffle blocks are introduced into the spillway increases well above that of spillway flow without baffle blocks. For the case shown in Figure 48, the area-averaged turbulence intensity is calculated to be 12%. For the spillway at the same discharge but without blocks, the area-averaged turbulence intensity is 4%. While turbulence intensity information at the exit plane was not used for TDG predictions in the current effort, this increase in turbulence will enhance jet dissipation as the water falls through the atmosphere prior to impinging the lower pool.

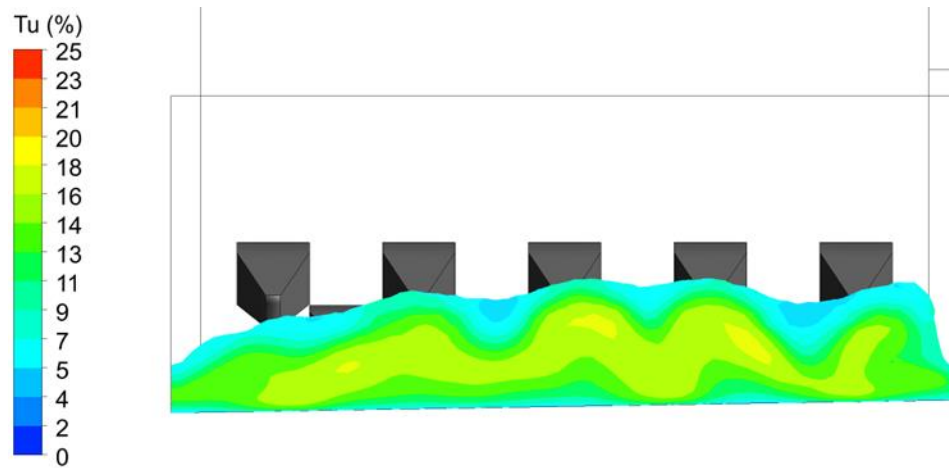


Figure 48: Turbulence intensity in the water phase at the spillway outlet (linear blocks case shown).

Table 17 below reports the values of α and β calculated for each of the block cases. The introduction of baffle blocks into the flow decreases the uniformity of velocity at the exit plane; consequentially, the correction coefficients are higher than those realized in the calibration models. This is an expected result. By definition, both correction coefficients tend to 1 for uniform cross-sectional velocity profiles. In flows with larger velocity gradients, the coefficients can become significantly larger than unity. Other examples in which α and β can be much greater than unity include flow downstream of bridge piers and a flooding river [21].

Table 17: Kinetic energy and momentum flux correction coefficients for baffle block cases. The specific discharge in each case is 260 ft²/s.

Block Case	Froude	α	β
Linear	2.21	1.72	1.24
LNSUB	2.81	1.47	1.16
Angled	2.97	1.25	1.04

Utilizing the calibration curves reported in Section 4.1.2 and the CFD results for baffle block cases shown in the current section, predictions of TDG at Boundary Dam can be made for proposed spillway modifications.

4.4. TDG PREDICTIONS

It is important to note at the onset of this section that the current TDG prediction effort is exploratory in nature. The attempt is to use *known, historic flow conditions and subsequent TDG levels* to make TDG predictions for potential hydraulics present at the dam if modifications to the spillway are implemented.

Figure 49 contains a plot of TDG predictions achieved by methods of the current effort—these are plotted at two different dashed series. Also shown in the graph are TDG predictions estimated by the method the engineering firm Hatch is using; here, a bold line is used. When examining the graph, it is important to keep in mind that only the *points* plotted represent meaningful results; the lines are provided to allow visual continuity between the predictions of each method.

For the prediction methods of the current research, TDG flux denotes the gain from the forebay-to-tailrace fixed monitoring stations shown in Figure 19 on page 43. It is worth stating that Configuration 1 is the current spillway geometry present at Boundary Dam; in this research effort, it is specifically the calibration model with a 13 kcfs discharge.

Consequently, TDG flux of approximately 7% saturation is realized for all models because it was specified as such in the calibration step. Configurations 2, 3, and 4 represent potential modifications which may be implemented at the dam—namely the linear, LNSUB, and angled configurations.

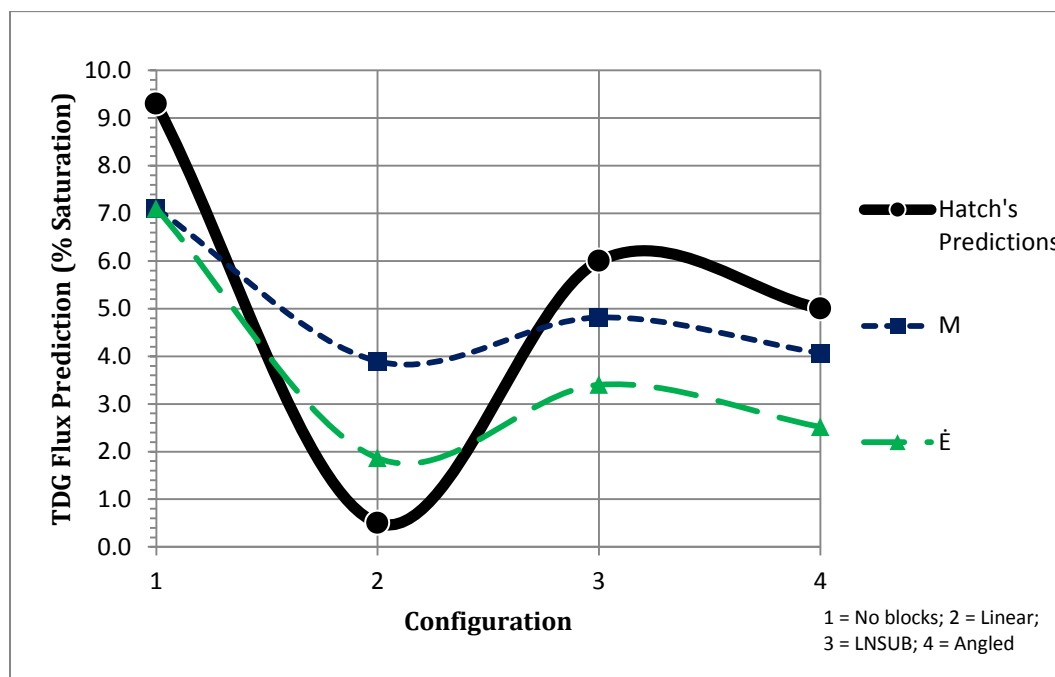


Figure 49: Initial TDG predictions. The y-axis denotes the predicted forebay-to-tailrace TDG flux, and the x-axis denotes different spillway configurations.

Upon first inspection of TDG prediction results, a few items arise. First, the predictions for Configuration 1 are all the same—as previously mentioned, this is a direct result of calibration. Secondly, for Configuration 1 all models of the current effort predict a TDG flux at Boundary Dam of 2.2% saturation less than that of Hatch’s model. This stems from field data available for the current research. Data averaged according to the procedure of Section 3.1 suggests that, for Configuration 1, the TDG flux at Boundary has historically been 7.1% on average. This result of 7.1% is reasonable, however, the reader should bear in mind that significant scatter is present in data monitored at hydropower projects. Therefore, the value of 9.3% predicted by Hatch’s model is also in the reasonable range.

Due to this discrepancy in the calibration data point, however, adjustments to the representation of results were made to allow for direct comparison between Hatch’s model and the currently investigated method. Each data point in Figure 49 was normalized by the maximum prediction achieved from that method. The results of normalization are shown in Figure 50. With this adjusted representation of data, it is more appropriate to make direct model-to-model comparisons.

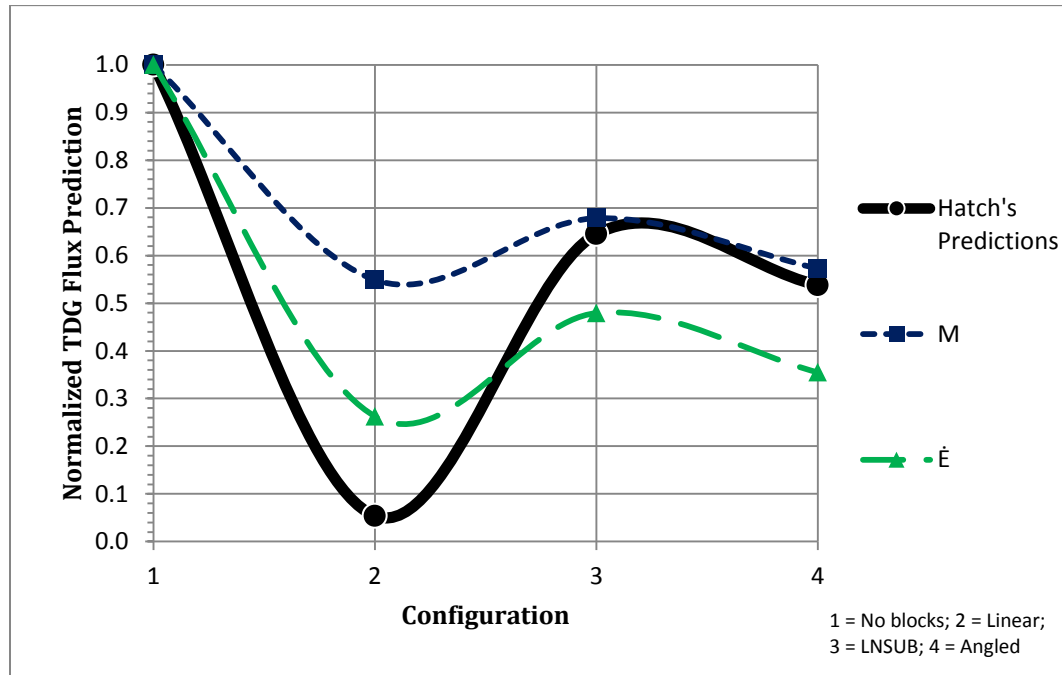


Figure 50: Normalized TDG predictions.

In examining Figure 50, it is readily apparent that the trends in TDG predictions of the present research match those of Hatch's. In terms of reducing TDG flux, the configurations are most preferable in the following order: linear, angled, and finally LNSUB. For these normalized results, the momentum function predictions for Configurations 3 and 4 match Hatch's predictions within 5% and 6.3% respectively.

For the linear blocks case, however, the specific energy rate and momentum approaches that have been investigated in the current research predicted a higher level of TDG flux than Hatch's model does. One possible explanation for the current model to over-predict TDG flux for the linear blocks case can be postulated by examining turbulence in each of the baffle block models.

Below, Table 18 shows the TKE observed at the spillway outlet for each of the baffle block runs. While the values of TKE reported here have not been validated (see Section 4.2.1 for a discussion on outlet sensitivity to inlet conditions), general trends observed can be informative.

Table 18: Turbulence kinetic energy in water exiting the spillway for all three baffle block cases.

Configuration	Area-averaged TKE (ft ² /s ²)
2 - Linear	46.8
3 - LNSUB	36.2
4 - Angled	37.7

In Table 18, Configurations 3 and 4 exhibit approximately the same magnitude of area-averaged TKE, on the other hand, water exiting the spillway in Configuration 2 exhibits TKE that is on the order of 25 – 30% higher than the other two alternatives. The higher level of TKE present in Configuration 2 will serve to dissipate the spillway jet as it plunges through the atmosphere, and ultimately the spilled water (and entrained air bubbles) will not plunge as deep into the lower reservoir. The expected effect, then, is that overall TDG flux would be reduced. While further investigation of this was not pursued, spillway jet TKE could be an interesting topic of focus for future TDG prediction efforts.

In the interest of comparing predictions from the current research with those of Hatch's, the final measure investigated was to adjust the current model's calibration data to match Hatch's. This was carried out in two different approaches, and the results are shown in Figure 51.

In the first approach—denoted in Figure 51 by \dot{E} and M —a value of 2.2% saturation was added to the single calibration data point of 7.1% (see Table 4, pg. 42). Here, the constant of 2.2% is achieved by subtracting 9.3% from 7.1% saturation—9.3% is Hatch's prediction for the 13 kcfs case without blocks, and 7.1% came from averaging field data reported by Rounds & Orlins [15]. In the second approach, a constant of 2.2% was added to *all* calibration values listed in Table 4—these series are denoted by " $\dot{E} + 2.2$ " and " $M + 2.2$ ".

Figure 51 shows the results of these adjustments. It becomes apparent that the predictions made by the specific energy rate method for Configurations 3 and 4 are close to those of Hatch's—a percent difference calculation yields 5.6% and 4.7% difference for Configurations 3 and 4, respectively, for the " $E+2.2$ " case.

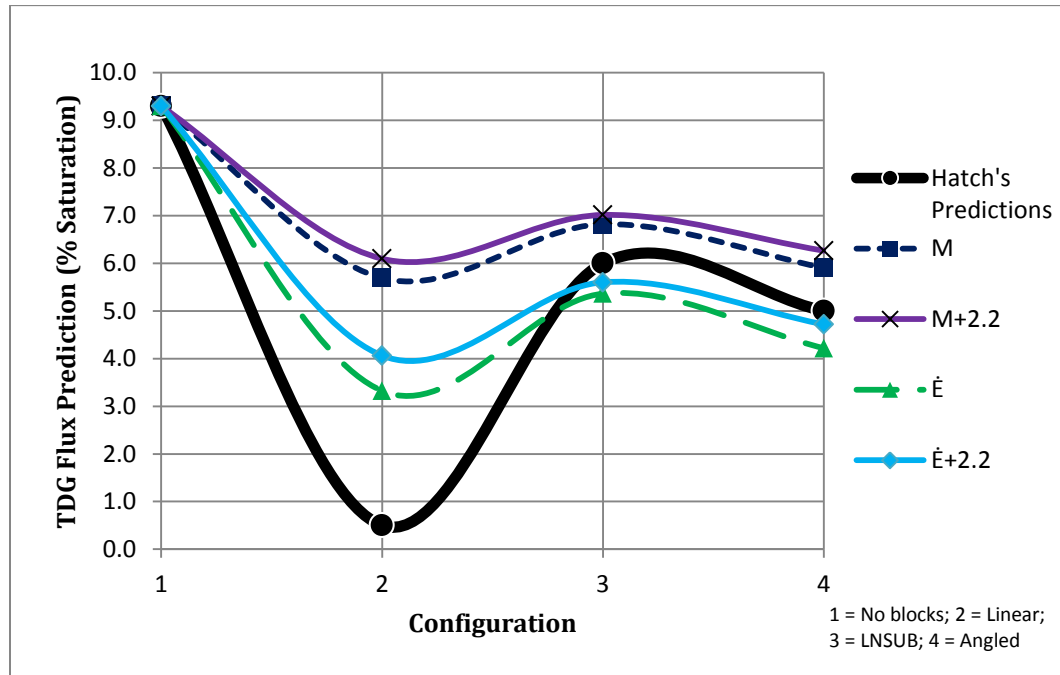


Figure 51: TDG predictions with the calibration data adjusted to match Hatch's.

Based upon TDG data currently available for the present research, it is not the author's intent to suggest these adjusted TDG predictions are fully justified. However, in the interest of making direct comparisons between the present modeling effort and Hatch's work, the adjustment in calibration data is valid.

The current results for Configuration 2 all remain substantially higher than the TDG flux predicted by Hatch for this case. It appears that the higher level of turbulent energy in this jet plays a significant role on how the jet behaves during the free fall before impinging the lower reservoir.

Overall, in terms of the trends observed from the current effort, TDG predictions were in agreement with those of Hatch's model. This discovery provides evidence that TDG production is indeed correlated to hydrodynamics of a spillway jet. Based upon the achieved results, it appears as though specific energy rate is the parameter which best correlates to TDG generation at a hydropower project with free jet dissipation.

5. CONCLUSIONS

5.1. GOAL OF STUDY

The goal of the current effort was to identify an efficient numerical methodology which correlates spillway flow characteristics to TDG generation. At the conclusion of this endeavor, a methodology for predicting trends in TDG flux across hydropower facilities with free, plunging jets is suggested. By analysis of historical flow and TDG behavior at Boundary Dam, it is concluded that the spillway modifications present themselves in the following order in terms of most favorable TDG reduction performance: linear blocks, angled blocks, and LNSUB.

In terms of general hydrodynamic spillway behavior, the introduction of baffle blocks decreases flow velocity and increases flow depth. While the result is a decrease in Froude number, flow remains supercritical throughout the spillway in all proposed baffle block configurations. For a flow rate of 13 kcfs at Boundary Dam, the introduction of baffle blocks into the spillway decreases the exit-flow Froude number by 57%, 46%, and 42% for the linear, LNSUB, and angled cases. In terms of specific energy, E , a 43%, 33%, and 38% reduction is realized for the linear, LNSUB, and angled block configurations. In the current effort, these values of energy reduction were investigated to see if a correlation existed between the amount of energy reduced and downstream TDG generation. To assess if a relationship is present, TDG predictions from Hatch's model were used for comparison. Despite the scatter present in TDG field data, the present model's predictions were in reasonable agreement with those made by the engineering firm Hatch. Similar trends were observed, and this encouraging discovery justifies further investigation of the currently sought TDG prediction method.

An overall conclusion of this study is that the specific energy rate does appear related to downstream TDG generation. Turbulence can also play a significant role in dissipating total jet energy; consequentially, spillway jet turbulence should be further investigated to numerically quantify how it influences TDG production.

In comparison to more detailed CFD models which predict TDG by solving mass transport equations, the methodology developed during the current effort has the benefit of

substantially decreased computational costs. In the current investigation, all models were run on four processors and took anywhere from several hours up to a week to run (depending on which mesh and model were under consideration). Due to this relatively minimal cost, the current method is well-suited to evaluate multiple TDG abatement alternatives as an initial step in the design process. Then, once the most promising TDG abatement alternatives had been identified, further study on a more comprehensive scale would be warranted.

5.2. KINETIC ENERGY AND MOMENTUM CORRECTION COEFFICIENTS

As part of the present research, kinetic energy and momentum flux correction coefficients, α and β respectively, were documented for a chute spillway at a range of flow rates. These values were in agreement with ranges found in literature and may be of use for analyzing jets of other, similar chute spillways. The observed ranges spanned from $\alpha = 1.03 - 1.06$, and values of β were very near unity, $1.01 - 1.02$. When baffle block configurations were considered, the ranges of both coefficients increased: $\alpha = 1.25 - 1.72$ and $\beta = 1.04 - 1.24$. The correction coefficients for baffle cases are specific to a given configuration, not discharge; therefore they are not as readily adaptable for use in other projects.

5.3. TDG REGIMES

Another point of interest was introduced in Section 3.1, and this is the notion that TDG flux at Boundary Dam can be broken into three somewhat separate regimes. These three regions must correspond to three different dominating physical phenomena. The first region involves low spill rates where TDG is actually stripped during the spill process. It could be hypothesized that at these flows the spilled water plunge depth is shallow enough to promote mixing such that dissolved gas release is greater than dissolved gas generation. In the second region, TDG flux increases along with increasing spill flow. In the third and final region it appears as though TDG flux asymptotically reaches a maximum value; some physical process leads towards saturation such that no further increase in downstream TDG supersaturation is possible.

The middle region of increasing TDG flux with increasing flow is the region that should be modeled by the sought predictive TDG tool; and, ideally, the minimum and maximum TDG

flux should be determined by the physical processes which create these limitations. In the current study, field data were used to distinguish these three regimes at Boundary Dam.

An explicit discussion of the above highlighted phenomenon was not encountered in the literature reviewed, but an investigation into the limiting physical processes would be informative for future TDG reduction efforts. One possibility could be to study the suggested regimes on a CFD model similar to the one Hatch is using, or a model such as the one developed by Politano et al. [32].

5.4. MODEL LIMITATIONS

The hypothesis at the onset of the current investigation assumed that energy of the spillway flow is the core driving mechanism which results in TDG supersaturation. The achieved results, and limited ability to assess model performance suggest that this hypothesis is reasonable; however, one of the key limitations of the developed method stems from lack of TDG data available for spillways that have undergone structural modifications. While trends from the current model were compared to, and are in reasonable agreement with predictions made by another TDG model, there are currently insufficient field data for full validation of the developed methodology.

To assess the accuracy of the new method, it would be necessary to form TDG predictions and compare them to field data at a hydropower facility that has implemented structural modifications to spillways. Cabinet Gorge is one facility which has installed baffle blocks with the goal of reducing downstream TDG pressures, however, this installation is very recent, and field data were not available at the time of the present research. Moving forward, Cabinet Gorge could serve as a potential facility to assess the accuracy of the developed TDG prediction method.

Also stemming from the limited amount of data currently available is the inability to fully address uncertainty in TDG predictions. This is a point worthy of attention in future investigations. As additional TDG data are documented within the hydropower community—specifically data that characterizes how structural modifications effect downstream TDG pressures—it will become feasible to evaluate uncertainty in TDG predictions. At the current time, uncertainties in TDG predictions from the gas transfer model Hatch is using are not available. Additionally, uncertainty in TDG predictions of the

developed method were not evaluated due to lack of experimental information that characterizes the influence of spillway modifications on downstream TDG levels (especially at facilities with free jet dissipation).

An additional limitation of the presented method is that historical TDG data must be available at a hydropower project in order to make TDG predictions for potential structural modifications. This is not a largely concerning limitation, as many facilities monitor TDG; however, the presented prediction method would not be viable for evaluating TDG at the construction of a new facility.

5.5. SENSITIVITY

As part of the current research, models were run with different inlet turbulence intensities. It was determined that outlet quantities including water velocity, area, and kinetic/momentum correction coefficients were all highly insensitive to turbulence intensity at the inlet. This finding was valuable because inlet turbulence conditions are not readily available for the spillway of interest. Findings of the sensitivity study justify that the presented results remain valid despite inlet turbulence uncertainties of the current project.

It was found that a tenfold increase in specified inlet turbulence intensity resulted in a 66% increase in turbulence intensity observed in the outlet water phase. The current investigation did not use turbulence parameters monitored at the outlet for predicting TDG, and therefore this sensitivity is not of concern. However, future investigations would benefit from resolving this source of uncertainty if they were to utilize turbulence quantities at the spillway exit.

5.6. MESH

While the currently employed meshes provide sufficient accuracy for this initial investigation, achieving a higher quality mesh for the baffle block runs would be a worthwhile effort for future research efforts to pursue.

The irregular shape of the blocks posed meshing challenges in the current work, and this resulted in higher discretization uncertainties realized for block cases than the calibration models. Future efforts should seek to achieve a higher quality mesh to increase the

precision of computed jet characteristics; this would provide further confidence in quantities computed on the spillway exit.

In achieving a quality mesh for the block cases, inlet conditions could be adjusted to capture a more accurate representation of wall layer flow behavior, velocity profiles, and also outlet turbulence. To achieve more accurate inlet conditions, a numerical model of the intake geometry upstream of the radial gate could be run to evaluate non-uniformities of flow as it enters the spillway chute. The results of such a model could then be used to specify inlet conditions for the CFD model of spillway flow used for TDG predictions. It would then be justified to take a next step related to the current research and closer examine how turbulence will influence jet breakup during the free fall.

In Figure 52, the region enclosed by a white oval highlights the domain used for the CFD models in the current effort. A promising next step for future research would be to use the same domain for CFD analysis, and then utilize energy and turbulence quantities at the spillway outlet to predict jet decay as the spillway water falls through the air.



Figure 52: The white oval indicates the domain region for the current CFD models. The black, dashed lines indicate the region future work should seek to *predict* by extrapolating energy and turbulence quantities at the spillway exit.

It is important to emphasize that it is not recommended that the CFD model domain be increased, rather that information at the spillway exit be extrapolated to characterize how

jet breakup during the fall will influence impingement energy and TDG generation. Ultimately this pursuit would allow for a more robust analysis of TDG production.

5.7. WALL LAYER FLOW BEHAVIOR

As previously discussed, the CFD models appear to capture the main features of spillway hydrodynamics, but do not capture what was termed the “wall layer” behavior. This appears to be the largest discrepancy between fluid dynamics within the model and the actual spillway.

While the absence of a wall layer is a source of error in the computational model, it is not a great concern in this initial consideration of TDG prediction results. This is because the total energy of the flow is much greater than the energy associated with the wall layer. In future investigations, an attempt to resolve the wall layer issue could be beneficial, as this aerated flow does influence outlet turbulence and the nature of jet dissipation. While reproducing this flow behavior would be challenging, a model could seek to replicate the wall layer by adjusting inlet conditions as well as specifying wall adhesion parameters within Fluent.

In general terms of spillway flow, aerated flow is beneficial for energy dissipation purposes and cavitation protection [58]. Therefore, the aerated wall layer phenomenon could be exploited to enhance energy dissipation at Boundary Dam, which could ultimately reduce downstream TDG pressures. Of course, design integrity of the spillway and radial gate would have to be ensured first.

5.8. CONCLUDING REMARKS

While the ability to draw major conclusions from the present effort is limited by lack of data that characterizes how installing impact energy dissipation devices influences downstream TDG pressures, overall, the present work does suggest that TDG downstream of a dam with free, plunging jets can be predicted by examining spillway jet characteristics. This discovery justifies further investigation of the presented predictive method, and a few potential directions have been identified which could help improve the efficiency and robustness of the proposed methodology.

BIBLIOGRAPHY

- [1] "Electricity in the United States - Energy Explained, Your Guide To Understanding Energy - Energy Information Administration." [Online]. Available: http://www.eia.gov/energyexplained/index.cfm?page=electricity_in_the_united_states#tab2. [Accessed: 10-Jun-2013].
- [2] "Census Bureau Projects U.S. Population of 312.8 Million on New Year's Day - Population - Newsroom - U.S. Census Bureau." [Online]. Available: <http://www.census.gov/newsroom/releases/archives/population/cb11-219.html>. [Accessed: 10-Jun-2013].
- [3] "Human Power Trainer -- Windstream Power." [Online]. Available: http://www.windstreampower.com/Bike_Power_Generator.php. [Accessed: 10-Jun-2013].
- [4] "Grand Coulee Dam, Bureau of Reclamation, Pacific Northwest Region." [Online]. Available: <http://www.usbr.gov/pn/grandcoulee/index.html>. [Accessed: 10-Jun-2013].
- [5] "Micro Hydro Electric Power System in Colorado - YouTube." [Online]. Available: <https://www.youtube.com/watch?v=edEhvmNlYqk>. [Accessed: 11-Aug-2013].
- [6] "Columbia River Basin map." [Online]. Available: <http://upload.wikimedia.org/wikipedia/commons/8/85/Columbiarivermapsnaakeriverhighlighted.png>. [Accessed: 19-Sep-2013].
- [7] W. J. Ebel, "Supersaturation of nitrogen in the Columbia River and its effect on salmon and steelhead trout," *Fishery Bulletin*, vol. 68, no. 1, pp. 1-11, 1969.
- [8] W. J. Ebel and H. L. Raymond, "Effect of atmospheric gas supersaturation on salmon and steelhead trout of the Snake and Columbia rivers," *Marine Fisheries Review*, vol. 38, no. 7, pp. 1-14, 1976.
- [9] "Bureau of Reclamation: Glossary," *U.S. Department of the Interior/Bureau of Reclamation*, 17-Feb-2012. [Online]. Available: <http://www.usbr.gov/library/glossary/#B>. [Accessed: 20-Jun-2013].
- [10] U.S. Army Corps of Engineers, Bureau of Reclamation, and Bonneville Power Administration, "Final Updated Proposed Action for the FCRPS Biological Opinion Remand." 24-Nov-2004.
- [11] USACE, "Water Quality Plan for Total Dissolved Gas and Water Temperature in the Mainstem Columbia and Snake Rivers." Jan-2009.
- [12] N. Morse-Dayton, "Boundary Dam," 29-Oct-2007. [Online]. Available: <http://www.flickr.com/photos/nmdayton/4317685137/>. [Accessed: 13-Sep-2013].
- [13] Columbia Basin Environmental, "Boundary Dam Spillway Evaluation 1 May - 25 July 2002." Jan-2003.
- [14] R. D. Sullivan, D. E. Weitkamp, T. J. Swant, and J. M. DosSantos, "Changing spill patterns to control dissolved gas supersaturation," *Hydro Review*, pp. 106-112, Aug-2004.
- [15] M. Rounds and J. J. Orlins, "Boundary Hydroelectric Project (FERC No. 2144)/Total Dissolved Gas Mitigation Studies Appendix 2/TDG Field Data Analysis: 2012 Annual Report." Jul-2013.
- [16] A. K. Biń, "Gas entrainment by plunging liquid jets," *Chemical Engineering Science*, vol. 48, no. 21, pp. 3585-3630, 1993.
- [17] R. W. Fox, P. J. Pritchard, and A. T. McDonald, *Introduction to Fluid Mechanics*, 7th Edition. John Wiley & Sons, 2009.

- [18] J. S. Gulliver and R. E. A. Arndt, *Hydropower Engineering Handbook*. McGraw Hill, 1991.
- [19] USACE, "Large Radial Gate Figure," *Wikipedia, the free encyclopedia*.
- [20] R. M. Khatsuria, *Hydraulics of Spillways and Energy Dissipators*. CRC Press, 2005.
- [21] T. W. Sturm, *Open Channel Hydraulics*. McGraw Hill, 2010.
- [22] USBR, *Design of Small Dams*, 3rd ed. Washington, D.C.: United States Department of The Interior, U.S. Government Printing Office, 1987.
- [23] D. A. Ervine, H. T. Falvey, and W. Withers, "Pressure Fluctuations on Plunge Pool Floors," *Journal of Hydraulic Research*, vol. 35, no. 2, pp. 257–279, Jan. 1997.
- [24] K. Moen, J. Groeneveld, P. Obalander, C. May, C. Simonsen, P. Rodrigue, and S. Smith, "Boundary Hydroelectric Project (FERC No. 2144) Study No. 3 Evaluation of Total Dissolved Gas and Potential Abatement Measures Final Report." Mar-2009.
- [25] "Total Dissolved Gas Criteria for Surface Water Quality Standards." [Online]. Available: http://www.ecy.wa.gov/programs/wq/swqs/criteria-freshwater/wac173201a_200-tdg.html. [Accessed: 05-Jul-2013].
- [26] "Hydrolab Water Quality Data Sonde Parameters - Stevens Water Monitoring Systems," *Stevens*. [Online]. Available: http://www.stevenswater.com/water_quality_sensors/datasonde_parameters.aspx. [Accessed: 05-Jul-2013].
- [27] C. Sweeney, K. Moen, and D. Kirshbaum, "Hydraulic Design of Total Dissolved Gas Mitigation Measures for Boundary Dam," presented at the Waterpower XVI, 2009.
- [28] D. A. Geldert, J. S. Gulliver, and S. C. Wilhelms, "Modeling Dissolved Gas Supersaturation Below Spillway Plunge Pools," *Journal of Hydraulic Engineering*, vol. 124, no. 5, pp. 513–521, 1998.
- [29] A. L. Urban, J. S. Gulliver, and D. W. Johnson, "Modeling Total Dissolved Gas Concentration Downstream of Spillways," *Journal of Hydraulic Engineering*, vol. 134, pp. 550–561, May 2008.
- [30] M. Politano, P. Carrica, and L. Weber, "Prediction Of Total Dissolved Gas Downstream Of Spillways Using A Multidimensional Two-Phase Flow Model," *Mecánica Computacional, Volume XXIV. Number 2. Hydric Resources and Environmental Engineering*, vol. XXIV, no. No. 2, pp. 285–295, 2005.
- [31] Q. Lu, L. Ran, L. Jia, L. KeFeng, and D. Yun, "Field Observation of Total Dissolved Gas Supersaturation of High-Dams," *Science China Technological Sciences*, vol. 54, no. 1, pp. 156–162, Jan. 2011.
- [32] M. Politano, P. Carrica, and L. Weber, "A Multiphase Model for the Hydrodynamics and Total Dissolved Gas in Tailraces," *International Journal of Multiphase Flow*, vol. 35, no. 11, pp. 1036–1050, Nov. 2009.
- [33] J. S. Gulliver, S. C. Wilhelms, and K. L. Parkhill, "Predictive Capabilities in Oxygen Transfer at Hydraulic Structures," *Journal of Hydraulic Engineering*, vol. 124, no. 7, pp. 664–671, 1998.
- [34] Y. Zhu, H. Oguz, and A. Prosperetti, "On the Mechanism of Air Entrainment by Liquid Jets at a Free Surface," *Journal of Fluid Mechanics*, vol. 404, pp. 151–177, 2000.
- [35] K. T. Kiger and J. H. Duncan, "Air-Entrainment Mechanisms in Plunging Jets and Breaking Waves," *Annual Review of Fluid Mechanics*, vol. 44, no. 1, pp. 563–596, Jan. 2012.
- [36] D. A. Ervine and H. T. Falvey, "Behaviour of Turbulent Water Jets in the Atmosphere and in Plunge Pools," *Proceedings of the Institution of Civil Engineers*, vol. 83 Part 2, pp. 295–314, Mar. 1987.

- [37] P. F. A. Manso, E. F. R. Bollaert, and A. J. Schleiss, "Evaluation of High-velocity Plunging Jet-issuing Characteristics as a Basis for Plunge Pool Analysis," *Journal of Hydraulic Research*, vol. 46, no. 2, pp. 147–157, 2008.
- [38] M. Politano, P. Carrica, C. Turan, and L. Weber, "Prediction of the Total Dissolved Gas Downstream of Spillways Using a Two-Phase Flow Model," in *World Water & Environmental Resources Congress*, 2004.
- [39] M. S. Politano, P. Carrica, C. Turan, and L. Weber, "A Multidimensional Two-Phase Flow Model for the Total Dissolved Gas Downstream of Spillways," *Journal of Hydraulic Research*, vol. 45, no. 2, pp. 165–177, 2007.
- [40] Seattle City Light, "Boundary Dam Water Spill," *Seattle City Light Facebook*. [Online]. Available: <https://www.facebook.com/photo.php?v=108008842604245&set=vb.140646799318965&type=3&theater>. [Accessed: 26-Aug-2013].
- [41] K. E. McGrath, E. M. Dawley, and D. R. Geist, "Total Dissolved Gas Effects on Fishes of the Lower Columbia River," Pacific Northwest National Laboratory, Richland, WA, 2006.
- [42] D. Weitkamp, "Total Dissolved Gas Literature 1980 - 2007, An Annotated Bibliography." Jan-2008.
- [43] "Northwest Fishletter." [Online]. Available: <http://www.newsdata.com/fishletter/289/2story.html>. [Accessed: 05-Jul-2013].
- [44] C. Fitzgerland, "NWAHA:Events/Committees:Archive," *Northwest Hydroelectric Association*. [Online]. Available: http://www.nwhydro.org/events_committees/archive.htm#2012_NWAHA_Annual_Conference_Papers_and_Presentations. [Accessed: 05-Jul-2013].
- [45] "Columbia River Operations for Fish > Northwestern Division > Northwestern Division Fact Sheet." [Online]. Available: <http://www.nwd.usace.army.mil/Media/FactSheets/FactSheetArticleView/tabid/2128/Article/1385/columbia-river-operations-for-fish.aspx>. [Accessed: 05-Jul-2013].
- [46] "Avista: Clark Fork River News," *Avista*, Spring-2013. [Online]. Available: <http://www.avistautilities.com/environment/clarkfork/pages/news.aspx>.
- [47] H. K. Versteeg and W. Malalasekera, *An Introduction to Computational Fluid Dynamics The Finite Volume Method*, Second Edition. Pearson Education Limited, 2007.
- [48] J. J. Orlins and J. S. Gulliver, "Dissolved Gas Supersaturation Downstream of a Spillway II: Computational Model," *Journal of Hydraulic Research*, vol. 38, no. 2, pp. 151–159, 2000.
- [49] R. LI, J. LI, K. LI, Y. DENG, and J. FENG, "Prediction for Supersaturated Total Dissolved Gas in High-dam Hydropower Projects," *Science in China E: Technological Sciences*, vol. 52, no. 12, pp. 3661–3667, 2009.
- [50] A. Hoque and S. Aoki, "Air Entrainment and Associated Energy Dissipation in Steady and Unsteady Plunging Jets at Free Surface," *Applied Ocean Research*, vol. 30, no. 1, pp. 37–45, Feb. 2008.
- [51] "ANSYS 14.5 Help." SAS IP, Inc., 2012.
- [52] T. Cebeci, J. Shao, F. Kafyeke, and E. Laurendeau, *Computational Fluid Dynamics for Engineers*. New York: Springer Berlin Heidelberg.
- [53] J. Blazek, *Computational Fluid Dynamics: Principles and Applications*, Second Edition. San Diego, CA: Elsevier Ltd., 2005.

- [54] F. R. Menter, "2-Equation Eddy-viscosity Turbulence Models for Engineering Applications." American Institute of Aeronautics and Astronautics, Aug-1994.
- [55] S. Kang and F. Sotiropoulos, "Numerical modeling of 3D turbulent free surface flow in natural waterways," *Advances in Water Resources*, vol. 40, pp. 23–36, May 2012.
- [56] H. Rahimzadeh, R. Maghsoodi, H. Sarkardeh, and S. Tavakkol, "Simulating Flow Over Circular Spillways by Using Different Turbulence Models," *Engineering Applications of Computational Fluid Mechanics*, vol. 6, no. No. 1, pp. 100–109, 2012.
- [57] I. Celik, U. Ghia, P. Roache, C. Freitas, H. Coleman, and P. Raad, "Procedure for Estimation and Reporting of Uncertainty Due to Discretization in CFD Applications," *Journal of Fluids Engineering*, vol. 130, no. 7, p. 078001, 2008.
- [58] P. Novak, A. I. . Moffat, C. Nalluri, and R. Narayanan, *Hydraulic Structures*, Fourth Edition. Taylor & Francis, 2007.
- [59] C. CHEN and Z. DONG, "An Experimental Study on Turbulence Characteristics of Flows Over Smooth Spillway Dam." *Science in China (Series A)*, Aug-1991.
- [60] ANSYS, "Volume of Fluid Model: Lecture 2."
- [61] X. L. Qu, L. Khezzar, D. Danciu, M. Labois, and D. Lakehal, "Characterization of Plunging Liquid Jets: A Combined Experimental and Numerical Investigation," *International Journal of Multiphase Flow*, vol. 37, no. 7, pp. 722–731, Sep. 2011.
- [62] B. Dargahi, "Experimental Study and 3D Numerical Simulations for a Free-overflow Spillway," *Journal of Hydraulic Engineering*, vol. 132, no. 9, pp. 899–907, 2006.
- [63] P. Kundu and I. Cohen, *Fluid Mechanics*, 2nd ed. Academic Press, 2002.

APPENDICES

APPENDIX A: ADDITIONAL DETAILS OF RELEVANT RESEARCH

Below, further details of literature discussed previously in this thesis regarding TDG prediction efforts are provided. Articles are presented in alphabetical order.

A multidimensional two-phase flow model for the total dissolved gas downstream of spillways, Politano et al., 2007 [39]

It is stated that the prediction of TDG downstream of spillways is a complex problem that is currently poorly solved. The generation of dissolved gas in rivers is dependent upon “3d effects, high turbulence, mass transfer at the free surface, and mass transfer with bubbles with different chemical compositions and solubilities.”

For the computational model, a 2D domain is used consisting of approximately 58,000 nodes. The time reported to reach convergent solutions is not reported. The result of their effort was a predictive model in which gas volume fraction, bubble size distribution at the inlet, and gas mass transfer at the free surface are the only unknown parameters. An important emphasis conveyed throughout the article is that bubble size plays a key role in the generation of TDG, with smaller bubbles having the largest contribution to supersaturation.

A multiphase model for the hydrodynamics and total dissolved gas in tailrace, Politano et al., 2009 [32]

The goal of this effort was to develop a 3D, two-phase flow model to capture hydrodynamics and predict TDG in the tailwater of Wanapum Dam. ANSYS Fluent was used for numerical modeling. For turbulence, the RANS-based Reynolds Stress Model (RSM) was implemented. One focus of the study was to investigate the effect which bubbles have on turbulence (and subsequent water entrainment) in the spillway water jet that develops in tailraces. In the field data reported, significant scatter is present.

Their solution process consists of two main steps. First the water profile was predicted using unsteady, variable time stepping on the VOF domain. Once a water surface profile was achieved, a second “rigid-lid” TDG model was used to model gas transfer.

The grid for VOF computations consisted of approximately $1.7\text{E}+06$ nodes and extended approximately 1000m downstream of the dam. The authors express that, due to the

extremely complex nature of the phenomenon at hand, the focus of their research is to present a model which can achieve reasonable solutions. In striving towards this goal, their model consists of three parameters tuned to match field TDG observations. The model relies on bubble probability density function, average bubble size, and gas volume fraction as external inputs. It is mentioned that ideally these inputs would be achieved from experimental data.

It is noted that using a two-phase VOF model to capture the free surface is complex; therefore, for large stilling basin domains it can take more than 2 months of CPU time (on a 4 processor PC) to reach a solution. For actual models run during this project a 128 processor Linux cluster (with 2GB of memory per processor) was employed. With this configuration, and with zero velocity and turbulence used throughout the domain for the initial condition, it took 60 days of wall clock time to reach statistically steady-state solutions for the first step of their process. Another 7 days were required for the TDG prediction computations.

In an effort to match model hydrodynamics with those observed in the field, the effect of bubbles on the turbulence field is investigated, and anisotropic turbulence values in the model are calibrated to achieve agreement with field data. The authors conclude that bubbles play an important role in turbulence suppression in tailrace flows; consequentially, bubbles influence the flow field and TDG distributions. In order to match TDG predictions with field data, a gas volume fraction and bubble diameter of 4% and 0.8mm, respectively, were used.

Dissolved gas supersaturation downstream of a spillway II: computational model, Orlins and Gulliver, 2000 [48]

This article discusses the computational model developed for analyzing spillway deflectors at Wanapum Dam on the Columbia River. A reduced-scale physical model (which includes the dam, stilling basin, and approximately 300m downstream) was used to aid in evaluating the various proposed spillway deflectors. The challenge with a Froude-scaled physical model is that it cannot accurately capture air entrainment or the transfer of gas across bubble-water interfaces—this is because Froude and Reynolds numbers do not scale together. For this reason, the 1:21.5 scale physical model was used to capture mean flow

characteristics and this information was used as inputs into the computational model. In this way the computational model was used to analyze the turbulent mixing and gas transfer to and from the water for TDG predictions.

The model presented in their work uses a 2D domain, which implies the assumption that flow is well-mixed laterally. The domain extends from where the spillway intersects the stilling basin apron to approximately 240m downstream. The entire river depth is covered, and the nominal cell size was 1.5m x 1.3m. Measurements taken on the physical model (using acoustic doppler velocimetry and particle image velocimetry) were interpolated to the computational grid nodes using the kriging algorithm. The commercial software package SURFER was used for computations. Bubble distribution in the flow, hydrodynamic data, and upstream depth-averaged TDG concentrations were used as inputs to the computational model. The upstream TDG concentration was used as an independent variable which could be changed to match particular flow conditions. From this information, steady-state TDG predictions are calculated for the tailwater of Wanapum Dam.

One of the sources of uncertainty in their effort was the difficulty experienced in taking measurements on the reduced-scale physical model. For instance, the placement of false walls in the tailrace of the physical model was required to constrain the bead-seeded flow to a certain transverse distance from a side view; without knowing the transverse distance, necessary bead locations could not be determined. One issue with the use of false walls is the constriction of lateral eddies in the tailwater flow to a smaller length scale, namely, the scale of the distance between the false walls.

The developed TDG prediction process was used to evaluate the existing spillway configuration as well as two proposed modifications to the spillway. Two coefficients were fit to field data, and computations were run for each configuration at the same discharge for two different tailwater levels. Overall, the study concluded the “low” spillway deflector would function best for the purpose of reducing TDG.

Modeling dissolved gas supersaturation below spillway plunge pools,
Geldert et al., 1998 [28]

The effort outlined in this article developed “physically based relationships” to predict TDG supersaturation levels downstream of spillways.

Two ideas that were incorporated into this model were the transfer of mass across the air-water interface at the water surface, as well as “an effective saturation concentration” dependent upon both the depth of the stilling basin and river downstream. The relationship developed for TGD predictions relies upon physical flow parameters, design specifications, and theory regarding bubble and mass transfer phenomenon.

It is summarized that downstream TDG levels “are largely determined by what happens in the spillway, stilling basin, and bubbly flow region immediately downstream.”

Modeling total dissolved gas concentration downstream of spillways,
Urban et al., 2008 [29]

A two-layer, steady-state gas transfer model for TDG predictions is presented. The model simulates the physical processes involved in gas transfer. The model utilizes relationships from literature which describe bubble and mass transfer, jet growth, turbulence decay, bubble rise velocity and coalescence. Field data from Ice Harbor Dam (located on the Snake River) was used to calibrate the model. Good agreement between the model and field measurements was achieved.

Conclusions were that bubble mass transfer is dominant in the stilling basin while free surface mass transfer is dominant further downstream from the spillways; peak TDG concentrations are relatively insensitive to the maximum range of air ejected or entrapped at entrainment locations; tailwater depth plays a significant role in TDG concentration; and increased water surface roughness increases the exchange of mass at the free surface.

Prediction for supersaturated total dissolved gas in high-dam hydropower projects, LI et al., 2009 [49]

This investigation was focused on hydropower projects in China. The authors state that research related to TDG originated in the U.S. and has focused on the Columbia and Snake Rivers, but now the issue of TDG supersaturation is becoming more important in China as they develop the “West-East Power Transmission Strategy.” This energy strategy has resulted in several high head dams being constructed, with additional high head projects in the planning stages. The investigators point out that all of the research for the Columbia and Snake Rivers has been focused on low to mid head dams, and for this reason the results from previous research studies are not applicable to the high head dams of which the

authors are interested. It is recognized that there is an empirical relationship between TDG production and discharge at any given facility, however, this relationship varies from one project to another, and general TDG formulae suitable for a wide range of projects have not been achieved.

The authors comment on the differences in hydraulics present in scour hole dissipation vs. plunge pools. They express that each configuration, for the same spill rate, will yield different levels of TDG supersaturation due to the variance in pressures and tail water depths. Figure 53 provides a comparison of scour hole dissipation versus plunge pool dissipation. The hydraulics present at Boundary Dam are more closely related to the plunge pool shown below.

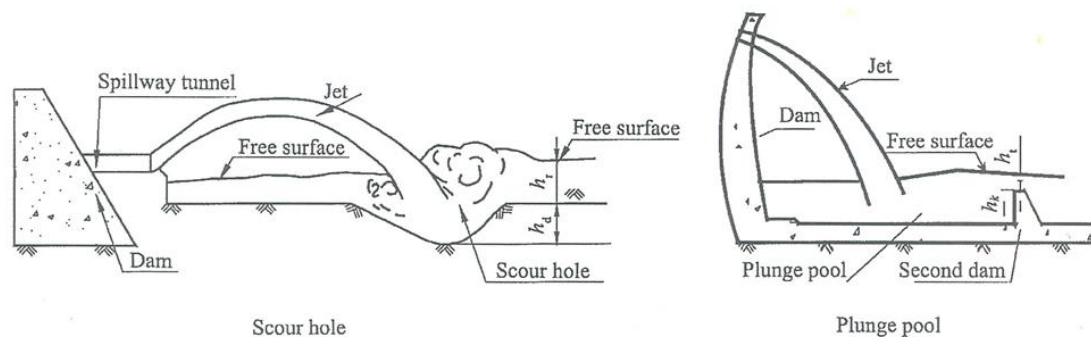


Figure 53: Comparing the difference between scour hole and plunge pool dissipation (LI et al., [49]).

For the study of TDG at high head dams in China, the main dependent variables considered were (1) hydrodynamic pressure and (2) water depth. To achieve hydrodynamic pressures for use in their TDG prediction equation, it states that physical models and dam design specifications were used. Calibration of the model equation yielded agreement with field data to within 5%. From this process, suggested ranges of correction coefficients are reported, however, the methodology used in achieving correction coefficient values is not fully clear. Therefore, the developed equations do not appear to be easily adaptable for predicting TDG below other hydropower facilities.

While the authors did use their model to make TDG predictions at a hydropower facility that was not yet been constructed, it doesn't appear they were able to validate model performance by predicting TDG supersaturation downstream of a dam and comparing the

model predictions to field data. The same challenge is experienced in the current research at Boundary Dam because field data for baffle block configurations are not available.

Prediction of the total dissolved gas downstream of spillways using a two-phase flow model, Politano et al, 2004 [38]

The effort is related to TDG studies for dissolved gas abatement at Wanapum Dam. The authors report that various studies have been conducted on the prediction of TDG, but most of them are based on experimental model testing. It is stated that models constitute an expensive approach and don't allow for optimization studies at feasible costs.

The reported research presents a two-phase flow model to predict gas volume fraction in the water, as well as the velocity of bubbles. To predict bubble sizes throughout the domain a transport equation is solved for bubble number density, and this is used in combination with void fraction information. For TDG predictions, a transport equation which considers the dissolution and absorption of air is used. The model consists of a 2D domain spanning from the end-sill to approximately 800m downstream of the spillway. The model is run with different inlet gas volume fractions and different inlet bubble radii to examine how TDG predictions compare to field data.

As with typical TDG field data, rather large scatter in the dataset is present.

Prediction of total dissolved gas downstream of spillways using a multidimensional two-phase flow model, Politano et al., 2005 [30]

A 3D model of Wanapum Dam was developed within Fluent for TDG predictions. For modeling turbulence, the modified $k - \epsilon$ closure was used. The grid contained approximately $1.77\text{E}+6$ cells. Gas volume fraction and the velocity of bubbles were used to achieve TDG predictions considering the dissolution and absorption of air mass. It is reported that the model is able to capture the main flow features downstream of the dam; however, "considerable discrepancy" is exhibited between the numerical model and experimental observations with regards to diffusion and entrainment of powerhouse flow into spillway flow.

APPENDIX B: FIELD DATA REDUCTION

In order to construct the graph shown in Figure 21, it was necessary to filter data provided in Rounds and Orlins' report [15]. In the report, data from the "short-term database" was used, which contains TDG data recorded at Boundary Dam during the period from 2006–2012. Based upon the ratio of *spilled flow to total outflow* that a give test was taken at, the data was broken up into eleven individual graphs in the report. Table 19 provides details on how data was divided for graphing.

Table 19: How data from the "short-term database" was divided for plotting purposes.

Corresponding Figure Number in Rounds and Orlins' Report [15]	Spilled Flow/Total River Discharge (%)	Spill Flow Discharge Ranges (cfs)	
		Minimum	Maximum
4	0 - 10	1,600	5,600
5	10 - 15	3,800	9,200
6	15 - 20	7,400	13,100
7	20 - 25	8,000	17,400
8	25 - 30	9,500	21,500
10	30 - 35	20,700	28,000
11	35 - 40	19,900	33,700
12	40 - 45	33,800	43,200
13	45 - 50	39,700	59,500
14	50 - 60	39,700	59,500
15	> 60	50,400	151,000

Figure 54 shows a sample of one of the eleven graphs used to average data for the needed TDG flux vs. spill flow rate shown in Figure 21 on pg. 45.

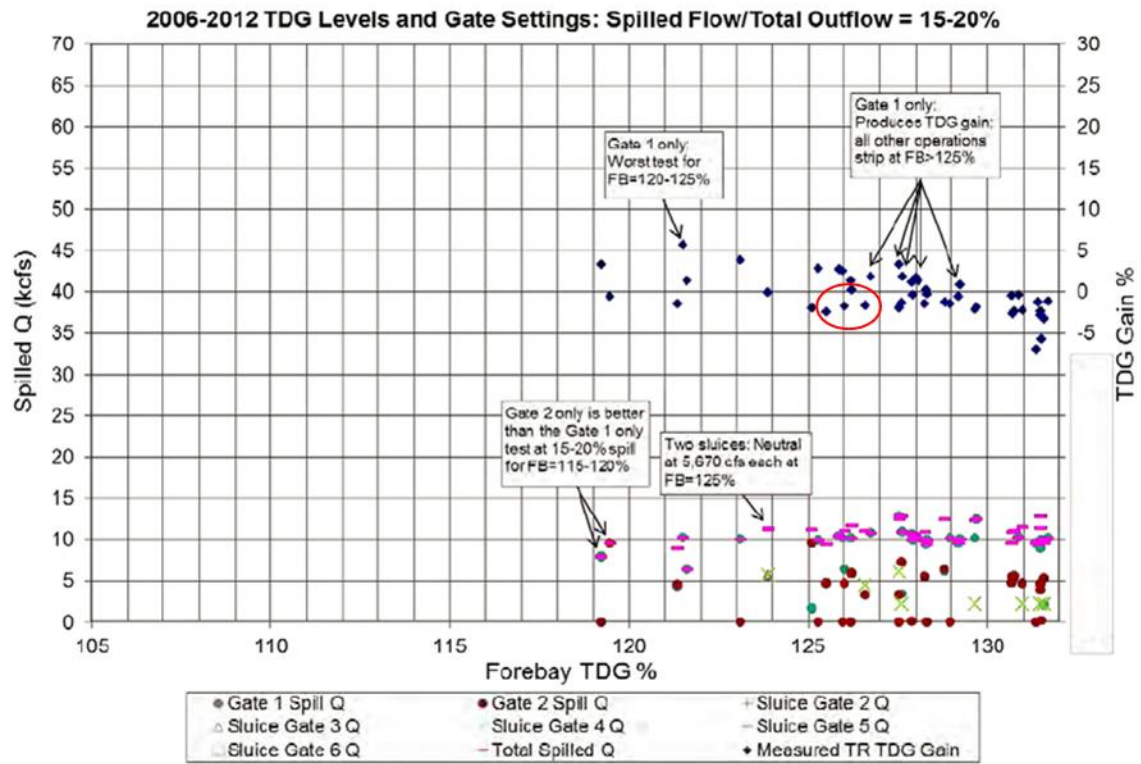


Figure 54: One of the graphs from Rounds and Orlins' report [15]. Data from the "Forebay TDG %" condition of 126% was averaged from this graph (and eleven others like it) to achieve the data plotted in Figure 21.

In the above figure, four points between 125 and 127 "Forebay TDG %" were averaged to achieve a TDG flux of -1.5% for the spilled flow/total outflow condition of 15–20%. The points used for averaging are circled on the above graph (in red). Any notes provided on the graphs were taken into account in determining whether or not to include a data point in averaging. For instance, an annotation on Figure 54 states that "Gate 1 only: Produces TDG gain; all other operations strip at FB>125%." Because of this note, none of the higher TDG fluxes between 125 and 127% Forebay TDG were used in averaging.

APPENDIX C: MODELING DETAILS

Below, information about specific parameters used for modeling efforts are presented.

Parameter	Settings	Specification	Units	Notes
<i>Meshing – 6 kcfs</i>				
	Maximum inflation thickness	2.5	ft	For all 6 kcfs models
	# Inflation Layers	15, 23, 34		For <i>coarse, medium, & fine</i> meshes
	Growth	1.20, 1.13, 1.09		For <i>coarse, medium, & fine</i> meshes
	Size on spillway inlet and outlet	0.92, 0.61, 0.41	ft	For <i>coarse, medium, & fine</i> meshes
<i>Meshing – 13 kcfs (*Note: these settings were also used for all corresponding Baffle Block Models)</i>				
	Maximum inflation thickness	5.71	ft	For all 13 kcfs models
	Number of inflation layers	15, 26, 43		For <i>coarse, medium, & fine</i> meshes
	Inflation growth rate	1.20, 1.12, 1.07		For <i>coarse, medium, & fine</i> meshes
	Size on spillway inlet and outlet	1.31, 0.77, 0.45	ft	For <i>coarse, medium, & fine</i> meshes
<i>Meshing – 17.5 kcfs</i>				
	Maximum inflation thickness	8.87	ft	For all 17.5 kcfs models
	Number of inflation layers	22, 34, 50		For <i>coarse, medium, & fine</i> meshes
	Inflation growth rate	1.20, 1.13, 1.09		For <i>coarse, medium, & fine</i> meshes
	Size on spillway inlet and outlet	1.31, 0.87, 0.58	ft	For <i>coarse, medium, & fine</i> meshes
<i>Meshing – 20 kcfs</i>				
	Maximum inflation thickness	10.76	ft	For all 20 kcfs models
	Number of inflation layers	25, 38, 56		For <i>coarse, medium, & fine</i> meshes
	Inflation growth rate	1.12, 1.08, 1.05		For <i>coarse, medium, & fine</i> meshes
	Size on spillway inlet and outlet	1.44, 0.96, 0.64	ft	For <i>coarse, medium, & fine</i> meshes
<i>Multiphase model – VOF</i>				
	Scheme	Explicit		
	Options	Open Channel Flow		
	Body force formulation	Implicit body Force		
<i>Viscous model – SST $k - \omega$</i>				
	Turbulence damping	1.000E+01		Damping Factor (default value)
	Kinematic viscosity	8.218E-04	lbm/ft-s	Kinematic viscosity at 12.75C
	Fluid density	6.231E+01	lbm/ft ³	Default value for water

		7.647E-02	lbm/ft ³	Default value for air
<i>Operating conditions</i>				
	Pressure	2.116E+03	lbf/ft ²	
	Reference pressure location	5.000E+00	X (ft)	
		2.000E+01	Y (ft)	
		2.700E+01	Z (ft)	
	Gravity	-3.219E+01	Y (ft/s ²)	
	Operating Density	7.647E-02	lbm/ft ³	
<i>Atmosphere pressure outlet</i>				
	From neighboring cell	Backflow direction specification method		
<i>Atmosphere inlet and outlet</i>				
	Turbulence intensity	1	%	
<i>Inlet mass flow</i>				
	Turbulence Intensity	2	%	Based upon information in [59]
	Inlet mass flow	Varies—refer to “Flow Rate” in Table 4	cfs	Mass flow rate is achieved by using “Flow Rate” and multiplying by water density
	Specification for free surface level	Varies—refer to “Spill Gate Opening” in Table 4	ft	
	Specification for bottom level	-4.306E-03	ft	
<i>Pressure outlets</i>				
	Turbulence intensity	5	%	
	Hydraulic diameter	$4A/(b+2*y)$	ft	
	Backflow direction specification method for momentum	From neighboring cell		
	Pressure specification method	From neighboring cell		
	Open channel flow	-3.554E+01	ft	Bottom level
<i>Walls</i>				
	Roughness (K _s)	2.490E-03	ft	Based upon information from Khatsuria, pg. 550 [20]
	Roughness constant	0.5		
<i>Reference values</i>				
	Length	y	ft	
	Velocity	$Q/(b*y)$	ft/s	

<i>Solution methods</i>				
	P-V coupling	PISO		
	Gradient	Green-Gauss Cell Based		
	Pressure	PRESTO!		
	Momentum	2nd order UP		
	Volume fraction	Compressive		
	TKE	2nd order UP		
	Specific dissipation rate	2nd order UP		
	Transient formulation	1st order Implicit		
<i>Solution controls</i>				
	Under relaxation factors	All default values		
	Pressure V-Cycle termination	0.001		

